668 | Juli 2013

SCHRIFTENREIHE SCHIFFBAU

Hendrik Dankowski

# A Fast and Explicit Method for Simulating Flooding and Sinkage Scenarios of Ships

TUHH
Technische Universität Hamburg-Harburg

# A Fast and Explicit Method for Simulating Flooding and Sinkage Scenarios of Ships

Vom Promotionsausschuss der

Technischen Universität Hamburg-Harburg

zur Erlangung des akademischen Grades

**Doktor-Ingenieur (Dr.-Ing.)**

genehmigte

**Dissertation**

von

Dipl.-Ing. (FH) Hendrik Dankowski, M.Sc.

aus Eutin

2013

**Vorsitzender des Prüfungsausschusses**

Prof. Dr.-Ing. Otto von Estorff

**Gutachter**

1. Gutachter: Prof. Dr.-Ing. Stefan Krüger

2. Gutachter: Prof. Dr.-Ing. habil. Apostolos D. Papanikolaou

**Zusätzliche Gutachter**

Prof. Dr.-Ing. Moustafa Abdel-Maksoud

Prof. Dr.-Ing. habil. Alexander Düster

**Tag der mündlichen Prüfung**

13. März 2013



Technischen Universität Hamburg-Harburg

Schwarzenbergstraße 95C

D-21073 Hamburg

http://www.ssi.tu-harburg.de/vss/

Bericht Nr.: 668

ISBN 978-3-89220-668-2

URN urn:nbn:de:gbv:830-tubdok-12229

## Abstract

Many severe ship accidents in the past were caused by a large water ingress followed by the progressive flooding of the watertight integrity of the ships and finally resulted in the sinking and total loss of the vessels. These accidents show a high demand for a better understanding of the flooding of ships with the help of numerical methods. This would allow to avoid such accidents in the future and to find new designs with an increased capability to withstand flooding. The circumstances of the accidents, which involve flooding are difficult to understand due to the complexity of the inner subdivision and the large number of resulting flooding paths. Hence, a fast numerical simulation method is developed in this thesis to analyse and predict such flooding events. The validation of the method comprises the comparison with experimental results from three test cases of a model test and the re-investigation of three severe ship accidents, which have been carefully investigated before: The accident of the  gateway, the HERAKLION and the ESTONIA. The results obtained with the new method in these applications are very promising.

A quasi-static approach in the time domain is chosen to compute the flooding of the inner subdivision and the resulting equilibrium floating position at each intermediate time step. The flooding paths are modelled with the help of directed graphs. The water fluxes through the openings are computed by a hydraulic model based on the Bernoulli equation. Large and partly flooded holes are taken into account, as well as conditional openings like breaking windows or the flooding through completely filled compartments. The effect of air compression can be taken into account as well if this is required for a certain case. After the determination of the new flood water distribution and the corresponding filling levels in each compartment, the resulting equilibrium floating position is computed. The simulation ends, either if the intermediate floating position does not change any more or if all buoyancy reserve is lost and the ship starts to submerge below the sea surface.

The method is developed within the ship design system E4, which ensures a consistent data model and allows the direct coupling with existing and new methods. All essential effects are taken into account without unnecessarily increasing the complexity of the model as this would lower the performance of the simulation method. The method enables the user to study many flooding scenarios within a short period, for example to investigate the influence of watertight doors that were left open.

## Zusammenfassung

Zahlreiche schwere Seeunfälle von Schiffen wurden in der Vergangenheit ausgelöst durch Wassereinbruch und anschließender weitergehender Flutung der wasserdichten Unterteilung, welche zum Sinken und dem Totalverlust der Schiffe führte. Daher besteht ein hoher Bedarf an numerischen Simulationsmethoden, mit denen diese Flutungsvorgänge genauer untersucht werden könnten. Dadurch könnten solche Unfälle in Zukunft vermieden werden und sicherere Schiffsentwürfe entwickelt werden. Die Rekonstruktion der Unfallvorgänge wird erschwert durch die hohe Komplexität der inneren Unterteilung von Schiffen und der daraus resultierenden großen Anzahl an Flutungswegen. Aus diesem Grund wird ein numerisches Berechnungsprogramm entwickelt, welches in der Lage ist, diese Vorgänge schnell und direkt zu analysieren und vorhersagen zu können, um so auch Kenntnisse über die einzelnen Zwischenflutungszustände zu erlangen. Die Validierung der Methode erfolgt anhand von drei Testfällen eines Modellversuches und drei realen Unfällen, die bereits umfangreich untersuchten wurden: Die Unfällen der European Gateway, der Heraklion und der Estonia. Die Ergebnisse der neuen Methode in diesen Anwendungen sind sehr vielversprechend.

Die quasi-statische Methode ermittelt den zeitlichen Verlauf der Flutung des Schiffes und die daraus resultierenden Schwimmlagen. Die Beschreibung des Flutungssystems, welches aus den Öffnungen und Räumen gebildet wird, erfolgt mit Hilfe gerichteter Graphen. Die Strömungen durch die Öffnungen der komplexen Unterteilung eines Schiffes werden idealisiert mit Hilfe der inkompressiblen Bernoulli-Gleichung berechnet. Teilgetauchte, große Öffnungen werden ebenso berücksichtigt wie zeitlich veränderliche Öffnungen, deren Eigenschaften im Laufe der Simulation unter bestimmten Bedingungen verändert werden. Somit können zum Beispiel berstende Fenster modelliert werden, die erst ab einem bestimmten Druckniveau durchlässig werden. Optional kann der Einfluss der Kompression von eingeschlossener Luft berücksichtigt werden. Nach Bestimmung der neuen Verteilung des Wassers und der Ermittlung der Füllstände in den einzelnen Räumen wird die korrespondierende hydrostatische Gleichgewichts-Schwimmlage bestimmt. Die Simulation wird fortgeführt, bis sich entweder diese Schwimmlage nicht mehr ändert oder das Schiff keine Auftriebsreserve mehr hat und von der Wasseroberfläche verschwindet.

Durch die direkte Integration der Simulationsmethode in das schiffbauliche Entwurfssystem E4 ist eine konsistente Datenmodellierung gewährleistet und eine Kopplung mit bestehenden und neuen Methoden möglich. Es wird Wert darauf gelegt, die entscheidenden Effekte hinreichend genau abzubilden, ohne die Komplexität unnötig zu erhöhen und damit die Geschwindigkeit der Simulation zu verringern. Dies erlaubt dem Anwender, verschiedene mögliche Varianten des Unfallhergangs innerhalb kürzester Zeit zu berechnen, um zum Beispiel den Einfluss einer eventuell geöffneten wasserdichten Tür auf einen Unfallhergang untersuchen zu können.

## Acknowledgement

First of all I want to thank my advisor Prof. Dr.-Ing. Stefan Krüger for his comprehensive and continuous support during my research work at his Institute of Ship Design and Ship Safety of the Hamburg University of Technology.

Special thanks go to Prof. Dr.-Ing. habil. Apostolos D. Papanikolaou for the fruitful collaboration, his very valuable comments and the hospitality during my visit at his institute.

Furthermore I want to thank the additional reviewers Prof. Dr.-Ing. Moustafa Abdel-Maksoud and Prof. Dr.-Ing. habil. Alexander Düster. I also thank Prof. Dr.-Ing. Otto von Estorff for chairing this doctorate commission.

Great thanks also go out to my colleagues at the institute M-6 for the in-depth discussions and inspirations. In particular I want to thank my office colleagues Dipl.-Ing. Philip Augener and Dr.-Ing. Hendrik Vorhölter for a great working atmosphere.

I am deeply thankful to Theresa for her never ending tremendous support, her patience and her extensive and very useful revisions. This thesis would not have been possible without you.

Finally I want to thank my parents Anke und Raimund who made all this possible with their versatile support during my years of studies and research work.

*We place absolute confidence in the Titanic. We believe that the boat is unsinkable.*

Philip Franklin, White Star Line Vice President on April 15th, 1912 at 8 a.m.
after he was informed that the Titanic was in trouble.

# Contents

# List of Figures

# List of Tables

# CHAPTER 1

# Introduction

The main objective of this thesis is the development of a fast, stable and reasonably accurate numerical simulation method to predict and revisit flooding scenarios in the time domain.

A comparison with the results of a standard benchmark model test and the re-investigation of the EUROPEAN GATEWAY, the HERAKLION and the ESTONIA accidents are performed for validation purposes. The aim of the presented method is to fill the gap between simple hydrostatic stability evaluations and more sophisticated but time consuming sea-keeping simulation methods.

The method is implemented in the ship design software environment E4, a first-principle ship design software used and developed at the Institute of Ship Design and Ship Safety of the Technical University of Hamburg together with partners from the German shipbuilding industry, among others the Flensburger Shipyard. This environment provides direct access to the complete ship data model and already implemented computational algorithms. A more detailed description of the coverage of the E4 software system can be found in Krüger et al. (1999) and Todd (2002).

## 1.1 Motivation

Damage stability calculations during the early design process are an essential indication of the ship's safety level to withstand any water ingress. Several accidents in the past have shown that it is very important to take into account critical intermediate stages of flooding, instead of only looking at the final stage of flooding in a damage case.

Uncertainties in the determination of critical failure modes in the case of a damaged ship are currently taken into account by including a sufficient safety reserve in the regulations. The shift from a deterministic to a probabilistic concept in current regulations provides a more advanced and rational approach in the assessment of the relevant damage cases. Risk-based methods are applied to judge upon the safety reserve of a ship in the case of damage to her watertight integrity. However, the main problem remains that the hydrostatic evaluation of each damage case relies mainly on the calculation of the final stage of flooding by the lost buoyancy method. The assessment of critical intermediate stages of flooding are only roughly described in the current

regulations, but the necessary treatment of the underlying physical concepts is not sufficiently explained.

In the scope of current regulations, the physical modelling of a damaged ship has not been improved, although the equivalent model test method of the Stockholm Agreement may be considered as a first step in introducing performance based standards in safety regulations.

Recently, there has been a shift from static assumptions to numerical flooding simulations in the time domain in the research community, which provide a better understanding of the physical behaviour of the ship during flooding. These numerical methods may be considered complementary to model tests. This work contributes to this attempt and presents a fast, explicit and stable numerical simulation of the continuous flooding development in the time domain.

## 1.2 Review of Previous Work

In the past, the flooding behaviour of ships after water ingress has been investigated in different ways. The first need to describe such events in a scientific and accurate manner arose after very severe ship accidents caused by the flooding of large open spaces happened and the existing models were no longer capable of describing the physical phenomena leading to these accidents.

In early investigations ,the timeline of events leading to the loss of a ship was evaluated manually by examining only a few intermediate stages of flooding. Parallel to this, numerical sea-keeping codes for the simulation of the ships motion in heavy weather conditions have advanced. Initially, these simulation codes were mainly intended for computing the motion of the intact ship in waves. In the nineties, extensive research has been carried out to model also the influence of entrapped flood water on the motion of the ship, which was typically done by describing the flood water behaviour by shallow water equations. However, these methods are limited to only a few compartments of simple geometry, since their focus were flooded vehicle decks on Ro-Ro ferries or entrapped water on the deck of fishing vessels.

The flooding of more complex compartment geometries with multiple external and internal openings has been introduced in the late nineties. Either existing sea-keeping codes have been extended by flooding models or newly developed methods were introduced. The latter was mainly motivated by the need to model the progressive flooding of large passenger ships. Currently, effort has been made to incorporate such time dependent flooding simulation methods into new regulations.

The International Maritime Organisation (IMO) started to deal with the aspect of large passenger ship safety (LPS) in 2001 on the 44th session of the Sub-Committee on Stability and Load Lines and on Fishing Vessels' Safety (SLF). To better characterise the survivability of a certain ship design, the *time-to-sink* term has been issued, which was changed to the expression *time-to-flood* on the following session. This development was followed by several research efforts of different groups, of which some will be described in more detail in the following. The 47th session in 2004 was the last SLF session, where this topic was on the agenda.

A valuable review about recent developments and trends in the assessment of damage stability of ships can be found in Papanikolaou (2007). A comprehensive study of previous work with respect to flooding simulations is also given in Ruponen (2007), Santos et al. (2009) and Khaddaj-Mallat (2010). An overview of software programs capable of the prediction of large-scale flooding following damage can be found in Konovessis (2006).

### 1.2.1 Numerical Codes

Examples of available numerical codes for the simulation of damaged ships in calm water or in the presence of waves are listed in the following, together with the main contributing institutes or companies. The list is sorted by the geographical location of the associated facilities from south to north and without any claim to be complete.

- CAPSIM developed at the Ship Design Laboratory (SDL) of the National Technical University of Athens (NTUA) in Greece.
- A Time domain flooding method developed at the Centre for Marine Technology and Engineering (CENTEC) of the Technical University of Lisbon, Portugal.
- FREDYN developed by the Maritime Research Institute Netherlands (MARIN) in Wageningen, Netherlands.
- ROLLS developed at the University of Technology, Hamburg (TUHH) and the Flensburger Shipbuilding Yard (FSG) in Germany.
- PROTEUS-3 by the team of the Ship Safety Research Centre (SSRC) associated with the University of Strathclyde, Glasgow in Scotland.
- SIMCAP developed at the department of Shipping and Marine Technology at Chalmers University of Technology, Gothenburg, Sweden.
- NAPA flooding module developed at the Helsinki University of Technology, Espoo, Finland.

All listed codes apply a hydraulic model based on the Bernoulli equation to compute the water flow through the openings. Further details of the codes are described in the following.

The CAPSIM software is a non-linear sea-keeping code, which includes the treatment of flooding through multiple openings. The theoretical foundations of this method have been first published in Zaraphonitis et al. (1997) and are further refined by Spanos (2002, in Greek only). The flood water is included in the determination of the vessels motion in irregular seas by the so-called lumped mass concept as described in Papanikolaou et al. (2000). A validation of this method by experiments has been for example carried out within the research projects NEREUS (Spanos and Papanikolaou, 2001) or SAFEDOR (Papanikolaou, 2009) and by various ITTC benchmark tests as summarised in Papanikolaou (2007).

Santos (1999) developed a numerical simulation method to address the physical phenomena of a flooded ship. He is currently working at the Centre for Marine Technology and Engineering (CENTEC) of the Technical University of Lisbon, Portugal. Santos has published several articles on this topic, for example on the experimental validation of his method together with an investigation of the European Gateway accident in Santos et al. (2002). Another publication (Santos et al., 2009) deals with the further validation of the developed method by applying it to the ITTC benchmark model test of a box-shaped barge.

The 24th ITTC Specialists Committee on Stability in Waves initiated three benchmark studies on the prediction of capsize of damaged ships in waves. The third part was conducted in 2006 (van Walree et al., 2007) and gives a good comparison and overview of several numerical codes feasible of simulating flooding events. It includes also some of the methods mentioned in this chapter. The model experiments described in this benchmark test will also serve as a validation of the new method presented in this thesis.

Over the past two decades, the FREDYN code has been developed at the Maritime Research Institute of the Netherlands (MARIN) mainly within the Cooperative Research Navies (CRNAV) project. The main objective of this software is the simulation of the non-linear motions of a manoeuvring naval vessel in waves. Its underlying theory is based on the work by de Kat (1988) and Hooft and Pieffers (1988), while a presentation of the FREDYN software itself can be found in de Kat et al. (1994). The extension by a flooding model together with an experimental validation can be found in van't Veer and de Kat (2000). The influence of entrapped air has been investigated by experiments and numerical simulations in Palazzi and de Kat (2004). An application on Large Passenger Ship survivability is published in van't Veer et al. (2004), where the focus is on the proper level of detail of the internal compartment layout and the influence of the water tightness of internal openings like doors.

The non-linear sea-keeping code ROLLS has initially be developed by Söding (1982) for the investigation of the E.L.M.A. Tres accident in 1981. The code has been further developed at the Institut für Schiffbau of the Universität Hamburg, Germany as described in the work of Kröger (1987) and Petey (1988). It determines the non-linear roll motion of ships in irregular waves combined with the equivalent wave concept by Grim (1961). Results for computing capsizing frequencies with this code have been presented by Söding and Tonguc (1986) and Petey (1990). The inclusion of flood water dynamics by applying shallow water equations to this problem is based on Dillingham (1981) and is described in further detail in Petey (1986). However, the inclusion of flood water is limited to a few additional tanks and leaks of rather simple geometry. The code focuses on a statistically appropriate simulation of the ship motions in irregular sea states.

The Ship Safety Research Center (SSRC) of the University of Strathclyde and the Safety at Sea consultant company use the damage stability code PROTEUS mainly for accident investigations, but also to determine the survivability of damaged ships in waves in a probabilistic manner. The method is based on Vassalos and Turan (1994) and Letizia (1996), while a summary of the applied model can also be found in Vassalos et al. (1998). The current version PROTEUS3 is based on the work of Jasionowski (2002). Several publications from different authors of this group followed, where a selection is given in the following.

A probabilistic model for the flood water ingress has been presented in Jasionowski et al. (2002). In Vassalos et al. (2004) the issue of the transient flooding of Large Passenger Ships is addressed by the numerical and experimental investigation of a verification study within the scope of the EUREKA project SAFENVSHIP.

In addition, the same group published a paper on how to derive data model information automatically from 2D drawings required for complex simulations such as evacuation or flooding methods (Majumder et al., 2005). Recently, special emphasis was put on the investigation of more complex and numerically intensive methods for modelling the flood water dynamics. A particle based approach is presented in Skaar et al. (2006), while a Volume-of-Fluid based CFD method is applied to the already mentioned ITTC benchmark test of a box-shaped barge in Strasser et al. (2009).

At the Chalmers University of Technology the SIMCAP code has been developed. A first and brief presentation of this code is given in Schreuder (2002), while its underlying theory is described in more detail in his master thesis (Schreuder, 2005). Each opening is discretised by several points with a prescribed area. The volume flux through the openings is determined by the sum over all fluxes through each point. Recently, this code has been coupled with structural Finite Element Analysis for the determination of the probability of survival of a Ro-Pax ferry after collision (Schreuder, 2011).

The latest development of a novel progressive flooding simulation method has been carried out by Pekka Ruponen and his team at the University of Helsinki. In his Ph.D. thesis (Ruponen, 2007) the underlying theory of the pressure-correction based numerical method is described, together with a detailed validation of this method by model test experiments published in Ruponen (2006). The initial main focus of this method is the flooding behaviour of a ship in calm water and not the sea-keeping behaviour of a damaged ship in waves. Further interesting aspects investigated with this method have recently been addressed in Ruponen (2009). These aspects are for example the influence of active counter actions after the damage occurred like the closure of watertight doors. Further validation of this method has been carried out by a comparison with a full-scale flooding test (Ruponen et al., 2010). The University of Helsinki and the NAPA company has actively participated in the EU project FLOODSTAND finished in 2012 (Jalonen et al., 2012). One particularly interesting aspect of this work is that the flooding method was developed in strong cooperation with one of the leading developers of ship design software, the NAPA company. The developed flooding module is now included in the current software release of the NAPA ship design software. Through this, flooding simulation methods are nowadays widely available in the naval architecture community. However, one important limitation of the NAPA flooding simulation model is that the impact of the seaway is only marginally taken into account.

The Korean Maritime & Ocean Engineering Research Institute (MOERI) carried out several experimental and numerical studies (Cho et al., 2010) to examine the flooding process of damaged ships in waves with its focus on cruise ships. This group also participated in the already mentioned ITTC benchmark study.

A quasi-static approach for flooding predictions in the time domain is also implemented in the Archimedes II program by Söding (2001) with its focus on the computation of cross-flooding times.

### 1.2.2 Accident Investigations

Probably the first application of a very simple hydraulic model in the investigation of a sinking sequence of a ship was done in the scope of the official S.S. Titanic accident investigation by Edward Wilding, one of the naval architects of Harland and Wolff, the yard which built the Titanic. This has been mentioned by Hackett and Bedford (1996), who reviewed the Titanic accident by the use of modern techniques. They also applied a hydraulic model in combination with a quasi-static calculation of the different intermediate stages of the sinking sequence. It is not clear whether or not their method has been further extended or applied to other cases as well.

The accident of the S.S. Heraklion in 1966 appears to be one of the first ferry accidents caused by water ingress on the vehicle deck. The investigations carried out directly after the accident did not involve any flooding simulation or motion analysis in natural seaways (Wendel, 1970). However, the recent review of this accident in Papanikolaou et al. (2012) used the NAPA flooding module to simulate the water ingress. The study from Krüger et al. (2012) applied the non-linear code ROLLS including the influence of water ingress and floodwater dynamics on the vehicle deck.

The next investigations to mention are the accidents of the European Gateway and the Herald of Free Enterprise. For this purpose, the British National Maritime Institute (NMI) developed a flooding simulation program called NMIFLOOD (NMI Ltd, 1983).

In recent years, further accident investigation have been performed, mainly to validate the developed numerical codes. The EXPRESS SAMINA accident has been investigated by Papanikolaou et al. (2003) and the method by Santos has been applied to study the EUROPEAN GATEWAY accident (Santos et al., 2002).

The very severe accident of the M.V. ESTONIA in 1994 has been investigated in the second instance by two consortia, one lead by the Swedish SSPA, the other one by the German HSVA. Following disputes about the first investigation lead to these additional studies. For the in-depth study of this accident, almost all numerical flooding simulation codes available at that time, have been used. The first consortium consisted of four partners: The University of Strathclyde applied the numerical code PROTEUS (Jasionowski and Vassalos, 2008), the Dutch model basin MARIN used FREDYN together with experiments to predict the flooding of Deck 4 (Carette et al., 2008) and the Chalmers University applied the SIMCAP code for the numerical simulations of foundering scenarios (Schreuder, 2008). The SSPA carried out manoeuvring tests and the final sea-keeping experiments (SSPA Consortium, 2008).

The second consortium lead by the HSVA used ROLLS to model the initial, transient phase of flooding (Valanto, 2009) and an quasi-hydrostatic approach for the later phase of the sinking sequence as described in detail in Kehren (2009).

# CHAPTER 2

# Theory and Basic Equations

Before investigating practical problems, the physical model together with the underlying basic equations and assumptions of the developed progressive flooding simulation method are described.

In general, the conservation principle of mass and momentum for the floodwater has to be fulfilled. The fluid flow for water and air is described by the Bernoulli equation, which can be obtained from the integration of the Euler equation along a streamline by applying the conservation of linear momentum. In addition, the equation of state is required for the description of the pressure density relation of the compressible air phase.

The conservation of mass is fulfilled by applying the continuity equation to each part of the flooding system as described in more detail in Subsection 3.1.1.

## 2.1 Basic Equations

Bernoulli's principle states that for an inviscid and stationary fluid flow, the overall mechanical energy composed of the pressure head and the kinetic and potential energy stays constant along a streamline. Formulated in head form, this is expressed by the following equation for the total head

$$\int_p \frac{1}{\rho\, g}\, \mathrm{d}p + \frac{u^2}{2\, g} + z - \frac{\varphi}{g} = const, \tag{2.1}$$

where $p$ is the fluid pressure, $\rho$ the fluid density, $g$ the gravitational constant, $u$ the fluid velocity and $z$ the level height. Any pressure losses are taken into account by the dissipative energy term $\varphi$ and are elaborately discussed in more detail in Section 2.4. This term will at first be neglected.

### 2.1.1 Equation of State

In addition, if the formation of entrapped air pockets is assumed to be relevant, the description of the flow dynamics in the compressible air phase requires at least one more basic equation. The equation of state of an ideal gas reads

$$p \cdot V = m \cdot R_s \cdot T, \tag{2.2}$$

where $R_s$ is the specific gas constant, $V$ the volume, $m$ the mass and $T$ the temperature of the gas in question. The assumed conditions of the ambient air phase, denoted by the index $e$ for environment, are summarised in Table 2.1. All other quantities like the air density $\rho_e$ are derived from these constants.

Table 2.1: Assumed parameters of the ambient air phase

| | | |
|---|---|---|
| Temperature | $T_e$ | 15 ° |
| Pressure | $p_e$ | 101325 Pa |
| Specific gas constant | $R_s$ | 287.058 $\frac{\mathrm{J}}{\mathrm{kg \cdot K}}$ |

For an isothermal process of a compressible ideal gas, the ratio of pressure and density is constant. As a result, the density of the air depends linearly on the pressure multiplied by the constant ratio of the air density $\rho_e$ at ambient pressure $p_e$ by

$$\frac{p}{\rho} = \frac{p_e}{\rho_e} = p \cdot \frac{V}{m} = R_s \cdot T = const, \tag{2.3}$$

$$\Rightarrow \rho = p \cdot \frac{\rho_e}{p_e}. \tag{2.4}$$

If the air flow velocities are neglected and only the pressure increase in air pockets is described, the mass is assumed to be constant as well, yielding in Boyle's law:

$$p \cdot V = m \cdot R_s \cdot T = const = p_0 \cdot V_0, \tag{2.5}$$

$$p = \frac{1}{V} \cdot p_0 \cdot V_0, \tag{2.6}$$

where $p_0$ and $V_0$ are a reference pressure and volume, respectively.

The air pressure $p$ inside a compartment is always taken as an over-pressure related to the environmental pressure $p_e$, because only the pressure differences of two compartments $p_a$ and $p_b$ are of importance to determine the fluid flux between these:

$$p = p_e + \tilde{p} \tag{2.7}$$

$$p_a - p_b = p_e + \tilde{p}_a - (p_e + \tilde{p}_b) = \tilde{p}_a - \tilde{p}_b. \tag{2.8}$$

This distinction is only relevant if air compression is taken into account, since the equation of state for an ideal gas is related to the absolute pressure.

### 2.1.2 Flow Description

The water flow through a small and deeply submerged opening connecting two compartments a and b (see Figure 2.1) is driven by the total head difference $\mathrm{d}H$ and can be formulated by

means of the Bernoulli equation for incompressible fluids

$$\mathrm{d}H = \frac{p_a - p_b}{\rho_w\, g} + \frac{u_a^2 - u_b^2}{2\, g} + z_a - z_b. \tag{2.9}$$

The squared velocities are typically small compared to the other terms and can therefore be neglected.

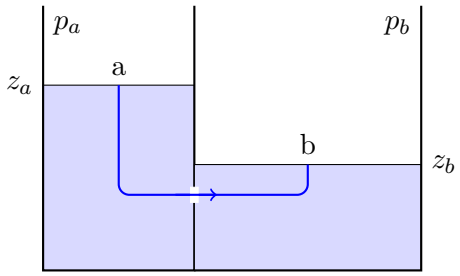


Figure 2.1: Water flow along a streamline between two compartments

The Bernoulli equation for a compressible air flow has the following form, which uses the additional relation for the air density from Equation 2.4:

$$\mathrm{d}H = \int_{p_a}^{p_b} \frac{1}{\rho\, g}\, \mathrm{d}p + \frac{u_a^2 - u_b^2}{2\, g} + z_a - z_b, \tag{2.10}$$

$$\int_a^b \frac{\mathrm{d}p}{\rho\, g} = \frac{p_e}{\rho_e\, g} \cdot \int_{p_a}^{p_b} \frac{1}{p}\, \mathrm{d}p = \frac{p_e}{\rho_e\, g} \cdot [\ln(p_b) - \ln(p_a)], \tag{2.11}$$

$$\Rightarrow \mathrm{d}H = \frac{p_e}{\rho_e\, g} \cdot \ln\left(\frac{p_b}{p_a}\right) + \frac{u_a^2 - u_b^2}{2\, g} + z_a - z_b. \tag{2.12}$$

For the air flow, only the differences in the air pressure are relevant, while the contributions of the other terms are negligible small.

For both cases of air (Equation 2.12) or water flow (Equation 2.9), the total head difference $\mathrm{d}H$ yields for the flow velocity of the fluid

$$u = \sqrt{2\, g \cdot \mathrm{d}H}. \tag{2.13}$$

The integration of the velocity over the area $A$ of the opening under the assumption of a flow direction that is perpendicular to the normal direction $\mathbf{n}$ of the opening leads to the total flux:

$$\dot{V} = \frac{\partial V}{\partial t} = Q = \int_A \mathbf{u} \cdot \mathrm{d}\mathbf{A} = \int_A \mathbf{u} \cdot \mathbf{n}\, \mathrm{d}A. \tag{2.14}$$

The dot product of an arbitrary vector with a perpendicular unit normal vector simply gives the magnitude of this vector, turning the vector integral into a one dimensional integral:

$$Q = \int_A \mathbf{u} \cdot \mathbf{n}\, \mathrm{d}A = \int_A u\, \mathrm{d}A \qquad \text{where} \quad u = |\mathbf{u}|. \tag{2.15}$$

## 2.2 Simple Test Cases

To illustrate the basic equations and the physics of the flow interchange between the compartments, three very simple generic cases are investigated as shown in Figure 2.2. For these cases it

is possible to find analytic solutions or at least stable numerical ones. This investigation is also used to study the influence of effects like air compression and air flow on critical aspects such as the time until the flooding is completed (time-to-flood), or the influence on the development of the water levels.

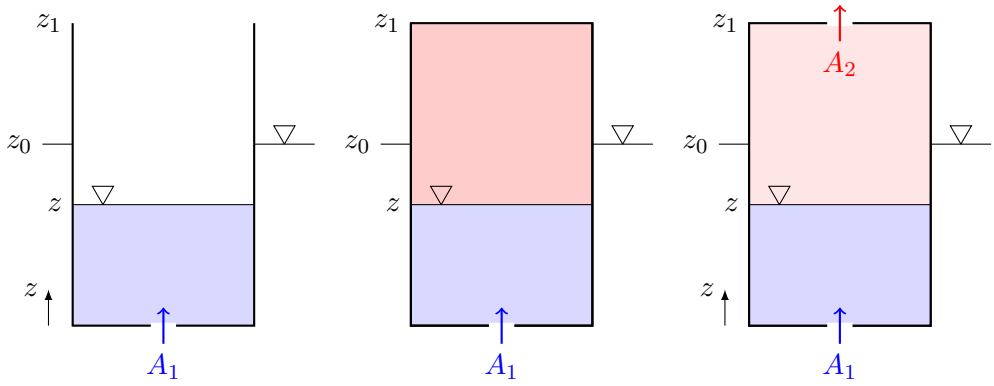


(a) Case 1 (b) Case 2 (c) Case 3

Figure 2.2: Test setup of three generic cases for water ingress with air compression and air escape

### 2.2.1 Simple Inflow

Test case 1 represents a simple inflow to a compartment from below without considering any influences of the air phase, see Figure 2.2a. The inflow velocity is only determined by the water height differences between the outside level $z_0$ and the water height $z$ inside the compartment, since the air pressure difference is zero and the influence of the water level velocity on the inflow velocity is assumed to be small. The interface kinematics are calculated with the help of the continuity equation, as the inflow flux $\dot{V}_w$ must be the same as the flux inside the compartment defined by the product of the water surface $S$ times the water level velocity $\dot{z}$. This gives the following relations:

$$u_w(t) = \sqrt{2\,g \cdot (z_0 - z(t))}, \tag{2.16}$$

$$\dot{V}_w(t) = u_w(t) \cdot A_1 = \dot{z}(t) \cdot S. \tag{2.17}$$

The resulting differential equation

$$\dot{z}(t) + a \cdot \sqrt{z_0 - z(t)} = 0 \qquad \text{with} \quad a = -\frac{A_1}{S}\sqrt{2\,g} \tag{2.18}$$

is of Bernoulli type for which the following analytic solution is found

$$z(t) = z_0 - \left[\frac{a}{2} \cdot (t + C_1)\right]^2, \tag{2.19}$$

where the integration constant is determined by the initial condition

$$z(t=0) = 0 = z_0 - \left[\frac{a}{2} \cdot C_1\right]^2, \tag{2.20}$$

$$\Rightarrow C_1 = \sqrt{z_0} \cdot \frac{2}{a}. \tag{2.21}$$

Inserting the integration constant gives a time dependent function of the water level, which is a quadratic polynomial with one maximum located at the final water level.

$$z(t) = z_0 - \left[\frac{a}{2} \cdot t + \sqrt{z_0}\right]^2, \tag{2.22}$$

$$\Rightarrow z(t) = -a \cdot t \left[\frac{a}{4} \cdot t + \sqrt{z_0}\right]. \tag{2.23}$$

The time-to-flood can be calculated by means of the final condition at $t_e$ using Equation 2.19. It is equal the negative integration constant:

$$z(t = t_e) = z_0 = z_0 - \left[\frac{a}{2} \cdot (t_e + C_1)\right]^2, \tag{2.24}$$

$$\Rightarrow t_e = -C_1. \tag{2.25}$$

### 2.2.2 Air Compression

For the second case 2, the compartment is assumed to be air-tight and air compression has to be taken into account, see also Figure 2.2b. Since no air flow occurs, the air mass stays constant, but the volume of the air pocket is reduced.

The resulting pressure increase has to be taken into account when calculating the inflow velocity by adding the air pressure differences to the Bernoulli equation

$$u_w(t) = \sqrt{2\,g \cdot (z_0 - z(t)) + \frac{1}{\rho_w} \cdot (p_e - p(t))}, \tag{2.26}$$

$$u_w(t) = \sqrt{2\,g} \cdot \sqrt{z_0 - z(t) + z_s \cdot \left(1 - \frac{p(t)}{p_e}\right)} \qquad \text{with} \quad z_s = \frac{p_e}{2\,g\,\rho_w}. \tag{2.27}$$

If the compartment is assumed to be filled with the air volume $V_{a,0} = V_0$ at the beginning, the pressure $p(t)$ is related to the filling level $z(t)$ according to Equation 2.6 as follows:

$$V_a(t) = V_0 - V_w(t) = S \cdot (z_1 - z(t)), \tag{2.28}$$

$$\frac{p(t)}{p_e} = \frac{V_{a,0}}{V_a} = \frac{z_1}{z_1 - z(t)}, \tag{2.29}$$

where $z_1$ is the total height of the compartment. This results in the following expression for the inflow velocity:

$$u_w(t) = \sqrt{2\,g} \cdot \sqrt{z_0 - z(t) \cdot \left(1 + \frac{z_s}{z_1 - z(t)}\right)}. \tag{2.30}$$

Together with the constant pressure height $z_s$ from Equation 2.27 and the constant term $a$ from Equation 2.18, this yields the following differential equation:

$$\dot{z}(t) + a \cdot \sqrt{z_0 - z(t) \cdot \left(1 + \frac{z_s}{z_1 - z(t)}\right)} = 0. \tag{2.31}$$

The final water level $z_e = z(t = t_e)$ is given by the condition that the inflow velocity becomes zero:

$$z_0 - z_e - z_e \cdot \frac{z_s}{z_1 - z_e} = 0, \tag{2.32}$$

$$z_e^2 - z_e \cdot (z_0 + z_1 + z_s) + z_0 \cdot z_1 = 0. \tag{2.33}$$

This quadratic equation leads to just one physically reasonable solution for the final water level $z_e$. The non-dimensional solution of this level $z_e$ is shown in Figure 2.3 as a function of the ratio of the total height of the compartment $z_1$ and the height of the outside water level $z_0$.

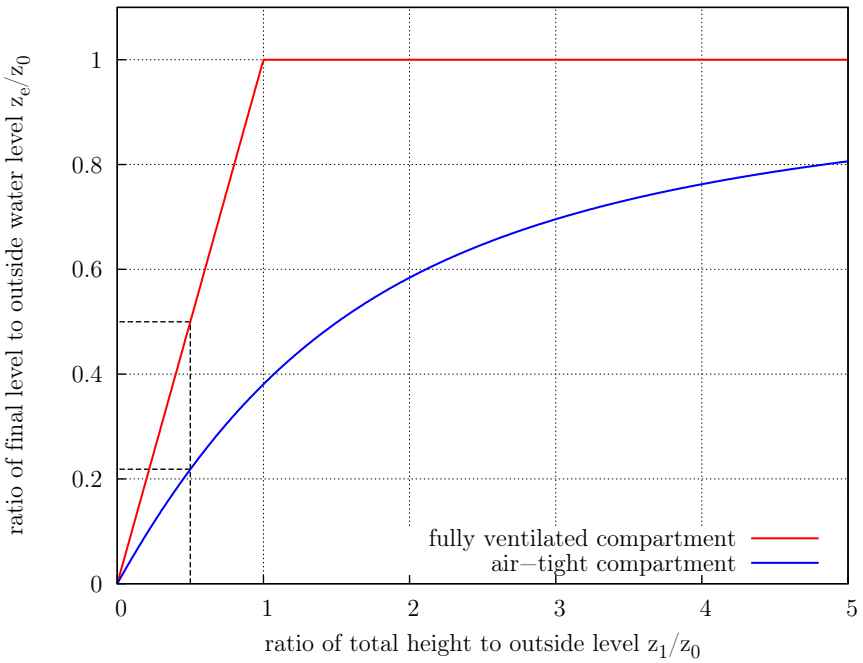


Figure 2.3: Non-dimensional final water level of a compartment subjected to water ingress as a function of the total height depending on the ventilation of the compartment

It is obvious that the difference in the final water level $z_e$ of an air-tight and a fully ventilated, non-air-tight compartment becomes smaller when the volume of the air pocket is relatively large compared to the total volume of the compartment. If the total height $z_1$ of the compartment is five times larger than the outside water level ($z_1/z_0 = 5$), approximately 80 percent of the outside water level is reached inside the air-tight compartment.

On the other hand, if the outside water level $z_0$ is above the total height $z_1$ of the compartment, resulting in ratios $z_1/z_0$ between 0 and 1, the influence is different: An outside water level two times larger than the total height ($z_1/z_0 = 0.5$) results in a final water level which is approximately 50 percent of the water level reached without air compression in a fully ventilated compartment, see also the dotted lines in Figure 2.3.

### 2.2.3 Ventilation

Another main influence on the water ingress is a possible ventilation capability of the compartment. In general, escape of air is also possible through openings which are not submerged completely at that moment, but it occurs mainly through ventilation pipes. The corresponding setup of case 3 is given in Figure 2.2c.

The escape of air mass from a compartment leads to a pressure *decrease*, while the air volume reduction caused by the water ingress comes with a pressure *increase*. The mass flux balance of the air flux through the opening $\dot{m}_k$ and the compartment air flux $\dot{m}_a$ lead to the following

equation:

$$\dot{m}_a(t) - \dot{m}_k(t) = 0 \qquad \text{with} \quad m_a(t) = \rho(t) \cdot V_a(t), \tag{2.34}$$

$$\Rightarrow \dot{\rho}_a(t) \cdot V_a(t) + \rho(t) \cdot \dot{V}_a(t) - \dot{m}_k(t) = 0. \tag{2.35}$$

The air mass flow $\dot{m}_k$ through the opening $k$ is given by the compressible Bernoulli equation according to Equation 2.12 neglecting minor terms

$$u_a(t) = \sqrt{2\,\frac{p_e}{\rho_e} \cdot \ln\left(\frac{p(t)}{p_e}\right)} = \sqrt{2\,\frac{p_e}{\rho_e} \cdot \ln\left(\frac{\rho(t)}{\rho_e}\right)}, \tag{2.36}$$

$$\dot{m}_k(t) = A_2 \cdot \rho(t) \cdot u_a(t). \tag{2.37}$$

Some of the entrapped air mass escapes at the same time when the air volume reduces. These are two developments, which lead to opposite changes in density (or pressure).

According to Equation 2.4, the ratio of pressure and density stays constant:

$$\frac{p(t)}{p_e} = \frac{\rho(t)}{\rho_e}. \tag{2.38}$$

The overall volume stays constant, meaning that the volume flux of air and water must be of the same amount. In addition, the air volume depends directly on the water level. The equation for the water flux is the same as in the air-tight compartment without air flow, but with the difference that the air pressure now depends on the air density:

$$\dot{V}_a(t) = -\dot{V}_w(t), \tag{2.39}$$

$$V_a(t) = S \cdot (z_1 - z(t)), \tag{2.40}$$

$$\dot{V}_w(t) = A_1 \cdot u_w(t) = A_1 \cdot \sqrt{2\,g} \cdot \sqrt{z_0 - z(t) + z_s \cdot \left(1 - \frac{\rho(t)}{\rho_e}\right)}. \tag{2.41}$$

This results in a system of two non-linear differential equations:

$$\dot{z}(t) + a \cdot \sqrt{z_0 - z(t) + z_s \cdot \left(1 - \frac{\rho(t)}{\rho_e}\right)} = 0, \tag{2.42}$$

$$\dot{\rho}(t) \cdot V_a(t) - \rho(t) \cdot \dot{V}_w(t) - \dot{m}_k(t) = 0. \tag{2.43}$$

Again, the solution for $z(t)$ and $\rho(t)$ can be found numerically. In this case, the final water level will be the same as in the first case of a fully ventilated compartment, but the time to reach this level will be longer.

### 2.2.4 Air Solubility

An additional effect that may have an influence on the water ingress is the solubility of air in water at high pressures, which can be modelled by Henry's law. This law states that the concentration $c$ of a solute air mass $m_{a,w}$ in a water volume $V_w$ is proportional to the pressure by a constant value, the so-called Henry's constant $k$

$$c = \frac{m_{a,w}}{V_w} = k \cdot p. \tag{2.44}$$

Taking into account the solubility, yields for the mass flux:

$$m_{a,w}(t) = k \cdot p(t) \cdot V_w(t), \tag{2.45}$$

$$\dot{m}_{a,w}(t) = k \cdot \frac{p_e}{\rho_e} \cdot (\rho(t) \cdot \dot{V}_w(t)), \tag{2.46}$$

$$\dot{m}_{a,w}(t) = k_0 \cdot (\dot{\rho}(t) \cdot V_w(t) + \rho \cdot \dot{V}_w(t)) \qquad \text{with} \quad k_0 = k \cdot \frac{p_e}{\rho_e}. \tag{2.47}$$

Integrating this in Equation 2.43 gives the following new differential equation for the air density:

$$\dot{\rho}(t) \cdot (V_a(t) - k_0 \cdot V_w(t)) - \rho(t) \cdot \dot{V}_w(t) \cdot (1 + k_0) - \dot{m}_k(t) = 0. \tag{2.48}$$

The air volume is reduced by the solute air in water and the water flux is increased by the solubility effect.

### 2.2.5 Sensitivity Analysis with Respect to Air Ventilation and Solubility

Even though, rather simple cases of the physical problem are considered until now, these already result in non-linear ordinary differential equations, which can hardly be solved analytically. In order to compare the different effects of air compression, air flow and air solubility, the equations are solved numerically with a standard Runge-Kutta scheme.

The selected parameters for the test setup as shown in Figure 2.2 are summarised in Table 2.2.

Table 2.2: Parameters for the sensitivity analysis

| | | |
|---|---|---|
| Outside water level | $z_0$ | 5.0 m |
| Initial water level | $z(t=0)$ | 0.0 m |
| Total height | $z_1$ | 8.0 m |
| Water surface area | $S$ | 1.0 $m^2$ |
| Opening area | $A_1$ | 0.1 $m^2$ |

The influence of the ventilation grade of a compartment on the development of the water levels is shown in Figure 2.4. In a fully ventilated compartment, the inside water level reaches the outside water level after around 10 seconds. Four different area ratios $\frac{A_1}{A_2}$ of the water inflow opening $A_1$ and the air outflow pipe area $A_2$ are investigated. The smaller the air pipe compared to the water inflow opening, the longer it takes to reach the final water level. If the compartment is completely air-tight, the final water level is around 50 percent of the one in a fully ventilated compartment.

This demonstrates that air compression can be neglected, if a large opening provides a sufficient degree of ventilation. A fully ventilated compartment can be assumed if the air pipe area is around 10 percent of the water inflow opening area. On the other hand, if the compartment is not sufficiently ventilated, entrapped air has an influence, at least on the flooding of the compartment where the air pocket is formed.

The influence of the solubility of air to water is shown in Figure 2.5. In this case the area ratio is $\frac{A_1}{A_2} = 200$. A quite high value of 5 percent solubility of air in water is chosen, which has only a small effect on the water level or on the air density. The solubility of air in water at atmospheric pressure is approximately 2 percent. For this reason, the effect of air solubility is neglected in the following.

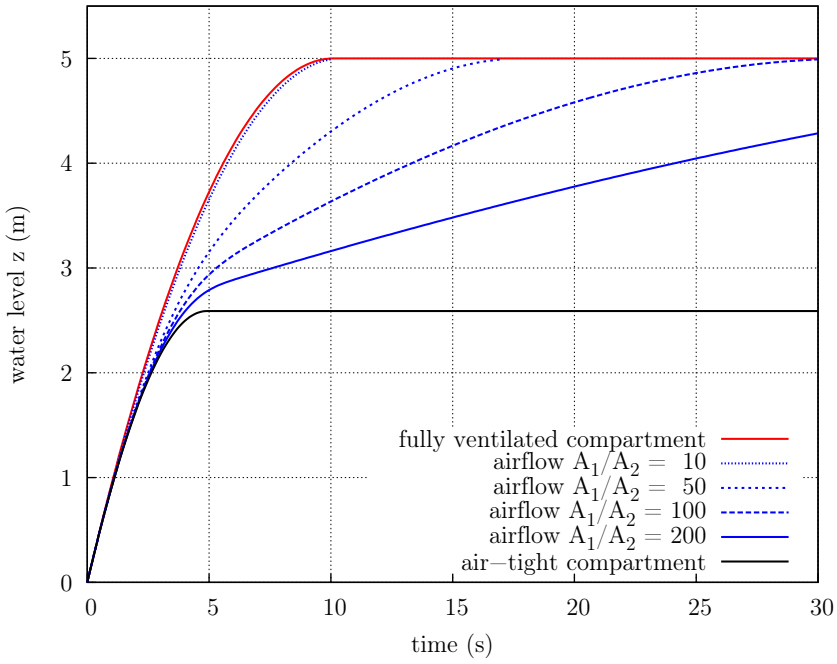


Figure 2.4: Water levels over time depending on the escape of air

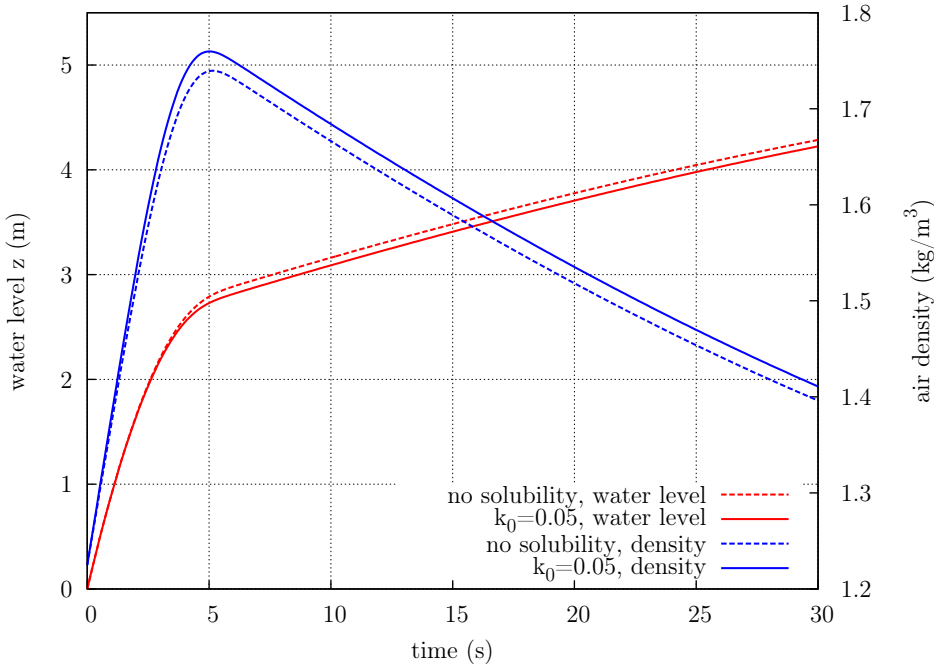


Figure 2.5: Comparison of water levels when taking into account air solubility with $k_0 = 0.05$ and $\frac{A_1}{A_2} = 200$

## 2.3 Opening Fluxes

The water flux through an opening depends on the size and the location of the opening and the surrounding water levels on both sides. It is useful to distinguish between different cases for which these parameters vary.

### 2.3.1 Small Openings

If the vertical extension of an opening is sufficiently small, it is reasonable to assume that the flux over the opening extension is constant. A water outflow discharge into air (Figure 2.6a)

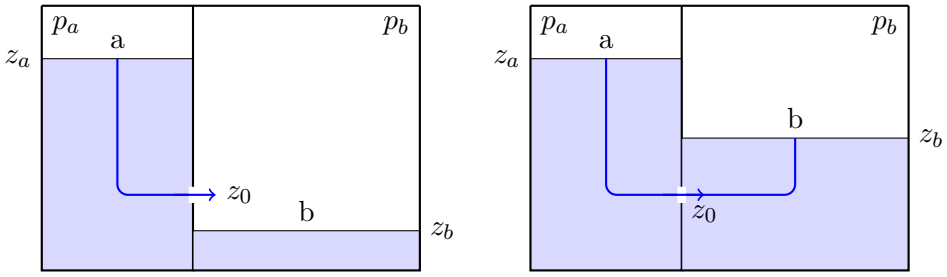


(a) Outflow into air (b) Deeply submerged opening

Figure 2.6: Outflow cases through a small opening

results in the following total head difference:

$$\mathrm{d}H = \frac{p_a - p_b}{\rho_w\, g} + \frac{u_a^2}{2\, g} + z_a - z_0. \tag{2.49}$$

By neglecting the water level velocity and assuming the same ambient air pressure ($p_a = p_b$) in the fully ventilated compartments, this simplifies to the so-called Torricelli theorem for the outflow velocity:

$$u = \sqrt{2\, g\, h} \qquad \text{with} \quad h = z_a - z_0. \tag{2.50}$$

The flux through a deeply submerged opening (Figure 2.6b) is independent of the location $z_0$ of the opening and given by the total head difference

$$\mathrm{d}H = \frac{p_a - p_b}{\rho_w\, g} + \frac{u_a^2 - u_b^2}{2\, g} + z_a - z_b, \tag{2.51}$$

yielding in the following formulation for the volume flux. Note that the formulation remains valid even if the flux direction changes, as the signum function returns 1 for positive and -1 for negative arguments:

$$Q = A \cdot u = A \cdot \mathrm{sign}(\mathrm{d}H) \cdot \sqrt{2\, g\, |\, \mathrm{d}H|}. \tag{2.52}$$

### 2.3.2 Large Openings

The determination of the flux through large openings is more challenging, since the cross section width and the fluid velocity may vary over the integration direction. In addition, the opening

can be oriented arbitrarily in space meaning that the integration direction for the opening area does not have to be the same as the earth fixed vertical direction. If any heel or trim movement occurs, which is usually the case, the opening moves out of its initial position and the orientation of the opening plane in space changes.

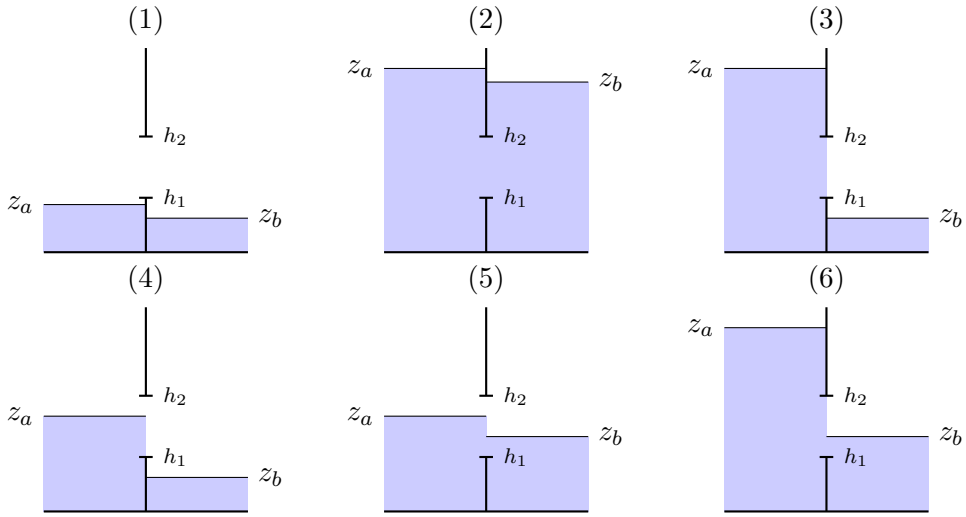


Figure 2.7: Submerging cases for large openings depending on the surrounding water levels

In Figure 2.7 the six possible combinations of water levels on both sides of an upright opening are given. However, in the sense of the fluid flow physics, only two different cases have to be distinguished. It is either a region of

- free outflow or
- deeply submerged flow.

All other cases can be developed from these elementary cases by superposition, if the opening flux determination is split into regions. For example, case 5 is a superposition of a free outflow from $z_a$ to $z_b$ and a deeply submerged flow from $z_b$ to $h_1$.

#### Simplifications for Large Openings

The flux determination through large openings simplifies for two cases:

1. small or zero vertical extension,
2. deeply submerged region.

If the vertical extension is small, the velocity is constant over the area of the opening. The flux through a deeply submerged region depends only on the water levels on both side, but not on the position of the opening itself.

A large opening has only theoretically a small or even vanishing vertical extension. For example staircases connecting decks or manholes are such openings, but only if the ship floats without any heel or trim. On the other hand, some parts of large openings are often submerged from both sides leading to deeply submerged flows in these regions. In this case Equation 2.51 applies

for the flow velocity $u$ and the volume flux in this region is given by

$$Q_s = A_s \cdot u, \tag{2.53}$$

where $A_s$ is the area of the deeply submerged part of the opening and $Q_s$ the corresponding volume flux through this part.

### Free Outflow

Only in the case of a free water outflow, the flux through the opening depends on the shape and location of the opening. In order to model any kind of opening shape, it is described as a planar polygon oriented arbitrarily in space.

For the flux integration, the opening is discretised in several z-stripes. This is required, because the velocity function is best described in the earth fixed vertical direction $z$, whereas the function of the opening area is best described in the direction $s$ lying in the polygon plane (see Figure 2.8).

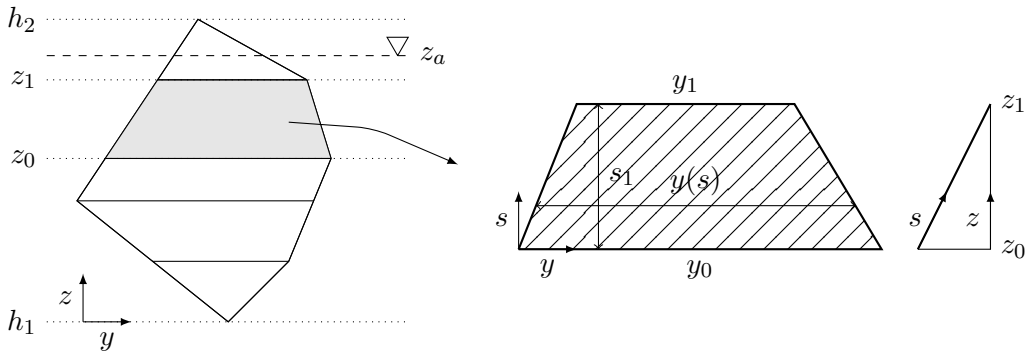


Figure 2.8: Arbitrary polygon and one stripe in z-direction

The relation between the earth fixed vertical direction $z$ and the integration direction $s$ is as follows:

$$z(s) = z_0 + s_z \cdot s \quad \text{with} \quad s_z = \frac{z_1 - z_0}{s_1} \quad \text{and} \quad s \in [0, s_1], \tag{2.54}$$

$$s(z) = \frac{z - z_0}{s_z} = \frac{z - z_0}{z_1 - z_0} \cdot s_1. \tag{2.55}$$

The width $y$ is a linear function of $s$:

$$y(s) = y_0 + s \cdot \frac{y_1 - y_0}{s_1}, \tag{2.56}$$

and the velocity function for the free outflow is given by:

$$u(z) = \sqrt{2\,g} \cdot \sqrt{z_a - z(s) + \alpha} \qquad \text{with} \quad \alpha = \frac{p_a}{\rho\,g} - \frac{p_b}{\rho\,g} + \frac{u_a^2}{2\,g}, \tag{2.57}$$

$$u(s) = \sqrt{2\,g} \cdot \sqrt{z_a - (z_0 + s_z \cdot s) + \alpha} = \sqrt{2\,g} \cdot \sqrt{h(s)}. \tag{2.58}$$

The constant factor $\alpha$ summarises all terms that are independent of $z$. The flux through one stripe is given by the integral

$$Q = \int_A u \,\mathrm{d}A = \int_s \int_y u(s) \,\mathrm{d}y \,\mathrm{d}s = \int_0^{s_1} u(s) \cdot y(s) \,\mathrm{d}s. \tag{2.59}$$

Inserting the velocity and width function and solving the definite integral (see Section 8.2 for details) gives the following flux value for one stripe:

$$Q = -\frac{2}{3\,s_z} \cdot \sqrt{2\,g} \cdot \left[ y_1 \cdot h_1^{\frac{3}{2}} - y_0 \cdot h_0^{\frac{3}{2}} + \frac{2\,(y_1 - y_0)}{5\,(z_1 - z_0)} \cdot (h_1^{\frac{5}{2}} - h_0^{\frac{5}{2}}) \right] \tag{2.60}$$

with

$$h_1 = h(s_1) = z_a - z_1 + \alpha \quad \text{and} \quad h_0 = h(0) = z_a - z_0 + \alpha.$$

This expression in Equation 2.60 is the more general formulation of the hydraulic models applied for example by Hutchison (1995) or Pawlowski (2003) for the determination of the accumulation of water on the vehicle deck of a damaged Ro-Ro vessel. These studies assumed upright openings of a constant width.

The flux through a rectangular weir is also given in Schröder and Zanke (2003):

$$Q = \frac{2}{3}\,B\,\sqrt{2\,g}\,h^{\frac{3}{2}}. \tag{2.61}$$

This is a rather simple case with a constant width $B = y_0 = y_1$ of an upright cross section ($s_z = 1$), no pressure difference ($\alpha = 0$) and the heights $h_0 = h = z_a - z_0$ and $h_1 = 0$. Applying these simplifications to Equation 2.60 results in the same formulation:

$$Q = -\frac{2}{3}\,B\,\sqrt{2\,g}\,(0 - B \cdot h_0^{\frac{3}{2}} + 0) = \frac{2}{3}\,B\,\sqrt{2\,g}\,h^{\frac{3}{2}}. \tag{2.62}$$

#### Correction for arbitrary orientation

The factor $s_z$ is determined by elementary geometric and trigonometric relations. As shown in Figure 2.9, the following relations hold:

$$s_z = \frac{z_1 - z_0}{s_1} = \frac{\mathrm{d}z}{s_1} = \cos\beta, \tag{2.63}$$

$$s_z = \cos\beta = \sin\alpha = |\mathbf{n}_p \times \mathbf{n}_w| \qquad \text{with} \quad \beta = 90^\circ - \alpha. \tag{2.64}$$

The required ratio $s_z$ can be computed directly from the current water plane normal vector $\mathbf{n}_w$ and the direction normal vector $\mathbf{n}_p$ of the opening. The length $s_1$ is not required and any trigonometric function evaluation is avoided.

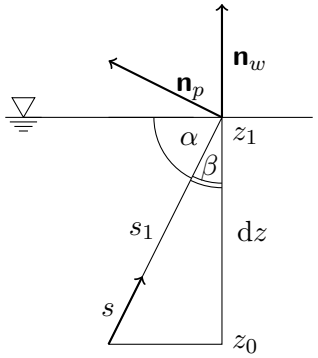


Figure 2.9: Correction factor $s$ for the arbitrary orientation of the opening

### Further Extensions

Large openings in regions of high curvature of the hull surface can be well approximated by two or three openings like the ones sketched above, even though in most cases the real shape of the damage opening is not exactly known. In addition, the same concept as sketched above may also be used to derive equations for other elementary opening shapes like triangles, circles or ship specific types like manholes.

Another influence might occur if the difference between the water levels is very large. The real shape of the fluid flow will differ from the assumed one, since the water surface will certainly not have a sharp discontinuity over the opening. The solution of the classical dam-break problem as described for example in Chanson (2005) or van't Veer and Zuidscherwoude (2012) is one possibility to better take into account the influence of the real shape of the water surface through the opening. A simple smoothing model for the mean water level is given in the appendix in Section 8.3. On the other hand, the phase where a very large difference in the water levels occurs, belongs typically to the short transient phase of flooding right at the beginning of the water ingress.

## 2.4 Modelling of Pressure Losses

Any obstruction of a fluid flow pattern like the flow through an opening leads to a certain loss in energy. The flow through two manholes is illustrated in two photos (see Figure 2.10), which were taken during the model experiments reported by Stening (2010) in the scope of the FLOODSTAND project.

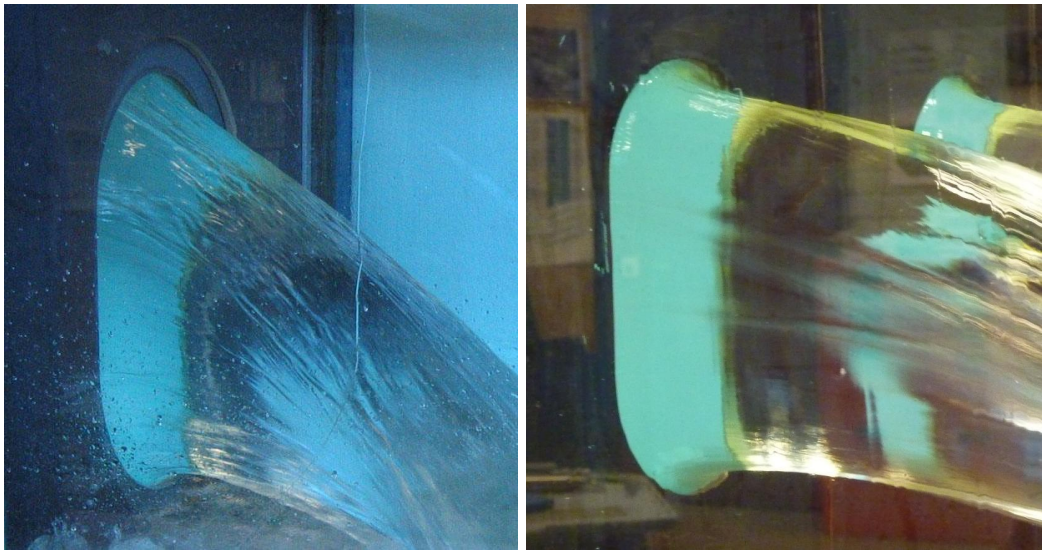

Figure 2.10: Contracted flow behind a manhole (Stening, 2010)

The loss is mainly caused by the flow expansion behind the opening and to a small degree by viscous effects. To be more specific, during the flow contraction no significant energy loss occurs, only a flow expansion leads to a larger and permanent energy loss (Stichlmaier, 2006). This is also the reason why the energy losses are in general higher through pipes compared to plates, since the flow through pipes consist usually of two expansion phases, one inside the pipe after the entrance and one after the flow leaves the pipe again.

The pressure losses over simple openings and through complex pipe systems are modelled by a dissipative energy term $\varphi_{ab}$, which is added to the basic Bernoulli equation. The dissipation is always positive since a streamline always looses energy from $a$ to $b$. For simple cross sections, the dissipative energy head amount $H_\varphi$ is assumed to be proportional to the pressure loss coefficient $k$ and the kinetic energy determined by the square of the actual velocity $\tilde{u}$:

$$H_\varphi = k \cdot \frac{\tilde{u}^2}{2\,g}. \tag{2.65}$$

To illustrate the relations, two consecutive pressure head losses $H_1$ and $H_2$ along the streamline of interest are considered. To determine the actual velocity $\tilde{u}$, the pressure head losses have to be added, while the ideal velocity $u$ is only influenced by the total head difference $\mathrm{d}H$. Together with Equation 2.65 this results in the following:

$$\tilde{u}^2 = 2\,g \cdot (\,\mathrm{d}H - (H_1 + H_2)), \tag{2.66}$$

$$u^2 = 2\,g \cdot \,\mathrm{d}H, \tag{2.67}$$

$$u^2 = \tilde{u}^2 \cdot (1 + k_1 + k_2). \tag{2.68}$$

In general, the relationship between the actual velocity $\tilde{u}$ and the ideal velocity $u$ through the opening is as follows:

$$\tilde{u} = u \cdot \frac{1}{\sqrt{1 + \sum k_i}} = u \cdot F. \tag{2.69}$$

The ratio $F$, also denoted as $C_d$, is the discharge coefficient or speed reduction factor. Values for this coefficient can be found in the literature (VDI-Gesellschaft, 2006), but may also be directly obtained by model experiments (Stichlmaier, 2006; Stening, 2010) or CFD analyses (Pittaluga and Giannini, 2006; Visonneau et al., 2010).

The relationship between the discharge coefficient $F$ and the sum $K = \sum k_i$ of the pressure loss coefficients is:

$$F = \frac{1}{\sqrt{1 + K}}, \tag{2.70}$$

$$K = \frac{1}{F^2} - 1. \tag{2.71}$$

A plot of the function $F(K)$ is shown in Figure 2.11. A typical value of $F = 0.6$ amounts to $K = 1.\bar{7}$.

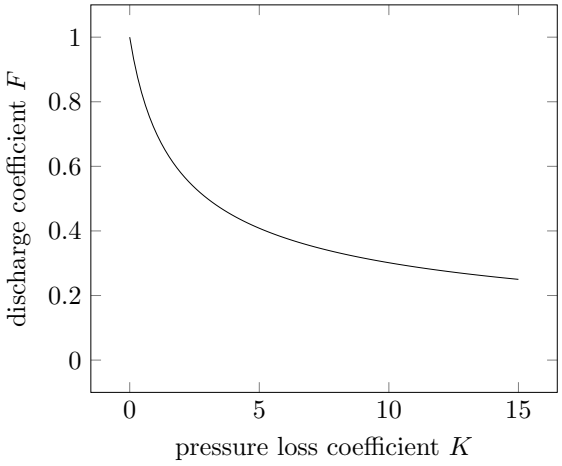


Figure 2.11: Relation between discharge and pressure loss coefficient

The IMO resolution MSC.245(83) for cross-flooding arrangements (IMO, 2007) also contains several empirical values of $k$ for different kinds of openings. It further says in the resolution, that the total speed reduction factor $F$ is obtained by the sum over all parts of the equalisation device:

$$F = \frac{1}{\sqrt{\sum k_i}}. \tag{2.72}$$

It is further stated, that to each system a pipe outlet component with $k_0 = 1$ has to be added to the sum. The old IMO recommendation for cross-flooding arrangements (IMO, 1973) states a different formula, which already includes the pipe outlet component for the system:

$$F = \frac{1}{\sqrt{1 + \sum k_i}}. \tag{2.73}$$

The pipe outlet value of 1 is not related to an actual real pipe outlet, this is probably only a practical explanation. Even if only one manhole is present, which is equivalent to the flow through an orifice without a pipe outlet, the summand 1 has to be included, as was shown clearly in the derivation of the formula for the speed reduction factor (see Equation 2.66 to 2.69). The misleading description of this summand 1 in the IMO resolutions is also discussed by Söding (2002b).

If it is assumed that the total pressure loss of a series of $n$ openings may be extrapolated from the discharge coefficient $f_1$ of a single opening, the overall discharge coefficient $F$ of the system can be calculated as follows:

$$k_1 = \frac{1}{f_1^2} - 1, \tag{2.74}$$

$$F = \frac{1}{\sqrt{1 + n \cdot k_1}} = \frac{1}{\sqrt{1 + n \cdot (\frac{1}{f_1^2} - 1)}}. \tag{2.75}$$

This is only valid if no interaction regarding the pressures losses between a series of manholes in a cross-flooding duct is assumed. For a more detailed analysis of especially cross-flooding ducts, experimental results for the pressure loss coefficients are available in Stening (2010). The main lack in the available experimental data is that the influence of the ship motion has not been investigated in sufficient details. The flow pattern through a door and thus the pressure losses will certainly be different at a heel angle of for example 30 degrees.

Scale effects might be considered if the discharge coefficients are obtained by model tests. However, no influence of the scale on the non-dimensional coefficients is present if the flow pattern can be assumed to be similar in model and full scale, i.e. dynamic similarity is given according to Walshaw and Jobson (1979, pages 251-256).

# CHAPTER 3

# Flooding of Complex Ship Compartmentations

This chapter describes the development of a numerical flooding method for ships and other floating objects based on the equations described in the previous chapter. Important implementation aspects are elaborated in detail. Moreover, the special requirements arising from complex compartmentations and typical opening properties on board of ships are emphasised. In addition, aspects like the treatment of entrapped air or the propagation through completely flooded compartments are described. The chapter concludes with an overview of the developed simulation model.

## 3.1 Flooding Paths

The connections between compartments of the ship by openings can be modelled by directed graphs. A simple example is shown in Figure 3.1, which describes the validation case B from Ruponen (2007).

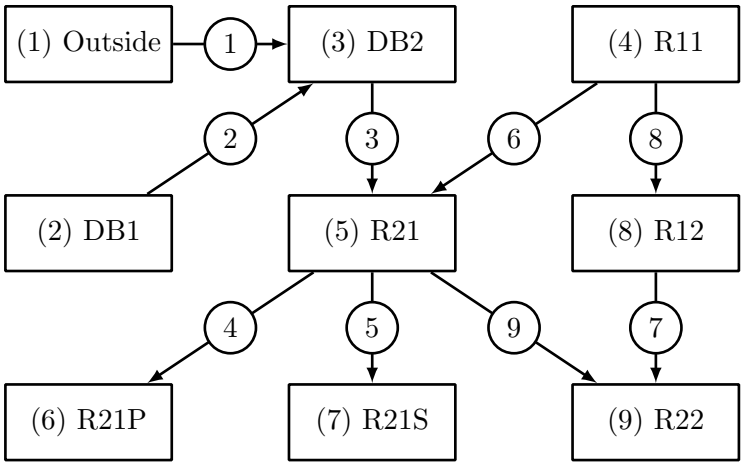


Figure 3.1: Graph of a simple subdivision model

The corresponding subdivision of the ship model is shown in Figure 3.2. Further details of this model test of a box-shaped barge will be described in Chapter 4.

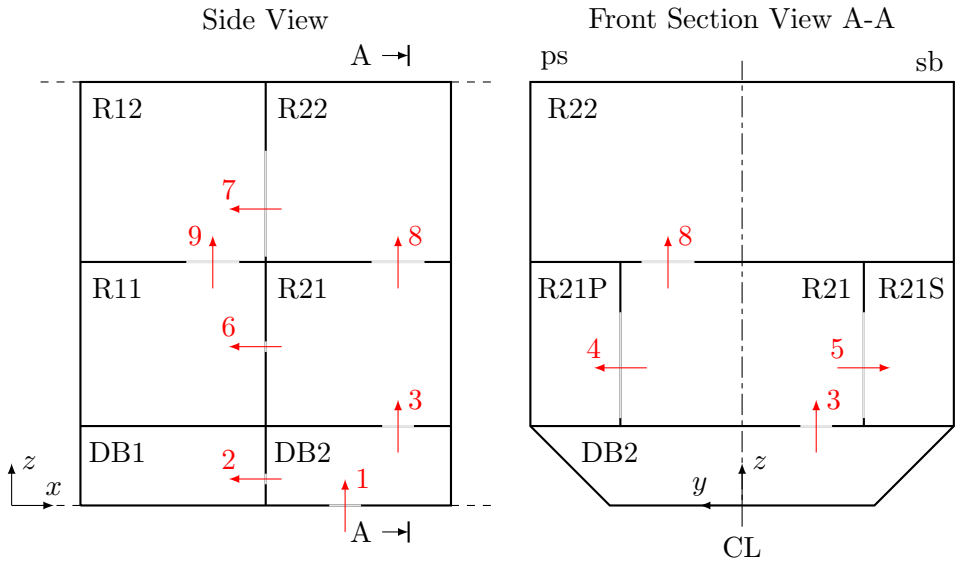


Figure 3.2: Geometry of the simple subdivision model

The graph is defined by nodes representing the compartments and edges representing the openings between the neighbouring compartments. Each node is defined by a unique ID and its name. As a sign convention, the positive direction of an edge is from a node with a lower to a node with a higher ID. This definition is required to have an initial sign direction, but gives no information about the actual flooding direction.

Using this kind of representation for the flooding paths is a very convenient and direct way. All methods and algorithms developed in the general graph theory (see for example Diestel, 2010) can be applied to flooding paths of ships if the required assumptions hold. This way information on for example the neighbours of the compartment in question or the number of independent flooding graphs can be obtained.

Moreover, the flooding graph serves to better illustrate the results of a flooding simulation. The total water volume passed through these edges or nodes of the graph can be calculated by integrating the flux over time for each element and helps to identify the most critical openings and compartments.

### 3.1.1 Mass Balance

The total flux of one compartment is given by the sum over all openings belonging to this compartment. For example, the flux $Q_{o5}$ for the compartment R21 with ID 5 equals the sum over all fluxes $q_k$ through the openings connected to this compartment (see Figure 3.1):

$$Q_{o5} = q_3 - q_4 - q_5 + q_6 - q_9.$$

The time integration of the flux to one compartment gives the amount of water transported in a certain time interval to one compartment from its neighbour(s):

$$\mathrm{d}V(t) = \int_{t_1}^{t_2} Q_o(t)\,\mathrm{d}t. \tag{3.1}$$

The change of water volume leads to new filling levels in the corresponding compartments. The determination of these new filling levels have to be done iterative, because the geometries of the compartments are usually of complex shape.

The filling level depends on the inclination of the waterline (i.e. the current trim and heel angle) and the fluid volume in the compartment. This relation can usually not be given analytically, especially if the ship moves. An example for the dependency of the water volume on the water level and the heel angle is shown in Figure 3.3, where this relation is drawn for a typical Ro-Ro cargo deck compartment for four different heel angles. The hydrostatic model of the compartment together with the water plane of an example filling is shown in Figure 3.4.

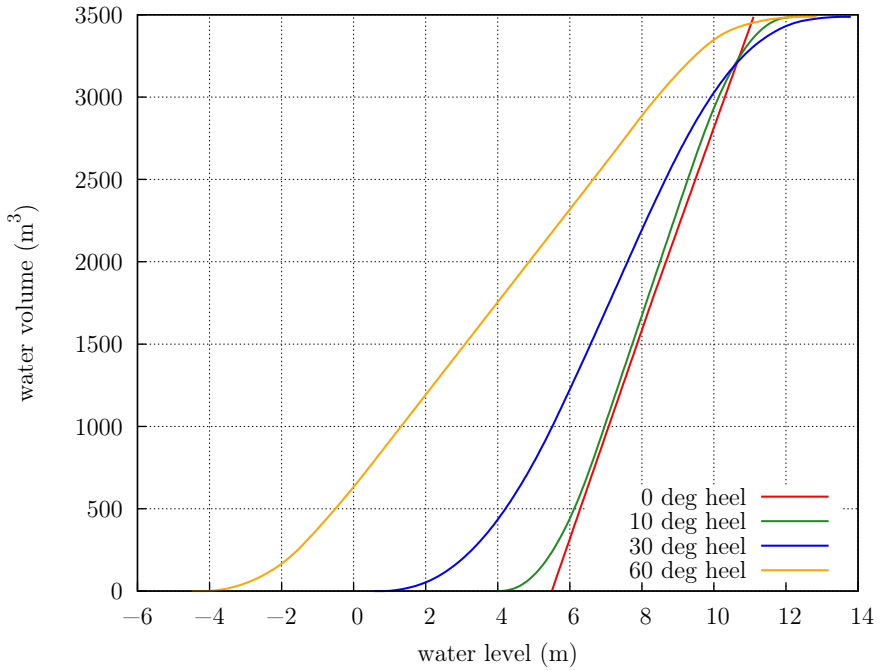


Figure 3.3: Water volume of a Ro-Ro cargo deck compartment depending on the water level and the heeling angle

To correctly determine the water level of a completely filled or empty compartment, it is crucial to accurately resolve the tails of the volume function over the water level. In addition, the gradient of the volume function, i.e. the current water plane surface, may include discontinuities if parts of the compartment does not extend over the whole height of the compartment.

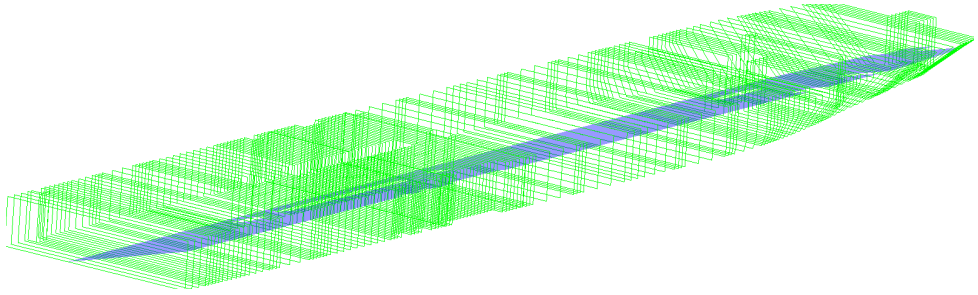

Figure 3.4: Computational model of a partly flooded Ro-Ro cargo deck

## 3.2 Flux Integration Scheme

The system of ordinary differential equations which has to be solved is of first order and non-linear. The volume flux $\dot{V}$ to one compartment must equal the sum of the fluxes $Q_o$ through all openings of the compartment. In addition, the fluxes through the openings depend non-linearly on the water heights $z(t)$, which again depend on the water volumes in each compartment:

$$\dot{V}(t) = Q_o(t) = f[z(t)] = f[V(t)]. \tag{3.2}$$

By using an explicit Euler forward scheme while assuming a constant flux for the non-linear function $f[t]$ during one time step $\mathrm{d}t$, the compartments are decoupled. The flux depends only on the water heights (or volumes) at the last time step $t_0$

$$\mathrm{d}V_0 = V(t_1) - V(t_0) = \mathrm{d}t \cdot Q_o(t_0). \tag{3.3}$$

To better account for the non-linearity and the coupling of the compartments, a weighted predictor-corrector scheme for the fluxes through the openings is used:

$$\mathrm{d}V_c = \mathrm{d}t \cdot (\omega \cdot Q_o(t_p) + (1-\omega) \cdot Q_o^*(t_0)), \tag{3.4}$$

$$\mathrm{d}V_c = \omega \cdot \mathrm{d}V_p + (1-\omega) \cdot \mathrm{d}V_0. \tag{3.5}$$

where $Q_o^*(t_1)$ is the flux after the prediction step at $t_1$ and $\omega$ is the relaxation factor. This integration scheme is illustrated graphically in Figure 3.5 and can be sketched as follows:

1. Predict opening fluxes $Q_o(t_0)$
2. Propagate predicted volume differences $\mathrm{d}V_0 = \mathrm{d}t \cdot Q_o(t_0)$ assuming a constant flux
3. Calculate new filling levels according to the predicted volumes $V^*(t_1) = V(t_0) + \mathrm{d}V_0$
4. Compute opening fluxes $Q_o^*(t_1)$ and the corresponding volume differences $\mathrm{d}V_p = \mathrm{d}t \cdot Q_o^*(t_1)$ based on the new filling levels
5. Reset volumes and propagate average volume differences $\mathrm{d}V_c$ according to Equation 3.4 to obtain the corrected volumes $V(t_1) = V(t_0) + \mathrm{d}V_c$
6. Calculate filling levels according to the corrected volumes $V(t_1)$ and proceed

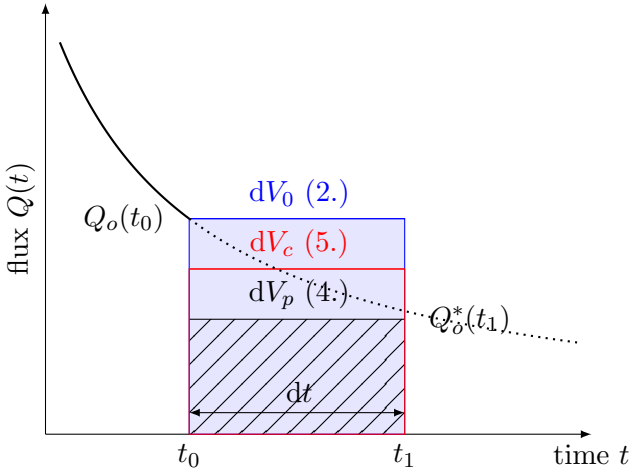


Figure 3.5: Flux predictor-corrector integration scheme for $\omega = 0.5$

The Euler forward scheme with an assumed constant flux over one time step can lead to fluctuations of the filling levels, caused by a change in the flux direction. This occurs, if the filling levels of two neighbouring compartments are very close and the assumption of a constant flux leads to the reversing of the compartment with the higher filling level to the compartment with the lower filling level in the propagated volumes and vice verse. How often this numerical phenomenon of overflowing occurs, depends on the length of the time step and the size of the opening. Even for a very small time step, the flux only becomes zero if the extrapolated volume change leads to exactly equal filling levels of neighbouring compartments in the next time step. The weighted predictor-corrector scheme smooths the flux by also using the flux values based on the predicted filling levels. This reduces the fluctuations of the flux and substantially stabilises the whole simulation.

## 3.3 Pressure Propagation through Full Compartments

If one or more neighbouring compartments become completely filled with water and the compartments are assumed to be fully ventilated, the corresponding compartments are directly coupled. The following conditions apply in this situation:

- The total flux of a full compartment must be zero.
- The water flux from partly filled compartments must be propagated through these full compartments.
- The only free variable remaining is the pressure in the completely flooded compartment.

These conditions lead to a non-linear system of equations, which must be solved to find the unknown pressure values. The system can be determined by constructing a sub-graph of all connected and fully flooded compartments.

Again, we consider an example of the flooding paths from the model tests illustrated in Figure 3.2. The DB2 compartment is assumed to be completely filled with water. In this case, the water coming from outside must be propagated through DB2 to the neighbouring compartments. All openings connected to DB2 are completely submerged at that point. The total flux to DB2 must be zero, which leads to the following conservation equation:

$$
\begin{aligned}
Q &= q_1 + q_2 + q_3, && (3.6)\\
&= A_1 \cdot \sqrt{\rho\, g \cdot (z_1 - z_3) + p_1 - p_3} \\
&\quad - A_2 \cdot \sqrt{\rho\, g \cdot (z_2 - z_3) + p_2 - p_3} \\
&\quad - A_3 \cdot \sqrt{\rho\, g \cdot (z_3 - z_5) + p_3 - p_5} = f(p_3) = 0. && (3.7)
\end{aligned}
$$

The dependency of $q_1, q_2$ and $q_3$ on the unknown pressure value $p_3$ together with the overall flux $Q$ is shown in Figure 3.6. Appropriate values for the opening areas and water levels are used.

This non-linear equation has to be solved for the unknown pressure value $p_3$. An analytic solution can only be found for less than three openings connecting to a completely filled compartment. However, the resulting non-linear system is usually not very large, since the number of equations is equal to the number of neighbouring, full compartments. This system can be solved with standard iterative algorithms like Powell's method described in Moré et al. (1980).

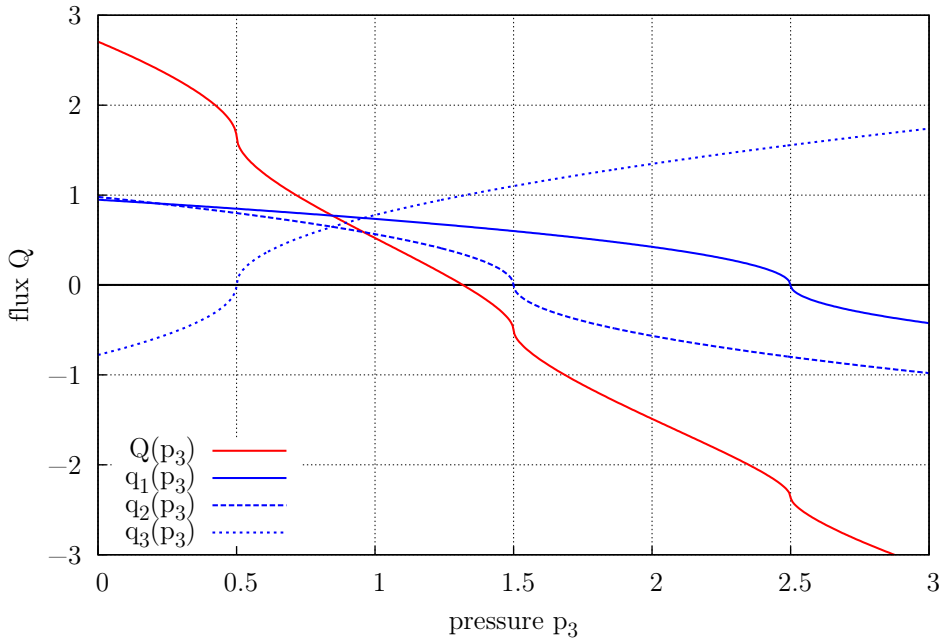


Figure 3.6: Volume fluxes depending on the internal pressure for a completely filled compartment

## 3.4 Conditional Openings

During the flooding process the conditions of openings can vary: Windows can break at a certain pressure height or internal doors can start to leak before they break completely. In addition, it is important to incorporate a time dependency to model the closure (or opening) of watertight doors, because these might not have been closed immediately at the beginning of the flooding process after the damage to the ship occurred.

### 3.4.1 Collapsing and Leakage

To model breaking doors or windows during the flooding process, a pressure head criterion is used for such openings. If the height of the water column $h_c$ above the lowest edge of the opening becomes larger than a predefined value, the opening breaks and stays open. The leakage of doors, which can already occur at relatively low pressure heads $h_l$, can be described by a discharge coefficient depending on the current pressure head $h_e$.

The pressure head dependency of doors and windows on ships has recently been studied for the first time in larger detail by the FLOODSTAND project in experimental and computational studies. The results are published in the corresponding project deliverable in Jakubowski and Bieniek (2010); Ruponen and Routi (2011). Examples for the leakage and structural failure of different door types from these model tests are shown in Figure 3.7.


Figure 3.7: Photos of the leakage and structural failure of semi-watertight doors during model tests (Ruponen and Routi, 2011)

The categories of water tightness for doors can be found in IMO SLF 47/INF.6 (2004), where it is also proposed to model the pressure head dependency of the watertight integrity of openings by a set of three parameters: The collapsing pressure height $h_c$, the height at which leakage starts $h_l$ and the area ratio $A_r = A_l/A_c$ between the leakage area and the submerged area of the opening, where the ratio may depend on the effective pressure head $h_e$, see also Figure 3.8.

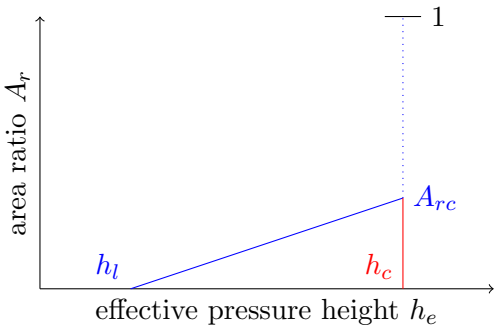


Figure 3.8: Example for the dependency of the area ratio on the pressure head

From the experiments performed by Jakubowski and Bieniek (2010) it has been observed that the area ratio $A_r$ is either constant or linear dependent on the effective water height above the lower edge of the opening. The maximum leakage before collapsing is usually in the range of 2 to 5 percent of the volume flux through the open door, depending on the type of door and the flow direction. If doors or windows start to leak before they collapse, which is the case for most non-watertight structures, this leakage occurs already at the very beginning when the water column height is still low.

In the present method, a collapsing condition represented by the maximum allowable pressure height $h_c$ is included. The leakage behaviour can be modelled by defining a constant maximum area ratio $A_{rc}$, assuming that the leakage starts already at zero pressure height ($h_l = 0$) and that the area ratio varies linearly until the collapsing of the structure.

### 3.4.2 Closure of Doors

A time dependent closure (or opening) of, for example, watertight doors can be modelled by a time-dependent discharge coefficient function. This function is defined by a start time of the closure and an end time when the door is assumed to be completely closed. In between, a linear variation is chosen. This condition can be used to study the influence of damage control procedures on board after a severe damage to the ship has been recognised by the crew.

### 3.4.3 Pump Elements

Another simple but valuable extension to the computational model are bilge pumps, which can slow down or even stop a further ingress of water after damage. A pump element can be represented as a flux, optionally time dependent, between two compartments, of which one can be the outside sea.

During fire-fighting scenarios, the water ingress and spreading caused by external or internal sources can be modelled with the help of pump elements. Another application are ballast operations to simulate for example the submerging process of heavy lift semi-submersible vessels as presented in Dankowski and Hatecke (2012).

### 3.4.4 Wave Elevation

Even though the presented method is not indented to model the behaviour of a damaged ship in waves, the modelling of a simple regular wave is assumed to be useful. This wave is used to describe a locally increased water height at openings where otherwise no water ingress would have been possible. For accident investigations like the ESTONIA accident presented later, this is essential to initiate a flooding process. Without this artificial design wave, no water ingress would have occurred at all, because the lowest opening has been above the mean calm water surface.

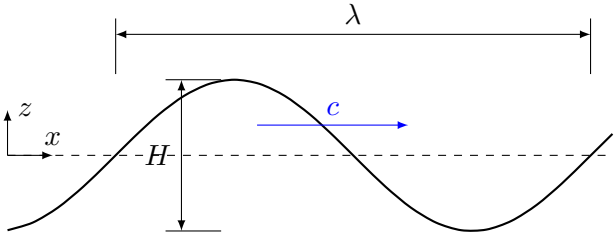


Figure 3.9: Description of a regular wave

According to linear wave theory, the regular design wave as shown in Figure 3.9 is simply described by a cosine function $z(x,t)$, where $c$ is the group wave velocity, $\lambda$ the wave length, $T$ the wave period, $H$ the wave height, $x_0$ a constant phase offset, $x$ the current position in the wave direction and $t$ the current time:

$$z(x,t) = \frac{H}{2} \cdot \cos\left[\frac{2\,\pi}{\lambda} \cdot (x + x_0 + c \cdot t)\right] \qquad \text{with} \quad c = \frac{\lambda}{T}. \tag{3.8}$$

The wave elevation is described in the earth fixed system, which means that each ship fixed point has to be transformed first by the actual heel, trim and encounter angle to the current position

in the wave pattern. It is assumed that the wave height will not change significantly across the extension of the opening, which allows to use the centre point of the opening to determine the increased water height at the opening due to the wave elevation.

Besides the increased water level, no other dynamic effects arising from the presence of waves are taken into account for the determination of the water flux through the openings. Other dynamic effects are for example the relative water velocity of the wave in relation to the motion of the ship or any further dynamic interactions between the ship and the waves. A more sophisticated statistical modelling of the water ingress in the presence of waves can be found for example in Hutchison (1995) and Söding (2002a). For now, the simple approach of a single regular wave is assumed to be sufficient. The accurate realisation of irregular waves on the basis of a sea state spectrum and its influence on the opening fluxes will be considered after the coupling with a sea-keeping simulation code.

## 3.5 Air Phase

In some cases, it may be necessary to take entrapped air into account, although in most cases the assumption of fully ventilated compartments is reasonable. The grade of ventilation and the requirement of modelling the air flow depends mainly on the size of the free and not submerged openings compared to the openings under water as shown in Subsection 2.2.5. The occurrence of air pockets may especially be important for the later phases of a sinking sequence. A detailed study on the effect of entrapped air can be found in Palazzi and de Kat (2004).

### 3.5.1 Air Compression

The simplest approach is to model only the compression of air pockets without any air exchange between the compartments. This can be done by assuming an ideal gas of constant mass and the compression to be isothermal according to Boyle's law. The influence of air compression on a simple test case can be found in Subsection 2.2.2. The pressure of the corresponding compartment with the entrapped air is increased by the reduction of the air volume according to Boyle's law as stated in Equation 2.6.

In this case the ambient air pressure $p_e$ has to be considered. The pressure $p$ is corrected by the ratio of the change in air volume from $V_{a,0}$ to the current air volume $V_a$

$$(p_e + \tilde{p}) \cdot V_a = (p_e + \tilde{p}_0) \cdot V_{a,0}, \tag{3.9}$$

$$\tilde{p} = (p_e + \tilde{p}_0) \cdot \frac{V_{a,0}}{V_a} - p_e. \tag{3.10}$$

If the total pressure values are used, this yields a simpler expression for the change in pressure during one time step $\mathrm{d}t$, where the air volume flux $\dot{V}_a$ must be equal to the negative overall water flux $\dot{V}_w$

$$p = p_0 \cdot \frac{V_a + \mathrm{d}t \cdot \dot{V}_w}{V_a}, \tag{3.11}$$

$$\mathrm{d}p = p - p_0 = p_0 \cdot \frac{\mathrm{d}t \cdot \dot{V}_w}{V_a}. \tag{3.12}$$

It should be noted that the influence of the compression of entrapped air pockets becomes smaller in full scale compared to the model scale. The pressure increase is approximately the same in

model and full scale, because it depends only on a volume ratio. However, the influence of the pressure difference $p_a - p_b$ between two compartments on the volume flow through the openings according to the Bernoulli equation Equation 2.9 becomes smaller in full scale compared to the water level differences term $z_a - z_b$.

### 3.5.2 Air Flow

Besides the air flow through air pipes, which are responsible for a sufficient ventilation of the compartments, there can also be an interchange of air between the different compartments through not completely submerged openings. The air flow can be described by the Bernoulli equation for compressible fluids (Equation 2.4), as it has been done by Ruponen (2007). The complication which arises here is the occurrence of an air flow through water formed of local bubbles. This type of flow is far from stationary and cannot be modelled by a simple hydraulic model based on Bernoulli's principle.

In addition, the simultaneous computation of internal air and water flow is difficult due to the large differences in density and velocity of both flows. This difficulty has also been observed by Ruponen (2007). He describes that a high number of iterations are required for the solution of the pressure correction equations in the presence of an air flow. Another aspect is that air flows much faster than water and therefore pressure differences in the air phase are reduced very quickly. Furthermore, it is also questionable how accurately all possible openings, that allow the escape or interchange of air, are known for a certain ship.

Consequently, the overall influence of the air flow on the global flow pattern and the flooding physics is usually small and can be neglected. For this reason, the air flow is for now excluded from the computational model. A different aspect are the air compression effects. These are taken into account by the simple approach presented in the previous section. However, the most important aspect here is the correct determination at what point in time the air starts to compress. A more detailed description of the determination of entrapped air follows in the next section.

### 3.5.3 Determination of Entrapped Air

An important aspect is the correct determination whether or not air is actually entrapped inside a compartment. It is required to know at what time air can no longer escape from the compartment and the air starts to compress building up a higher pressure. For the determination of this point in time, it is necessary to identify the location of all openings of the compartment in question and its neighbouring compartments relative to the corresponding water levels on both sides of the openings.

Two strategies are possible: Air is assumed to be entrapped in one compartment if *all* openings are completely submerged, either

1. by the internal water level *or* the water levels of all surrounding compartments, or
2. only by the internal water level.

This is also illustrated in Figure 3.10, where two compartments A and B are shown. The water flows from a bottom opening in B through a large opening to A and at the same time air can escape from an additional vent opening in B. The air from A escapes through the upper part of the large opening to B.

The water levels for three different situations are marked with the numbers 0, 1 and 2.

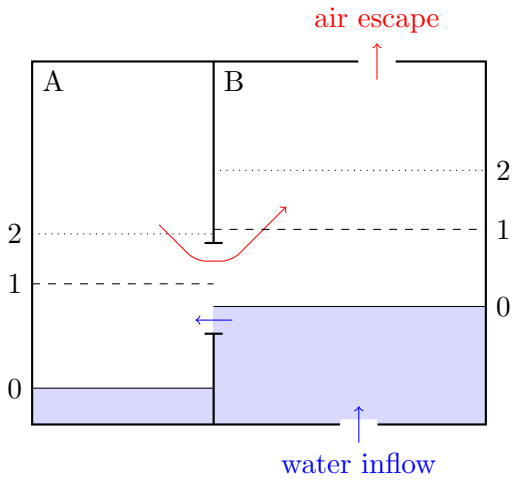


Figure 3.10: Two situations for a possible air-tight locked compartment

In situation 0, air can flow through the upper part of the large opening from A to B and escapes through to the top opening in B. In the next situation 1, air is entrapped in A. This corresponds to the first assumption that air is entrapped, if the internal water level or the water levels of the neighbouring compartments are above the upper edge of all openings in question. This situation typically occurs before situation 2. In this situation, both internal water levels completely submerge the large opening connecting A and B, which prevents any air interchange between the two compartments.

It is expected that the second assumption of situation 2 is the most realistic one, because air can still escape in situation 1 as air bubbles arise through the large opening, even against the water column in compartment B. A small pressure increase probably occurs, but this increase is directly reduced by the escape of the air bubbles. In addition, to assume a later start of the air compression is also the more conservative approach, since the formed air pockets are smaller and more water can enter the flooded ship. This aspect will also be investigated in more detail for the model test case B described in Section 4.4.

## 3.6 Aspects of Implementation

The presented method is implemented in the ship design software E4. The chosen programming language is Fortran. Due to its simplicity and capability of fast numerical evaluations, this language is very convenient for the implementation of numerical methods to solve engineering problems. Another advantage is, that a lot of well validated and fast algorithms are already available in the E4 software package. These are for example hydrostatic computations that are required for the determination of the volume and moments of a compartment, the robust, iterative Newton based methods to identify the equilibrium floating position of the ship, geometric algorithms, root finding techniques, equation system solvers and several others.

On the other hand, due to its modular concept, the extension of the software by new methods is straight forward. The new numerical flooding simulation is directly integrated into the E4 system and split into a library for the computational kernel called by the executable method, which contains the user interaction part and the post-processing. In addition, this method

is linked with already existing libraries for the user interface, the direct access to the ships database, plotting routines, hydrostatic computations and other relevant parts. In the future, the presented method can also be coupled with already implemented sea-keeping simulation codes like the non-linear code E4-ROLLS (Kröger, 1987).

Most parts of the computational data models of the investigated ships are already defined in the database of the design software. For flooding simulations, these data models have to be extended by the definitions of the relevant openings. It is also required to extend the hull description by non-watertight parts like the superstructure, the bridge and the funnel. The compartmentation has to be refined as well, because the flooding simulation takes the influence of non-watertight structures like walls and doors into account.

The distribution of the ingressed flood water in the internal subdivision of the ship leads to additional heel and trim moments. As the fluid shifting moments of each compartment are directly taken into account by the prescribed method, a correction of the vertical centre of gravity due to free surface effects is not required in any case.

### 3.6.1 Visualisation Techniques

To obtain a good insight into the vessel's reaction caused by the flood water ingress and spreading inside the inner subdivision of a ship, a three dimensional visualisation of the flooding sequence in the time domain is implemented. Due to the tremendous amount of data produced by a flooding simulation, an animation of the vessel and its motion together with the openings relative to the water surface is very useful to identify critical stages of intermediate flooding.

All of the required data for the visualisation is derived from the data model in the E4 database. The hull form is first triangulated, as so is the water surface. The whole scene is directly rendered with the help of the OpenGL library. A more advanced visualisation would be possible by using the exported data in external visualisation programs, but from an engineering point of view, this technique is the best choice for a fast and in-depth view of the flooded situation of the vessel.

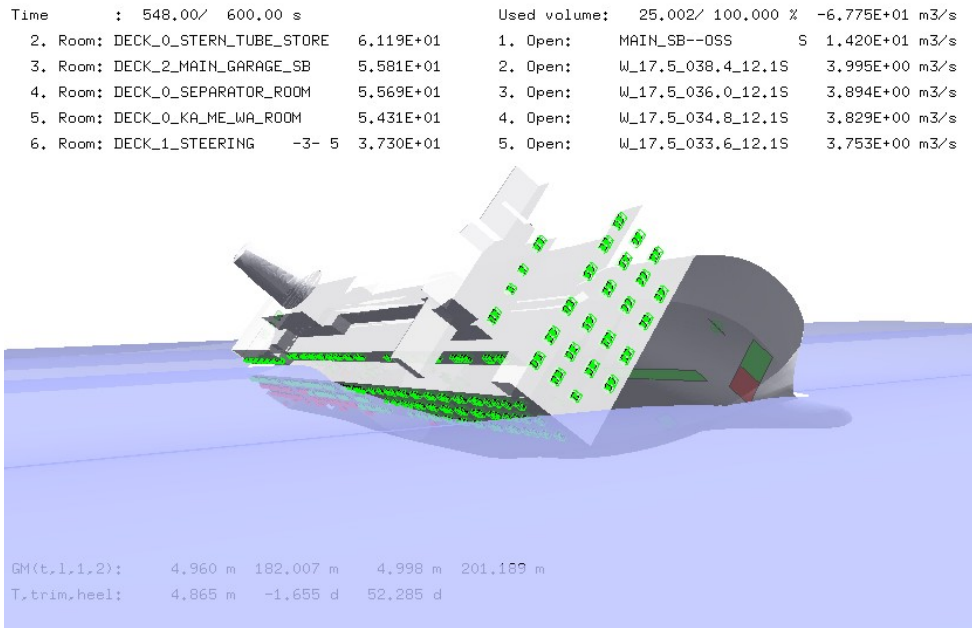


Figure 3.11: Visualisation frame of the ESTONIA investigation

One frame of this animation is depicted in Figure 3.11. The hull of the vessel is shown in transparent grey, together with the water surface in light blue. Openings through which water flows are coloured in red, while openings which are not submerged or which can still hold the hydrostatic pressure head are shown in green.

Additional information is given at the top and bottom of the screen. Here the top five of the openings with the largest absolute flux and the compartments with the largest relative volume fillings are listed. In addition, the time step and the relative used buoyancy volume are stated. In the lower left corner, the draught, trim and heel together with the $\overline{\mathrm{GM}}$ stability values are shown.

### 3.6.2 Definitions of Openings

To reduce the effort for the opening definitions, the description is currently restricted to planar rectangles, oriented arbitrary in space. The definition consist of the following parameters:

- The name of the opening
- The coordinate triple of the centre $(x, y, z)$
- The two IDs of the connected compartments (ID1, ID2)
- The extensions in the three coordinate directions $(dx, dy, dz)$
- The discharge coefficient $C_d$
- The pressure head criterion $P_h$

An opening is defined as a planar opening rotated around one axis out of an coordinate plane. An example for the definition of one opening in the $x$-$y$ plane is given in Figure 3.12. In this case, the $dx$ value is always positive, the $dz$ extension is always negative and the third component $dy$ depends on the rotation direction out of the $x$-$z$ plane.

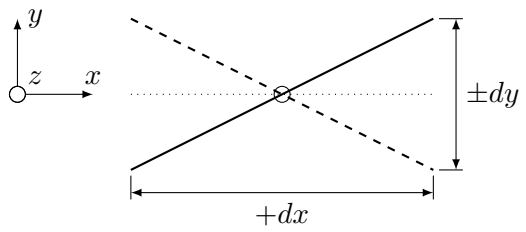


Figure 3.12: Examples of the opening definition for the $x - y$ plane

The sign convention for the definition of the openings is given in Table 3.1. The extension component for the rotation axis is always negative, the signs of the other extensions depend on the kind of opening. The chosen sign convention avoids identical and conflicting definitions of openings.

Table 3.1: Sign convention for openings

| | Sign convention | | | |
|---|---|---|---|---|
| Rotation axis | dx | dy | dz | Example |
| x | − | + | ± | side door in a longitudinal bulkhead |
| y | ± | − | + | staircase opening in a deck |
| z | + | ± | − | door in a transverse bulkhead |

### 3.6.3 Simulation Overview

The flow chart of one time step of the simulation is given in Figure 3.13. After the initialisation of the data, the loading condition of the vessel and a few other parameters like the requested simulation duration is selected. The relevant openings are separately described and directly chosen from the database.

Before the time loop is started, the flooding graph is automatically derived from the opening description, which contains the references to the compartments. At the beginning of each time step, conditional openings are checked, if for example certain openings will break. The pressure iteration for completely flooded compartments follows.

The next three steps are the explicit integration of the system of differential equations as described in Section 3.2. These steps consists of the computation of the opening fluxes, the propagation of the water volumes together with an update of the filling levels of the compartments. If the predictor-corrector scheme is applied, these three steps are repeated to obtain an averaged value for the opening fluxes.

If air compression is taken into account, all compartments are now checked if air is entrapped and the simple air compression model is applied, which changes the pressure in the corresponding compartment. The iteration of the new floating equilibrium based on the new distribution of the flood water inside the vessel is computed. A typical convergence criterion is the maximum change of the water levels in the compartments over one time step together with the movement of the vessel. If the convergence check is negative, the simulation proceeds to the next time step until the defined maximum simulation time is extended, convergence is reached, or the ship actually starts to vanish from the sea surface when no more buoyancy reserve is available.

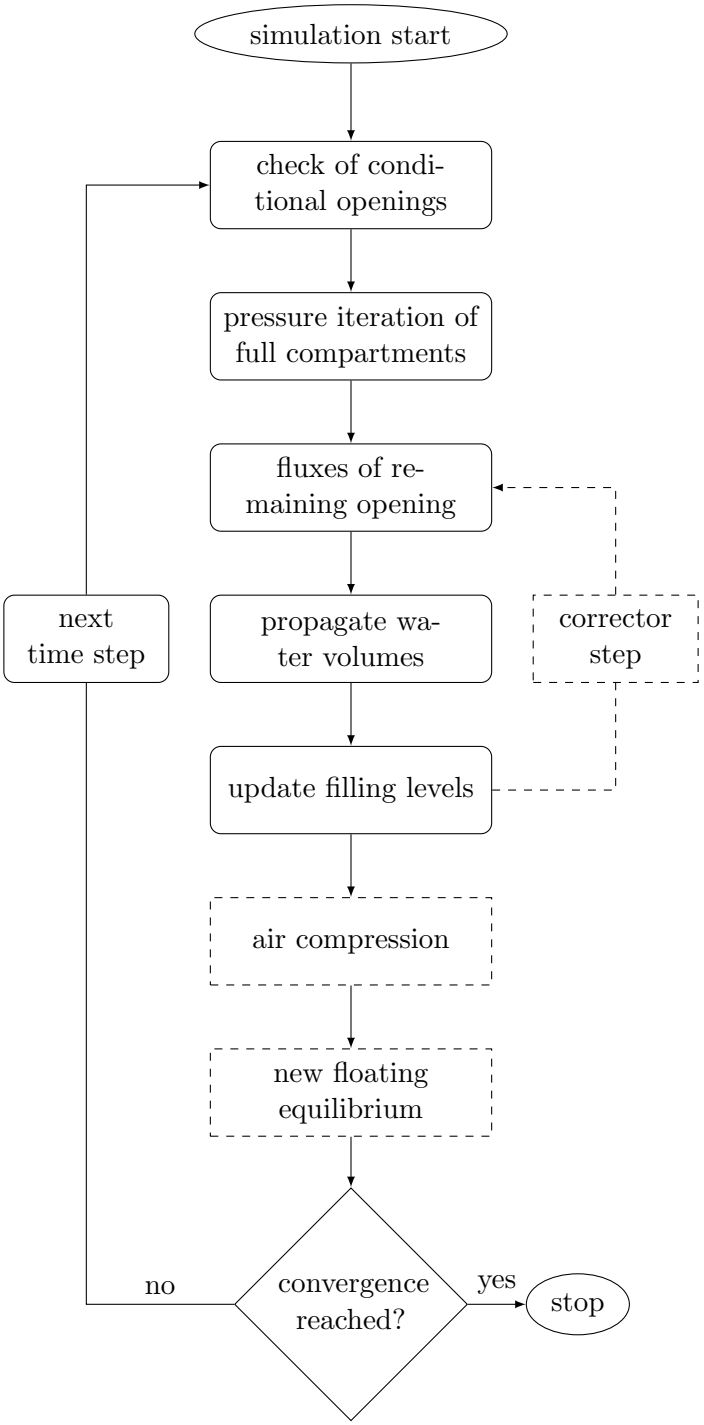


Figure 3.13: Flow chart of the numerical flooding simulation

# CHAPTER 4

# Validation with Model Test Results

As a first validation of the presented method, a comparison with model test results of a box-shaped barge carried out by Ruponen (2006) at the Ship Laboratory of the Helsinki University of Technology is performed. The main dimensions of the barge are given in Table 4.1.

Table 4.1: Main dimensions of the test barge

| | | |
|---|---|---|
| Length over all | $L_{\mathrm{OA}}$ | 4.000 m |
| Height | $H$ | 0.800 m |
| Moulded Breadth | $B$ | 0.800 m |
| Draught design | $T$ | 0.500 m |
| Displacement | $\Delta$ | 1.450 $\mathrm{m}^3$ |
| Vertical centre of gravity | $\overline{\mathrm{KG}}$ | 0.278 m |

A photo of the barge model is shown in Figure 4.1, where the front of the barge is on the left side. The mid ship part of the barge is built of perspex and it is located right in front of the main section. It contains all relevant compartments and the measurement equipment for the different model tests.

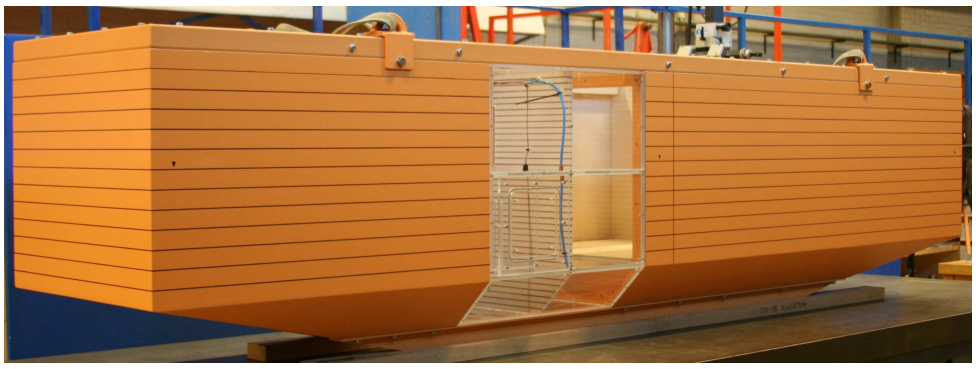

Figure 4.1: Photo of the test barge (Ruponen, 2006)

The validation with this benchmark test investigates also the capability of the new method to take into account the following critical aspects:

- Complex flooding sequences of multiple compartments
- The influence of the selected time step
- Differences in the computation in full and model scale
- Effects of air compression

All of the three test cases involve the flooding of multiple compartments. A sensitivity analysis of the time step and the influence of air compression is elaborated in more detail for the test case B. The comparison of the computation in model and full scale is presented for the third test case C.

## 4.1 Description of the Computational Model

The computational model of the buoyancy body is shown in Figure 4.2 including the stiffener at the bottom and the additional perspex plates at the lateral sides.

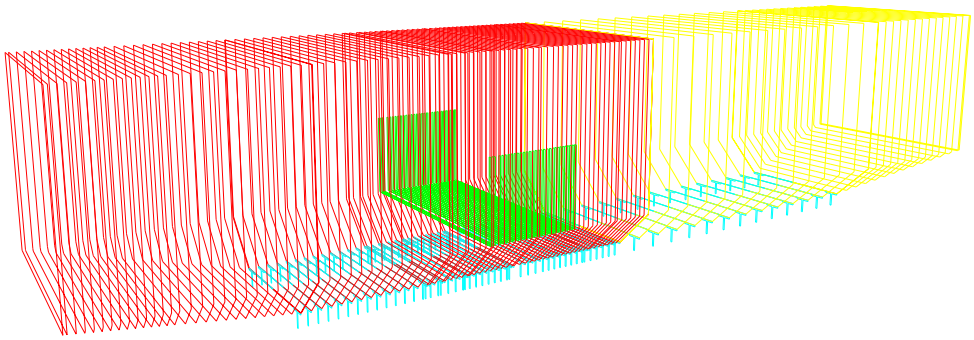

Figure 4.2: Computational model of the buoyancy body of the test barge

Detailed views on the inner subdivision of the perspex mid ship part are shown in Figure 4.3 together with the names of the compartments of interest. For each test case, a sketch of the side and section view of this mid ship part will be given to illustrate the current flooding situation.

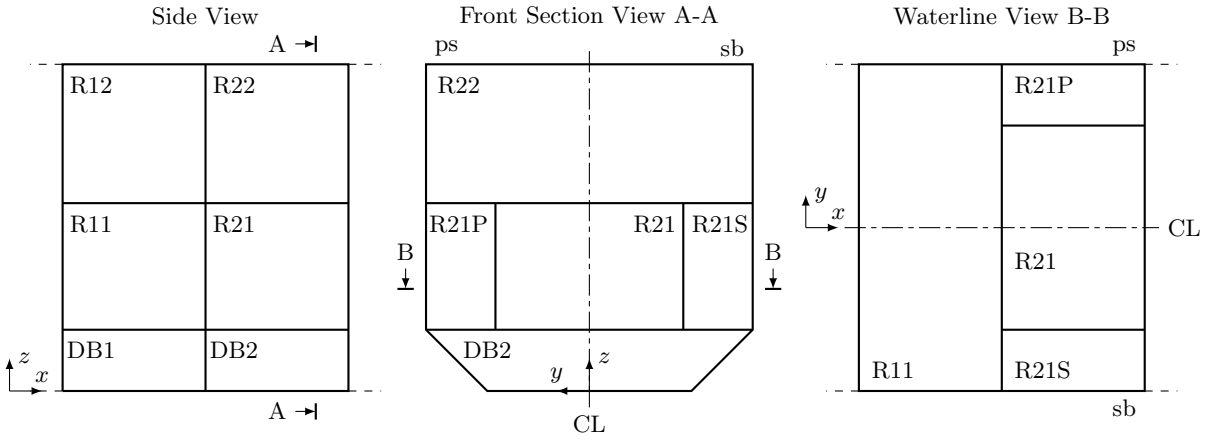


Figure 4.3: Detailed views of the mid ship part and the compartments of the test barge

Ruponen used three out of six model tests as validation cases for the numerical method, which he developed in the scope of his Ph.D. thesis (Ruponen, 2007). An overview of the naming between the extensive technical report of the model tests (Ruponen, 2006) and the validation cases in his thesis is given in Table 4.2 together with the naming in this thesis.

Table 4.2: Naming of the model test cases in different sources

| Technical Report (Ruponen, 2006) | Ph.D. thesis (Ruponen, 2007) | This thesis - |
|---|---|---|
| Test06 | Validation Case A | Model Test Case A |
| Test03 | Validation Case B | Model Test Case B |
| Test05 | Validation Case C | Model Test Case C |

## 4.2 Computational Setup

The detailed geometry of the barge, the openings and all other relevant model data such as the location of the water height sensors are given in Ruponen (2006). The properties of the relevant openings are summarised in Table 4.3.

Table 4.3: Properties of the openings of the test barge

| Point-Name | $X$ (mm) | $Y$ (mm) | $Z$ (mm) | $dx$ (mm) | $dy$ (mm) | $dz$ (mm) | $C_d$ (-) |
|---|---|---|---|---|---|---|---|
| Bottom damage DB1 | 2327.5 | 0.0 | 5.0 | 60 | 40 | 0 | 0.78 |
| Bottom damage DB2 | 2672.5 | 0.0 | 5.0 | 25 | 25 | 0 | 0.83 |
| DB1-DB2 pipe | 2500.0 | 0.0 | 77.5 | 18 | 0 | 18 | 0.80 |
| DB2-R21 manhole | 2800.0 | 175.0 | 145.0 | 40 | 60 | 0 | 0.78 |
| R21-R21P fire door | 2672.5 | 235.0 | 265.0 | 20 | 0 | 200 | 0.75 |
| R21-R21S fire door | 2672.5 | -235.0 | 265.0 | 20 | 0 | 200 | 0.75 |
| Large side damage F | 3500.0 | -395.0 | 200.0 | 40 | 0 | 100 | 0.80 |
| Large side damage A | 1500.0 | -395.0 | 200.0 | 40 | 0 | 100 | 0.80 |
| R21S side damage | 2672.5 | -395.0 | 305.0 | 40 | 0 | 60 | 0.78 |
| R21-R11 pipe | 2500.0 | 0.0 | 305.0 | 18 | 0 | 18 | 0.80 |
| R12-R22 open WT door | 2500.0 | 0.0 | 575.0 | 80 | 0 | 200 | 0.75 |
| R12-R11 staircase | 2395.0 | -180.0 | 455.0 | 100 | 10 | 0 | 0.78 |
| R22-R21 staircase | 2740.0 | -180.0 | 455.0 | 100 | 10 | 0 | 0.78 |

With these data, a detailed computational model of the same scale as used in the model tests has been defined. If not mentioned otherwise, a time step of 0.2 seconds is sufficient for a stable numerical simulation and to receive accurate results (compared to 0.05 seconds used by Ruponen). The influence of the time step on the simulation results is presented in more detail for test case B (see Section 4.4). The heeling angle will not further be mentioned in the following, since it is negligibly small for all three test cases. However, the evaluation of the new floating equilibrium is performed for all three degrees of freedom, i.e. the draught, heel and trim angle.

The water height sensors shown in Figure 4.4 are wires, which measure its wetted lengths electronically. To compare the obtained computed values with the provided results for the

water levels from the model tests, the filling heights must be computed at the positions of the sensors. The filling height for each pipe is given by the distance between the bottom point of the sensor and the current planar water surface of the selected compartment.

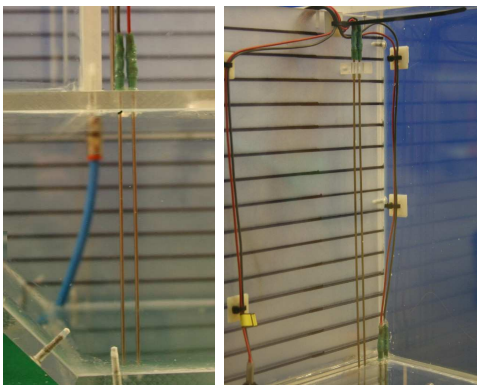

Figure 4.4: Photos of the water level sensors used in the model tests (Ruponen, 2006)

## 4.3 Model Test Case A

Validation case A represents a large side damage as sketched in Figure 4.5. All compartments are assumed to be fully ventilated, i.e. no air compression needs to be taken into account. The water starts to ingress through the large side damage and immediately spreads through the whole lower deck. After the lower deck compartments R11 and R21 are completely filled, the up-flooding through the staircase openings to the upper deck starts. Convergence is reached after the water levels on the upper deck in the compartments R12 and R22 equal to the outside water level.

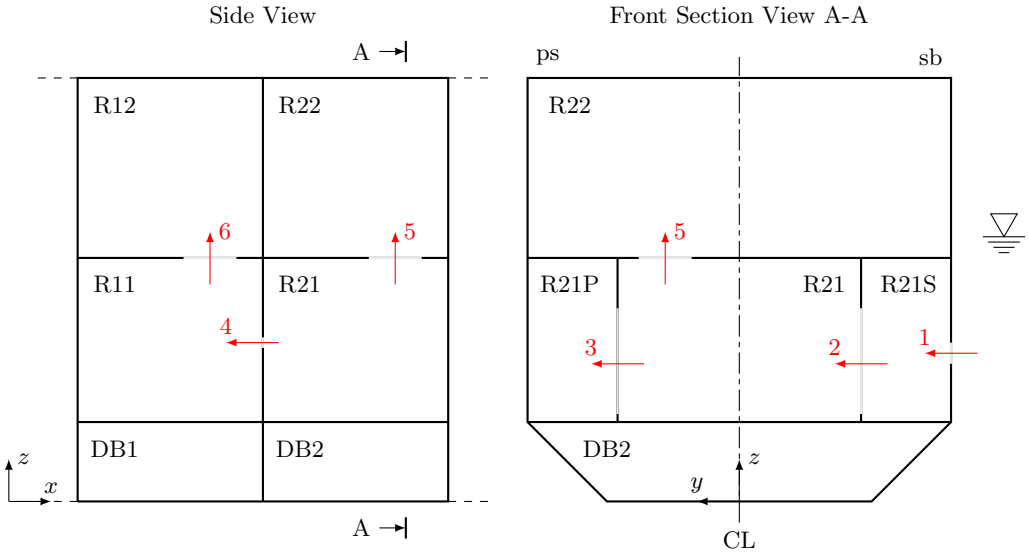


Figure 4.5: Model test case A - Side and section view of openings and compartments

The results of the new method are labelled with the prefix “calc. *value* D.”, the measured values with “meas. *value* R.” and the computed values by Ruponen with “calc. *value* R.”.

The simulated trim and heave motions (Figure 4.6 and 4.7) show a very good agreement with the measurements and the computed values from Ruponen.

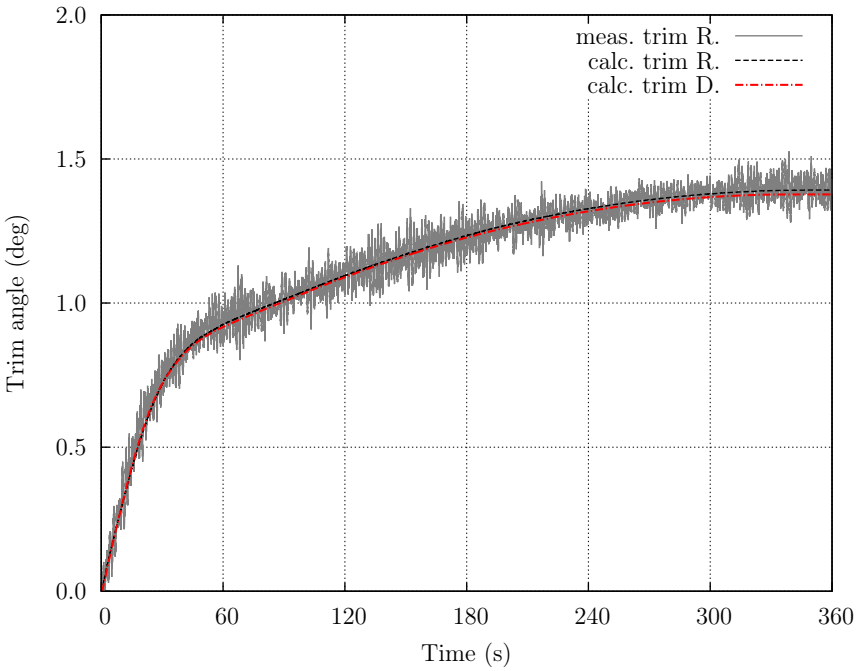


Figure 4.6: Model test case A - Trim angle

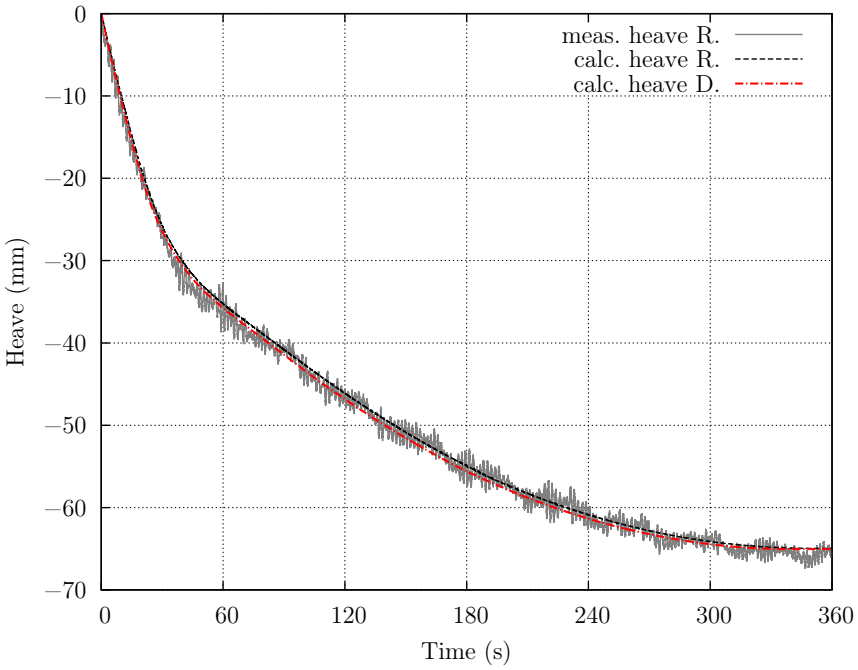


Figure 4.7: Model test case A - Heave motion

The water levels of both side compartments are shown in Figure 4.8. During the first transient phase of flooding, the water level in the side compartment R21P is underestimated by both simulation methods, while the flooding in the starboard compartment R21S next to the large

side damage on the starboard side is predicted to be faster in both simulation methods compared to the measured values.

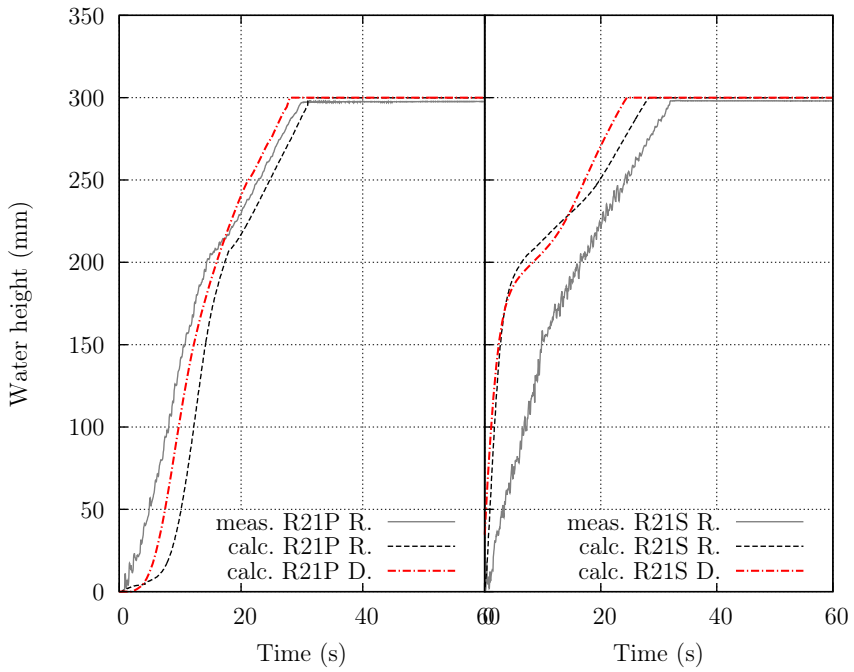


Figure 4.8: Model test case A - Water levels of the side compartments

As already mentioned in Ruponen (2007), this difference is mainly caused by the sudden and intensive water jet ingress through the side damage leading to an immediate flooding of the whole lower deck. The immediate spreading of this water jet delays the flooding of the starboard side compartment and accelerates the raise of water in the port side compartment. This transient flow is not captured by the applied hydraulic models for the water fluxes through the openings by neither of the two simulation methods. However, the influence of this effect on the overall flooding process is negligible small.

The small discrepancy between the two simulation methods themselves is probably due to the fact that air flow and air compression are not considered by the new method in this test case, which slightly delays the flooding process as shown in Subsection 2.2.5.

The water levels of the other two lower compartments R11 and R21 are shown in Figure 4.9. The simulated and measured results match very well. The only deviation from the measured values occurs in the water level of the aft compartment R11. This might be caused by the formation of an air wedge in the upper back corner of R11 right below the upper deck due to the large trim at that point and explains why this compartment is not completely filled up with water during the model tests. To take this effect into account, the forming and the compression of the air wedge in this compartment could be modelled (see also Subsection 3.5.3). However, the overall influence is negligibly small.

In Figure 4.10 the water levels of the compartments R12 and R22 on the upper deck are shown. The only difference to the measured results can be seen for the aft compartment R12. The flooding is delayed in the model test compared to the results of the simulation, due to the air pocket that is formed in the upper aft part of R11 located right below R12, which delays the up-flooding through the staircase opening.

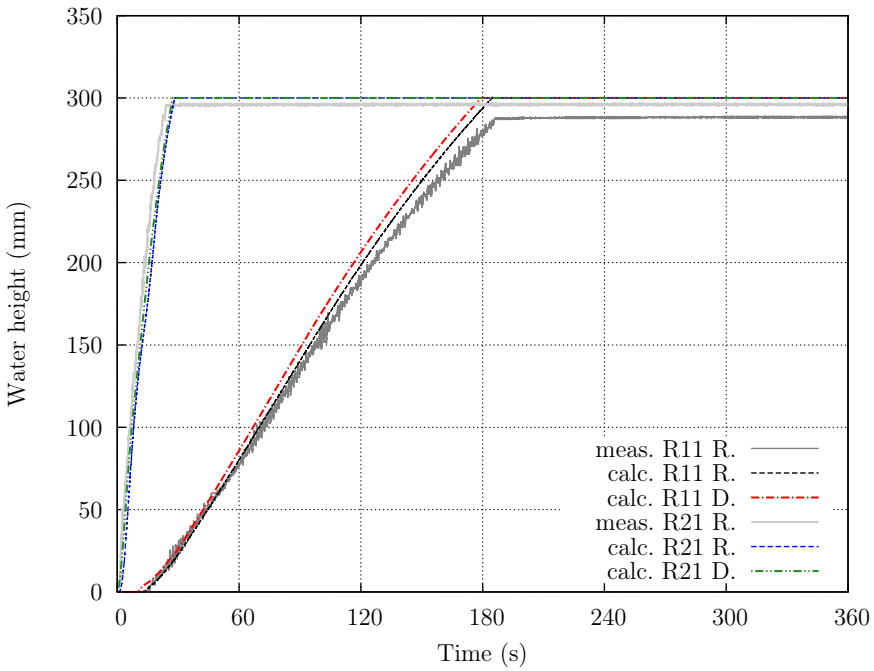


Figure 4.9: Model test case A - Water levels of the lower compartments

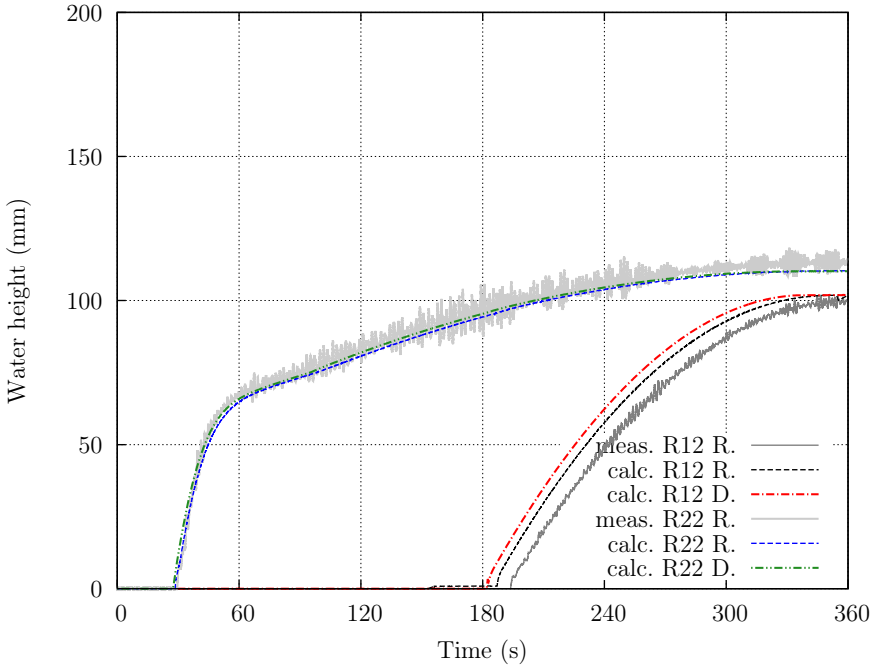


Figure 4.10: Model test case A - Water levels of the upper compartments

## 4.4 Model Test Case B

The second test case is challenging, because it does not only include air compression effects, but also complex up-flooding events. The setup is shown in Figure 4.11. The water ingress

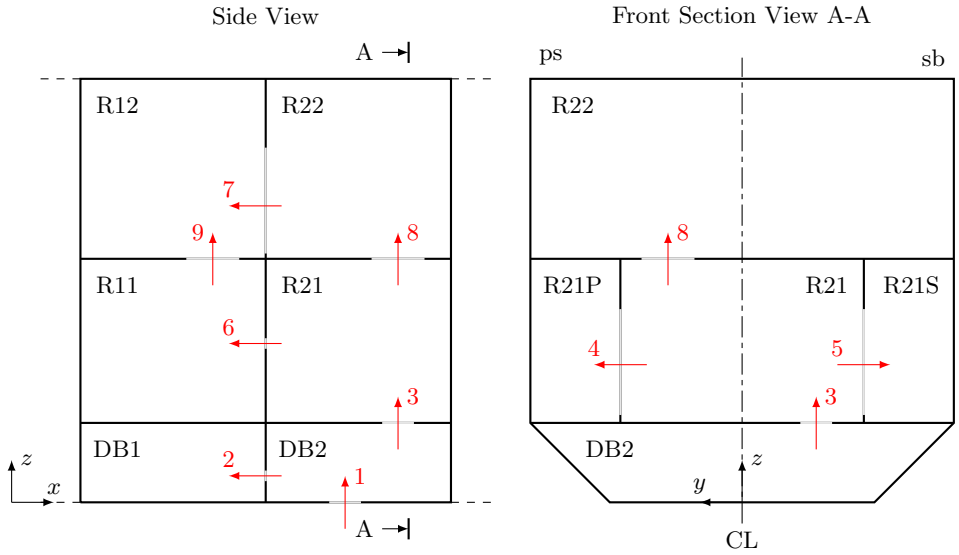


Figure 4.11: Model test case B - Side and section view of openings and compartments

starts through the bottom damage in DB2 before the other double bottom compartment DB1 is flooded. After DB2 is completely filled, the water proceeds further to the lower deck and its side compartments. A complex sequence of flooding occurs when the upper deck becomes flooded, since the front and aft compartments R22 and R12 are not only flooded both from below, but are additionally connected by a large opening.

The results obtained for the trim motion shown in Figure 4.12 agree very well with the measured values, only at the end of the flooding process, both computed results are slightly too small. In addition, the effect of different time step sizes on the trim motion is studied. The results for large time steps (5 and 2 seconds) deviate distinctly from the measured values. If the time step is reduced below 0.5 seconds, the results clearly converge to the measured ones. A smaller time step does not show any further change in the computed results, which also means that it is not required to choose a very small time step of 0.05 seconds as used by Ruponen. The convergence study shows, that a time step of 0.2 seconds is an appropriate choice to compute this test case in model scale. The computational cost scales typically linear with the time step. A halved time step results in twice the runtime to compute one simulation of the same duration, because the number of time steps is doubled.

The values of the heave motion that are computed by the new method are located below the measurement values for the first three minutes and for the last minute, as shown in Figure 4.13. This behaviour can be explained by the modelling of air compression in DB1, which will be investigated in greater detail in the following.

Looking at the lower double bottom compartments, the compressed air pocket in DB1 plays an important role, since all other compartments, including DB2, are sufficiently ventilated. The water levels of DB1 are shown in Figure 4.14 and the over-pressure of the air (difference to ambient pressure) is given in Figure 4.15. The results for two different determinations when the air compression starts are shown here, labelled with (1) and (2) in the figures.

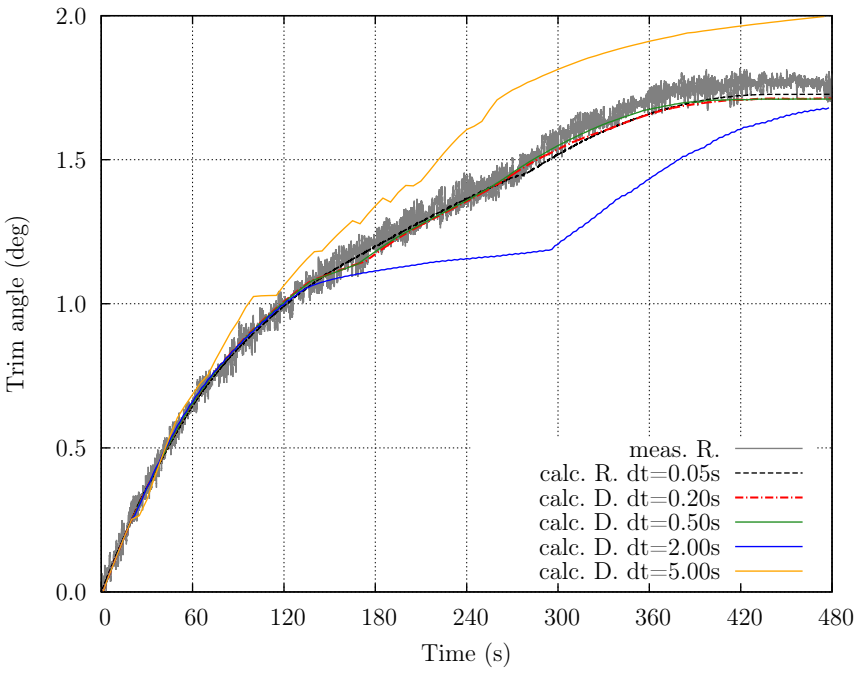


Figure 4.12: Model test case B - Trim Motion

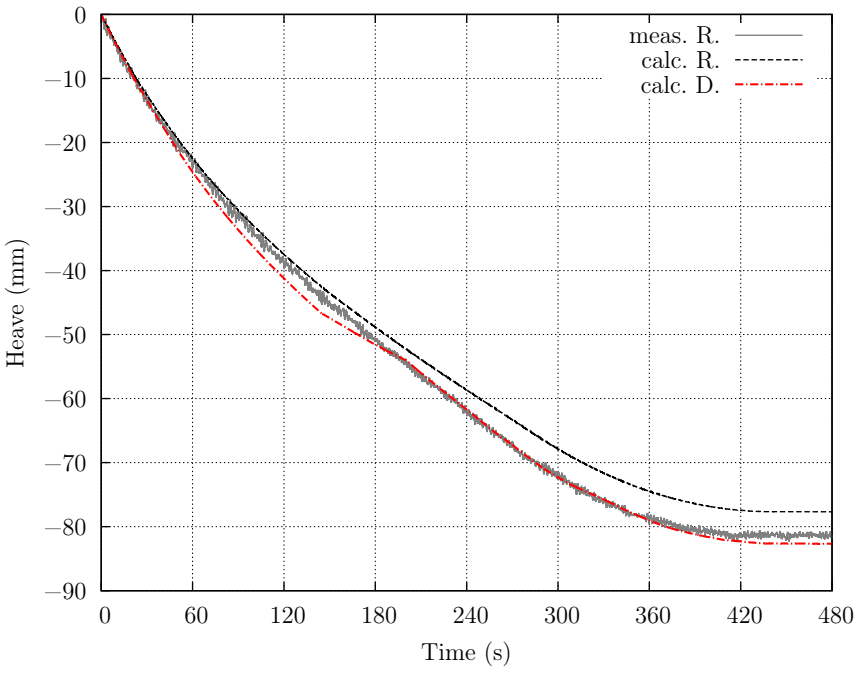


Figure 4.13: Model test case B - Heave Motion

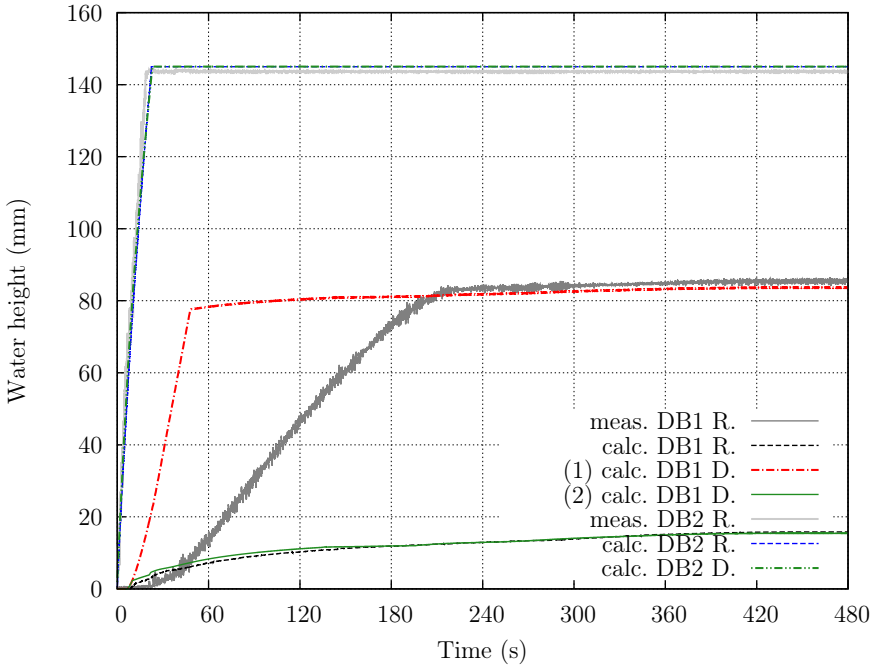


Figure 4.14: Model test case B - Water Heights in DB1 and DB2 for different air compression assumptions

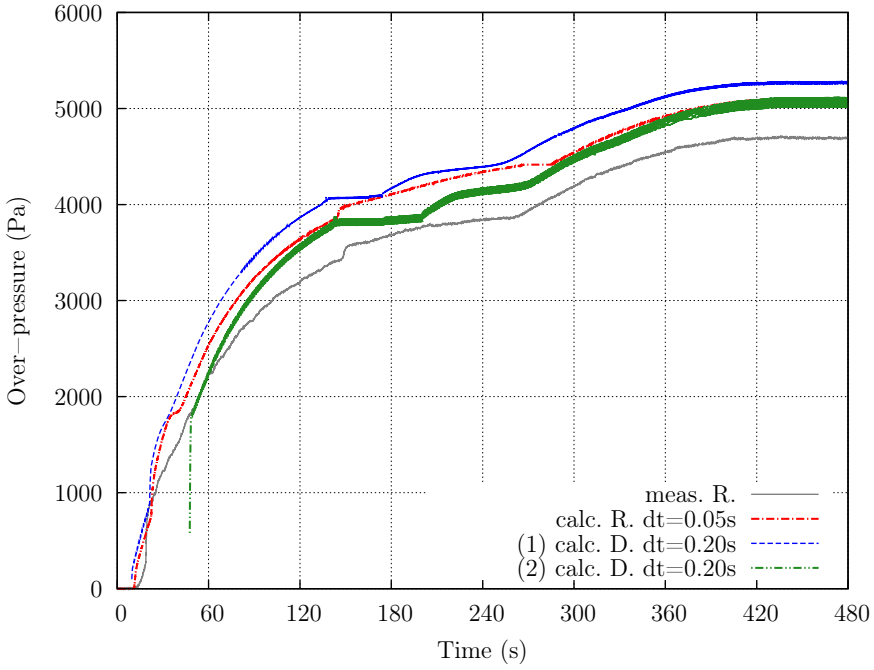


Figure 4.15: Model test case B - Over-pressure in DB1 for different air compression assumptions

As mentioned in Ruponen (2007), an air bubble flow arising from DB1 allowed some air to escape, resulting in a lower over-pressure in that compartment, which allows more water to enter. The main effect here is actually the point in time when an escape of air is no longer possible (compare also Subsection 3.5.3). If air compression is assumed to start after *one* side of the opening is submerged, the pressure increase starts earlier and less water can enter the compartment. The results obtained for this case (1) are similar to those obtained by Ruponen. When it is in case (2) assumed that air flow is prevented after *both* sides of the opening are submerged, the same water level as the measured one is reached, even though the gradient of the water level development differs. The real behaviour is comparable to the generic test case (see Subsection 2.2.5) when air flow is taken into account as well. The air flow influences mainly the gradient and the time to reach the final water level, but not the final level itself. The oscillations in the over-pressure for the second case (2) are slightly higher compared to (1), which might be caused by the more sudden increase of the pressure and the smaller compressed air pocket. However, these oscillations are not reflected in the water levels of the compartment. If not mentioned otherwise, strategy (2) for the determination of entrapped air is applied in all other simulations.

The water levels on the lower deck in the part between double bottom and upper deck are shown in Figure 4.16. It is observed, that both simulation codes give very similar results, with only the small difference, that the water level increase of R21 obtained by the new simulation code is a little slower at the beginning. The same behaviour is observed for the water levels of the two side compartments (see also Figure 4.17). However, the deviations from the measured values are very small.

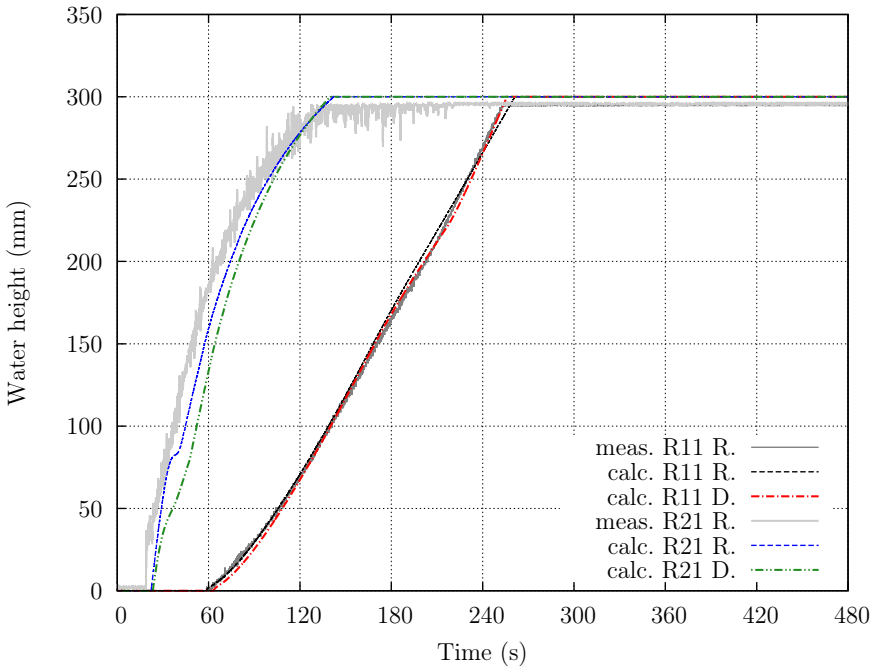


Figure 4.16: Model test case B - Water Heights in R11 and R21

The development of the water levels in the upper deck compartments R12 and R22 are shown in Figure 4.18. They strongly depend on the flooding sequence. The aft compartment R12 is flooded from the R11 compartment below, but also from a large opening to the compartment R22 in the front. This compartment is connected to R21 by the staircase opening and it is the first one on this deck, that is flooded. Especially in the first phase of the flooding process, differences

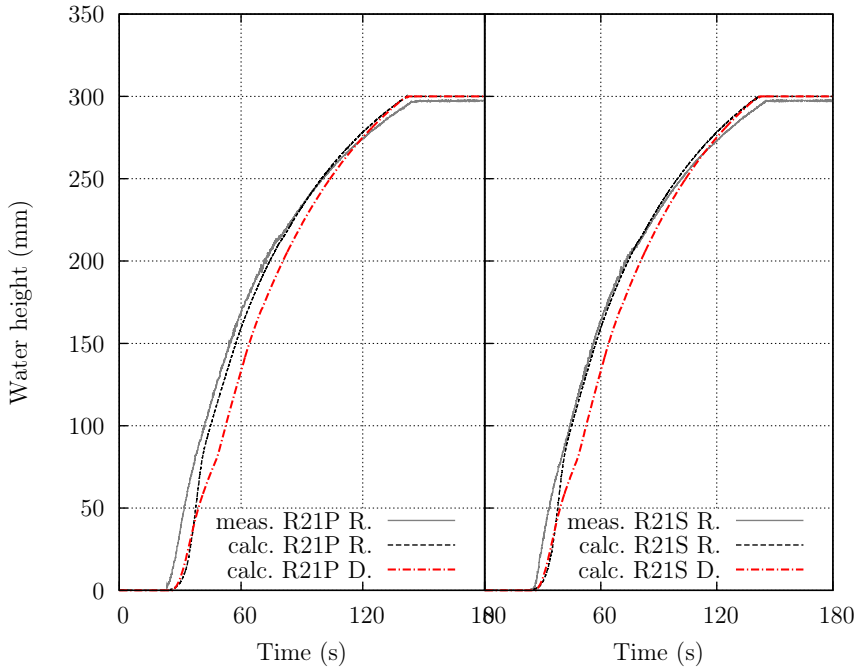


Figure 4.17: Model test case B - Water Heights in R21P and R21S

in the water levels compared to the measured values occur. However, both simulations reach the same final water levels at the end and are slightly below the measured values. This is probably caused by a small amount of air compression on the upper deck.

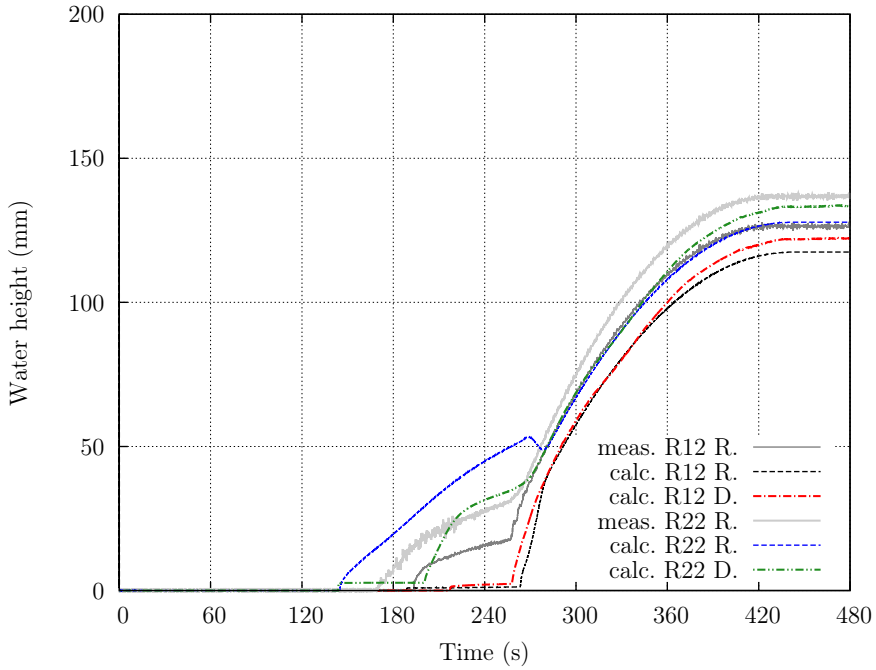


Figure 4.18: Model test case B - Water Heights in R12 and R22

To conclude, the presented test case B shows the applicability of the proposed method. It is even reliable for this demanding test case involving air compression in the lower part of the model

and complex flooding sequences on the upper deck. In addition, air should only be treated as entrapped if both sides of all openings of the corresponding compartment are submerged. This gives more appropriate results than only claiming that one of the openings must be submerged. This strategy for the determination of entrapped air yields reliable results even if the air flow itself is not modelled.

## 4.5 Model Test Case C

Finally, the third test case C serves as an validation for a slow and progressive up-flooding process. The water ingress starts in compartment DB1 and spreads through DB2 upwards to the upper decks. The setup is shown in Figure 4.19. A reduced time step of 0.1 seconds is required to correctly model the influence of the air compression in the DB1 compartment. For time steps greater than 0.1 seconds, the simulation does not converge to reasonable results.

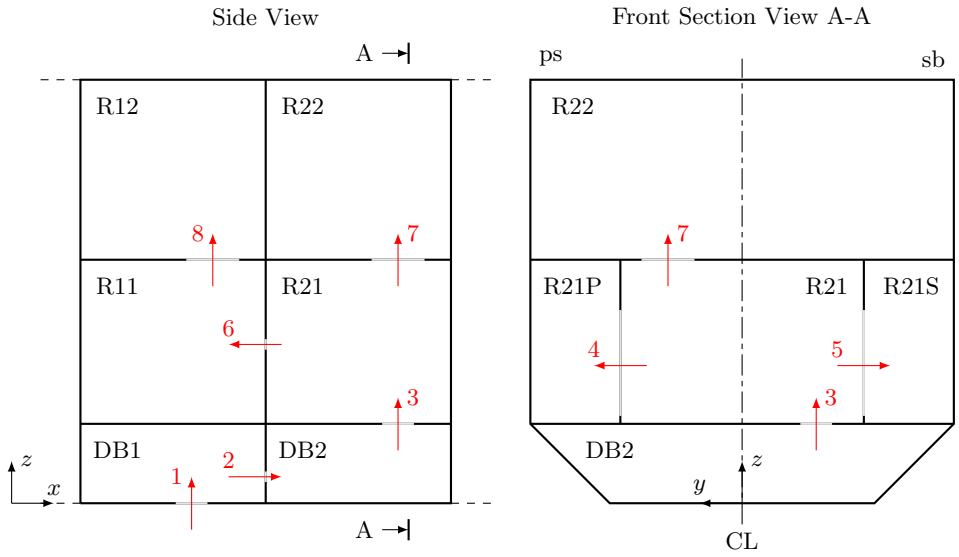


Figure 4.19: Model test case C - Side and section view of openings and compartments

The simulated ship motions are compared to the measured and computed results from Ruponen in Figure 4.20 and 4.21. The general flooding behaviour is well reproduced by the newly proposed method, but the predicted heave and trim motion is negligibly smaller.

It is known from the model tests, that DB1 is not completely filled with water at the end, due to the presence of an air pocket formed above the opening that connects the compartments DB1 and DB2. Even though an air compression model is used (see Subsection 3.5.1), the final estimated water level for the double bottom compartment DB1 is below the measured and computed values from Ruponen, see Figure 4.22.

Before the air compression starts, a small amount of air escapes through the connecting pipe from DB1 to DB2. The lower air volume leads to a smaller pressure increase and allows more water to ingress. This is probably the reason, why the new computational code, which does not take into account air flow, predicts a delay of the flooding.

This delay can clearly be seen in Figure 4.23 and 4.24, where the water levels of the compartments on the lower deck are shown. Apart from this delay in time, the general shape of the water level development in these compartments is well reproduced.

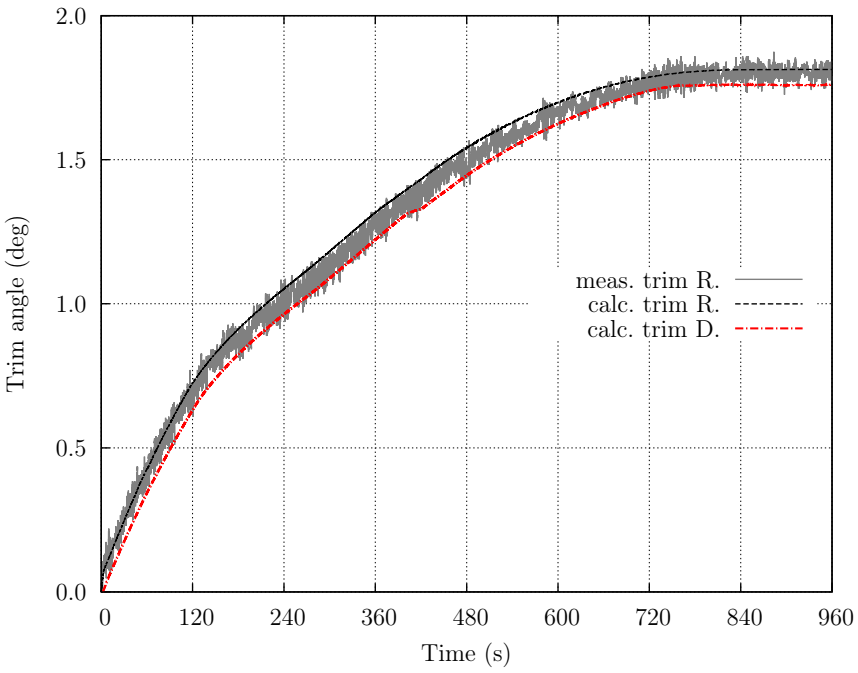


Figure 4.20: Model test case C - Trim motion

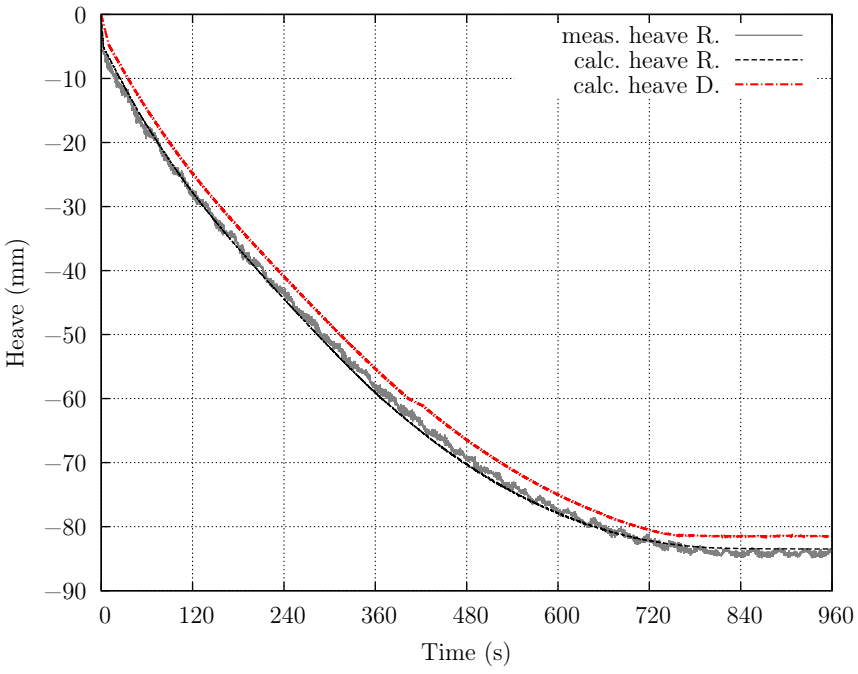


Figure 4.21: Model test case C - Heave motion

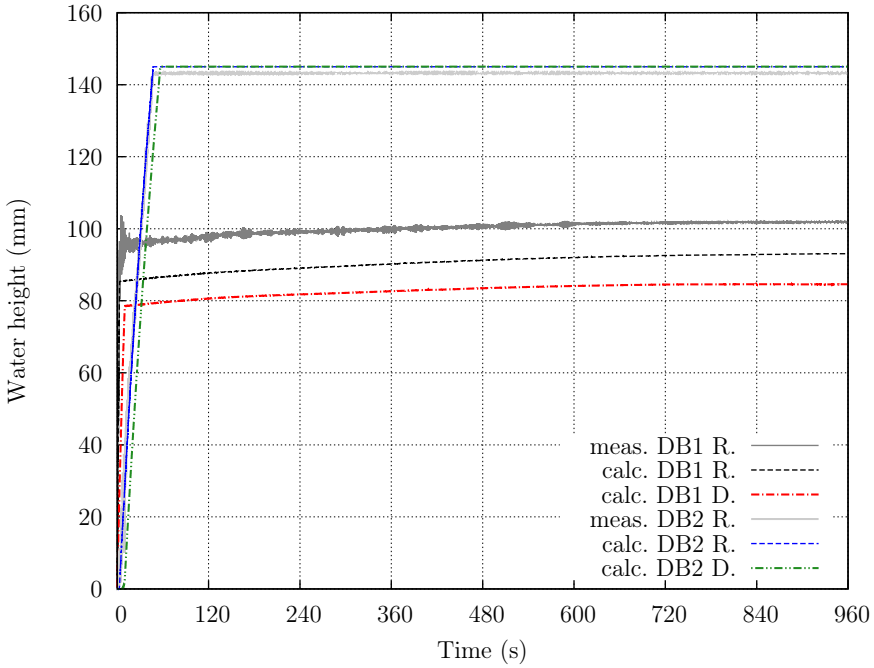


Figure 4.22: Model test case C - Water levels of the double bottom compartments

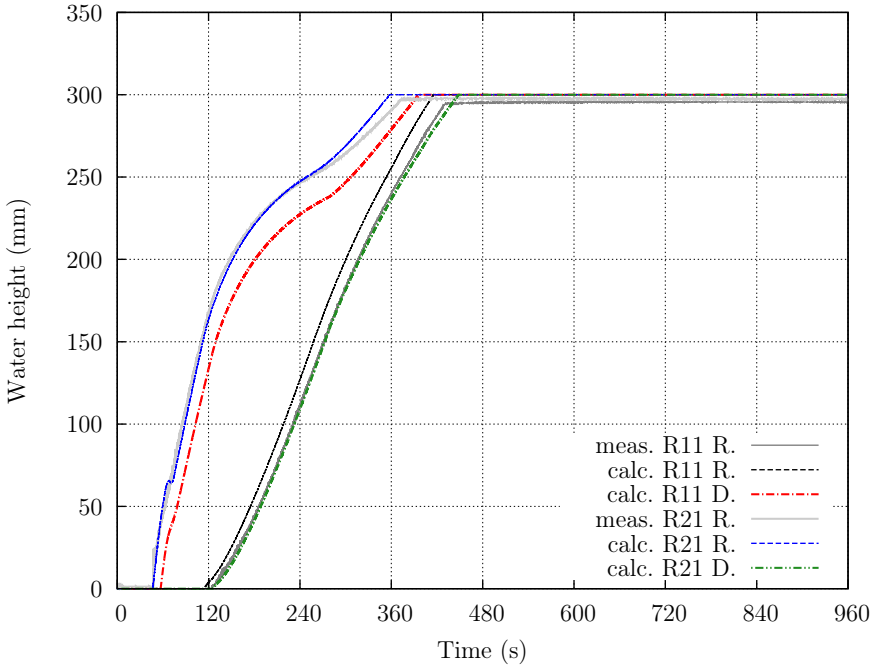


Figure 4.23: Model test case C - Water levels of the lower compartments

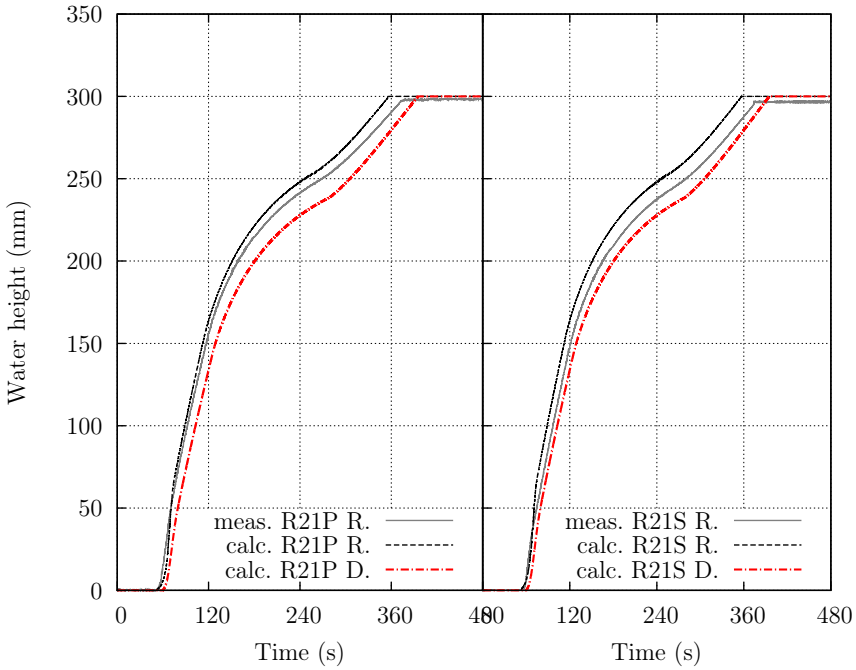


Figure 4.24: Model test case C - Water levels of the side compartments

This is also true for the flooding of the upper compartments, as shown in Figure 4.25. The flooding starts a few seconds later, since it already took some time for the water to fill up the lower parts of the model. The overall amount of flood water is slightly lower due to the overestimated pressure in DB1.

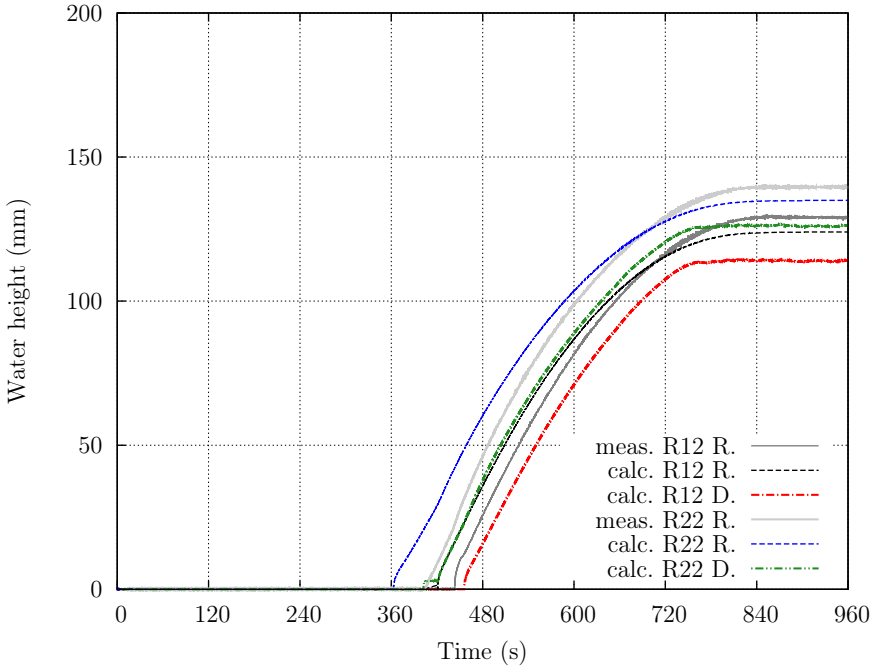


Figure 4.25: Model test case C - Water levels of the upper compartments

## 4.6 Full Scale Test

To investigate the influence of scale effects, the test case C is repeated with a computational model on the full ship scale resulting in a barge of 40 meters length, according to the model scale of 1:10. The geometry and the weights are scaled, while the non-dimensional discharge coefficients are kept constant.

At first, this allows to study if the computational method is independent of the scale of the data model. Secondly, the influence of the scale on effects like air compression (see for example Vassalos et al., 2004) and the time-to-flood can be studied. The results of the simulations performed with the full scale data model are scaled back to model size by applying Froude similarity.

The first result is that the trim motion for the full scale simulation fits even better to the measurement results, as can be seen in Figure 4.26. The same is true for the double bottom compartments, whose water levels are shown in Figure 4.27.

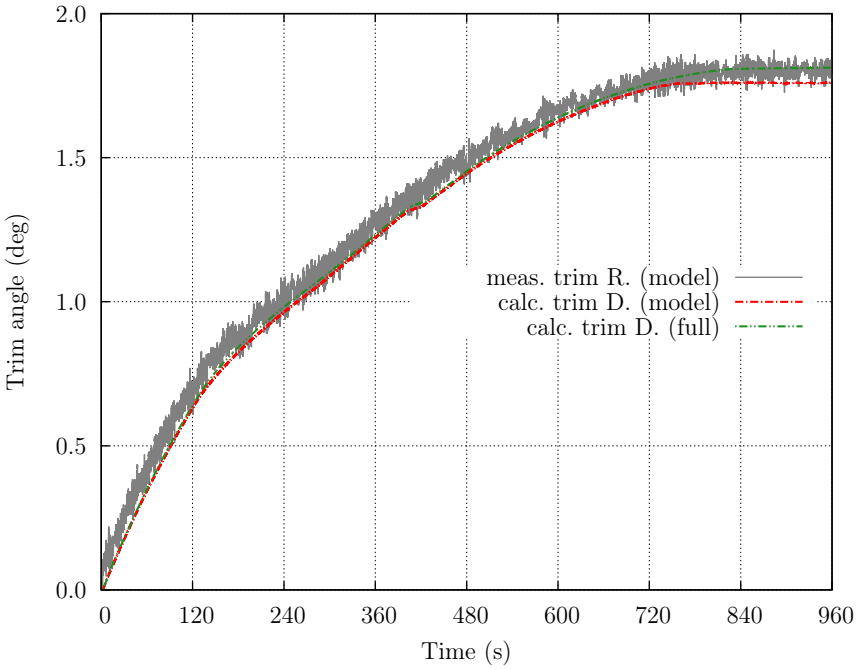


Figure 4.26: Full scale test case C - Trim motion

A second remarkable result is the fact that the model can be scaled for the simulations, which shows that the assumption of Froude similarity is valid in this case. The only difference occur for the cases in which air compression and air flow effects are relevant. In this specific case, the computed results fit the measurement results even better. This can be explained by the influence of air flow and the ventilation grade of the compartments. In model scale, the opening sizes are larger compared to the volume of the corresponding compartment leading to a higher ventilation grade compared to the relations in full scale. For this specific case, the ventilation grade of DB1 during the measurement of the model tests is comparable to the simulation of the full scale case under the assumption of no ventilation. Reasons for the higher grade of ventilation during the model tests than expected, are most likely transient effects during the initial flooding phase.

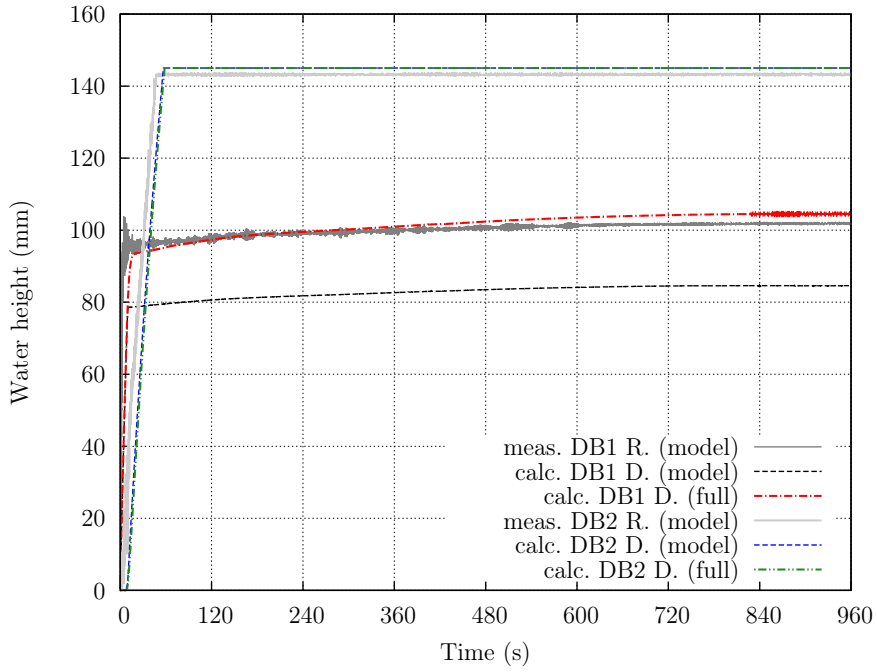


Figure 4.27: Full scale test case C - Water levels of the double bottom compartments

## 4.7 Conclusion of the Validation by Model Tests

The validation of the newly developed flooding method by comparing its results to the benchmark model tests as recommended by the ITTC for this type of problem has been successfully carried out. The time-dependent spreading of the flood water and the motion of the barge are correctly computed by the newly proposed method. The predictor-corrector integration scheme allows a comparable large time step. However, if the time step size is chosen too large, this results in non-physical results as shown in Figure 4.12. A recommended time step for the computation of model tests for the selected integration scheme is 0.1 seconds with air compression and 0.5 seconds, if air compression is not relevant. For full scale simulations, a time step of 1 second is an appropriate choice. A short convergence study is recommended in any case.

If the forming of air pockets has a significant influence on the overall flooding process, the time step has to be reduced to avoid instabilities in the numerical simulation. In addition, the influence of air flow is negligibly small, because the grade of ventilation is typically lower in full scale than in model scale, as discussed for test case C. On the other hand, the correct determination of the point in time when air compression starts, plays an important role, as shown for test case B.

Higher order integration schemes like Runge-Kutta methods might be contents of further research, especially if the influence of the air phase plays an important role. The air density is 1,000 times smaller than the water density and depends on the air pressure whereas water is usually assumed to be incompressible. In addition, air typically flows much faster than water. Thus, the coupling with the air phase requires a much smaller time step or a higher accuracy for the solution of the underlying equations.

# CHAPTER 5

# Accident Investigations

Three severe ship accidents, which were caused by the flooding of the watertight integrity of the vessels, will be investigated in the following to further validate the numerical flooding method. The selection of the chosen accidents depends on the available data material on the ships and the suitability of these cases to apply the newly developed flooding method.

The investigation of real practical problems is the best possibility to find further requirements for a numerical method. A result from a numerical simulation can better be judged upon its plausibility when its results are compared to examples, which have been experienced in the real world. Therefore, theses studies are intended to reveal the capabilities but also the limitations of the developed numerical code.

## 5.1 The European Gateway Accident

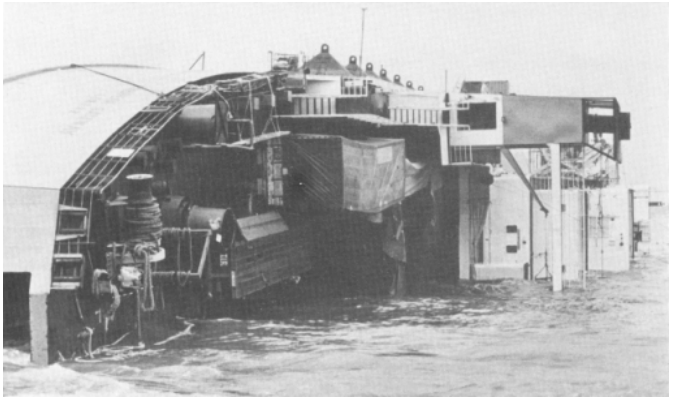

Figure 5.1: Photo of the grounded European Gateway after the accident (Harwich Lifeboat Station, 2010)

The accident of the European Gateway (see Figure 5.1) will be re-investigated with the described simulation method to validate the newly developed method and to increase the knowl-

edge about the details of the flooding events that finally lead to the loss of the ship. A short summary of this investigation is also published in Dankowski and Krüger (2012).

The accident occurred on Sunday, 19th December, 1982 close to the port of Harwich, United Kingdom, where the European Gateway collided with the Speedlink Vanguard ferry. The collision scenario of both vessels is shown in Figure 5.2. The bulbous bow of the Speedlink Vanguard caused a large damage to the starboard side shell of the European Gateway, which was located almost mid ship in longitudinal direction and below the waterline. This opening led to a sudden water ingress in the Auxiliary Engine Room. A second larger damage occurred above the waterline to the main vehicle deck caused by the upper bow section of the Speedlink Vanguard.

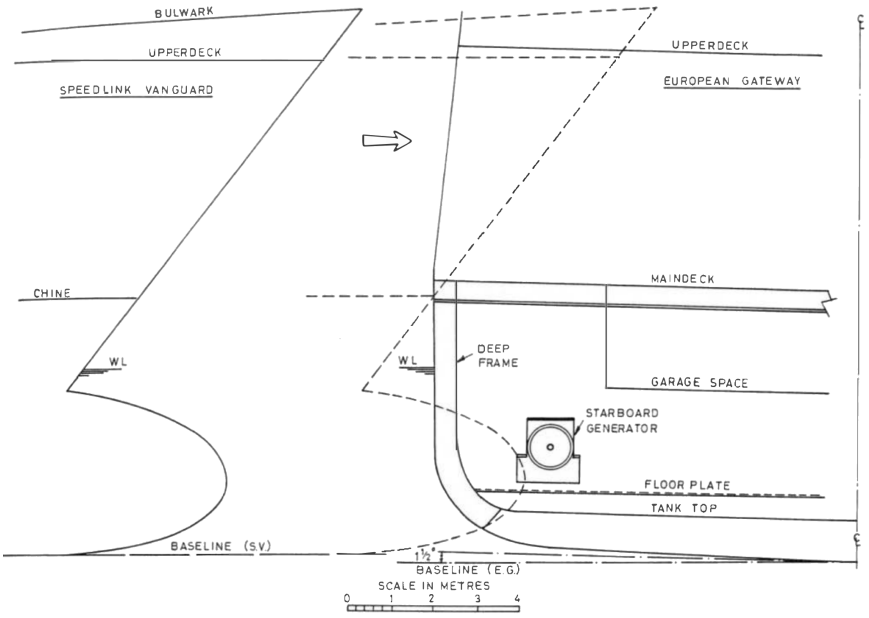


Figure 5.2: Collision scenario of the Speedlink Vanguard (side view) and the European Gateway (section view from forward) (Spouge, 1985)

The European Gateway capsized in less than three minutes in shallow water at a relative calm sea state with a wind speed of around 14 knots from astern (Spouge, 1985). Six people lost their lives and one person is still missing.

This accident is well suited for the validation of new methods, because it is well documented by several technical reports. In addition, the interesting effect of transient asymmetric flooding caused the sudden capsize of the ferry. It is important to investigate, if a new flooding simulation method is capable of modelling this complex failure mode. The immediate spreading of the flood water through the whole Auxiliary Engine Room was prevented by two generators in that compartment. The generators and other obstructions caused an asymmetric distribution of the flood water during the first transient phase of flooding. This is confirmed by one of the officers who saw a three feet high wall of water crossing the Auxiliary Engine Room from the starboard side, two to three seconds after the collision (NMI Ltd, 1983).

After a short review of previous investigations followed by a general description of the European Gateway and the loading condition during her last voyage, different scenarios of the accident will be investigated. First, the most likely scenario that led to the capsizing is simulated. In addition, the phenomenon of transient asymmetric flooding is further evaluated. At last, the influence of the watertight doors is discussed.

### 5.1.1 Previous Accident Investigations

For the formal investigation of the accident, two parties published technical reports. The first one was prepared on behalf of the Department of Transport by the National Maritime Institute (NMI), United Kingdom. In 1985 the British government merged NMI with the British Research Association to the today still existing British Maritime Technology (BMT) company. The program NMIFLOOD developed at the NMI was used to simulate the flooding process. The asymmetry of the flooding is taken into account by a manual shift of the centre of gravity of the flood water. The NMIFLOOD program was also used for the investigation of the HERALD OF FREE ENTERPRISE accident (Dand, 1988).

The German consultants SCHIFFKO were employed by the operator Townsend Thoresen (European Ferries) to investigate the accident. They computed the flooding of the vessel by a manual calculation of eight steps based on the current flood water situation in the compartments at each time step (Arndt, 1983). The asymmetry was taken into account by general assumptions on the flood water behaviour in the Auxiliary Engine Room. The Official Report of Court summarised the investigations of the court hearing in a formal matter. A year later, an additional technical paper by one of the NMI authors was published (Spouge, 1985).

The last technical paper on this accident (Santos et al., 2002) intents to validate the author's own flooding model by reproducing the capsizing event. To model the transient asymmetric flooding effect, the Auxiliary Engine Room is subdivided into two side and one centre compartment.

All relevant technical papers are listed in the following:

- Official Report of Court (unpublished)
- Report for the Department of Transport by NMI Ltd (1983)
- Report for the European Ferries company by Arndt (1983)
- Technical paper by Spouge (1985) published in Transactions of the Royal Institution of Naval Architects (RINA)
- Technical paper for the Ocean Engineering Journal by Santos et al. (2002)

### 5.1.2 General Description of the Vessel

The passenger ferry EUROPEAN GATEWAY was built in 1974 as hull number 2256 by the Schichau Unterweser Yard, Bremerhaven, Germany. At the time of the accident, it was operated by the British ferry company Townsend Thoresen serving the route from Felixstowe in the United Kingdom to Zeebrugge in Belgium. The main particulars are listed in Table 5.1.

Table 5.1: Main particulars of the EUROPEAN GATEWAY

| | | |
|---|---|---|
| Length over all | $L_{\mathrm{OA}}$ | 133.46 m |
| Length between perpendiculars | $L_{\mathrm{PP}}$ | 122.85 m |
| Breadth Moulded | $B$ | 19.90 m |
| Depth to Upper Vehicle Deck | $H_1$ | 11.65 m |
| Depth to Main Vehicle Deck | $H$ | 6.30 m |
| Draught Design | $T$ | 5.80 m |
| Service Speed | $V_S$ | 18.50 kn |

A photo of the vessel in service is shown in Figure 5.3. A more detailed description of the vessel is published for example in Doskocil and Thomsen (1976).


Figure 5.3: Photo of the European Gateway (Thornton, 2012)

The ship data model consists of the hull form and the inner subdivision. It is derived from original drawings provided by the yard and the operator and supported by the data published in Doskocil and Thomsen (1976). The original damage control plan is shown in Figure 5.5.

After the salvage, the European Gateway was repaired and put back in service on several routes. In recent years she served as the Penelope a route between Greece and Italy until April 2011 before she was chartered to MARFAMAR and now serves routes in North Africa. A photo of the vessel from 2011 is given in Figure 5.4.


Figure 5.4: Photo of the Penelope in Drapetsona, Greek on 24th October 2011 (Brekas, 2011)

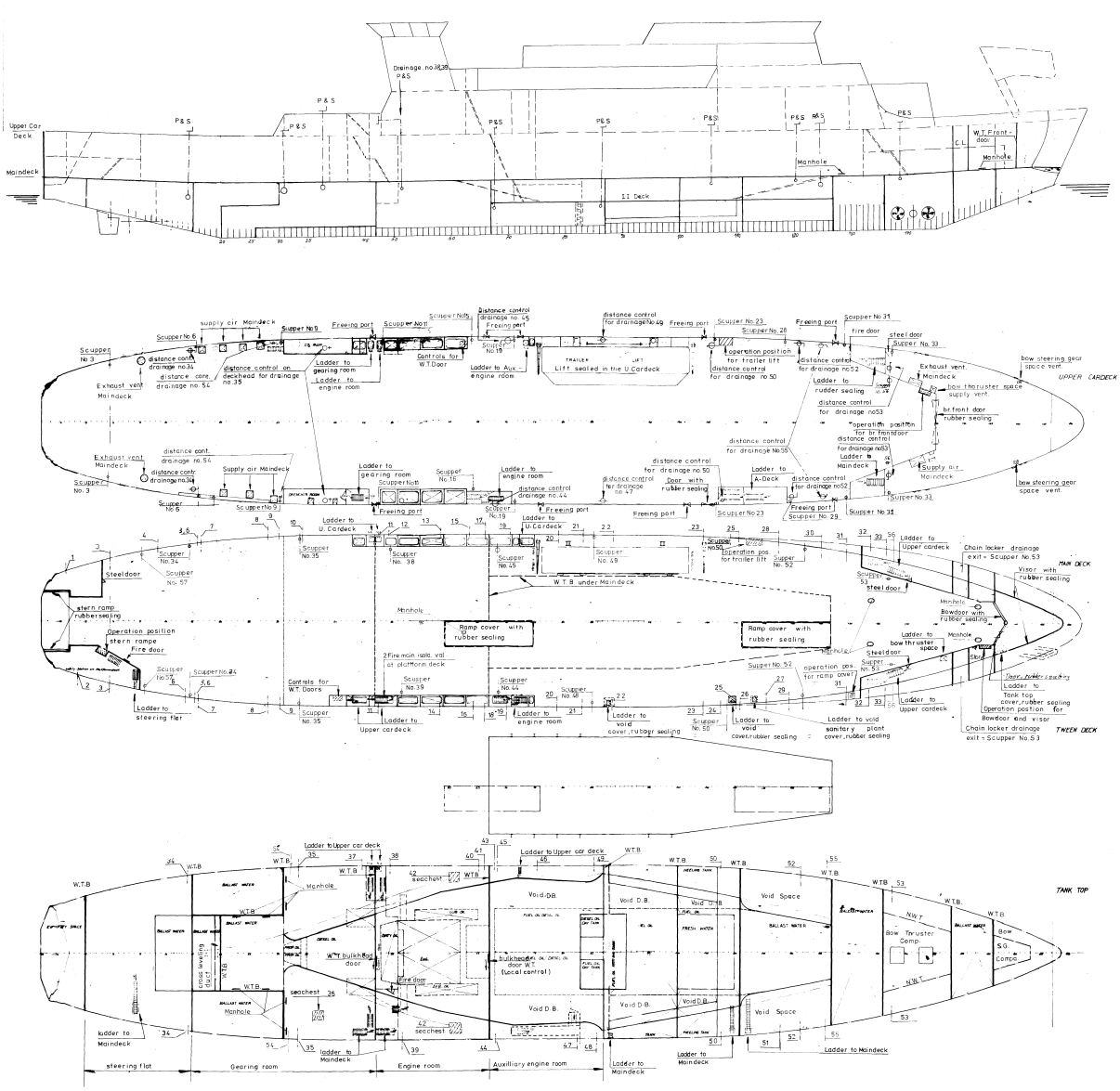


Figure 5.5: Original damage control plan of the EUROPEAN GATEWAY obtained from the Yard's drawing archive

### 5.1.3 Final Voyage Condition

The final loading condition of the EUROPEAN GATEWAY on her last voyage is taken from Spouge (1985) and summarised in Table 5.2. The corresponding intact lever arm curve is shown in Figure 5.6.

### 5.1.4 Critical Openings and Flooding System

The damage of the hull caused an opening to the Auxiliary Engine Room and small holes in the double bottom compartment. In addition, the side shell of the main vehicle deck was penetrated resulting in a large side hole above the main deck. The dimensions and the locations of the large damages to the side shell are derived from drawings published in Spouge (1985). The

Table 5.2: Loading Condition of the EUROPEAN GATEWAY at the time of the accident

| | |
|---|---|
| Shell Plating Factor | 1.004 - |
| Density of Sea Water | 1.020 t/m$^3$ |
| Ships Weight | 6578.105 t |
| Longit. Centre of Gravity | 56.379 m.b.AP |
| Transv. Centre of Gravity | -0.056 m.f.CL |
| Vertic. Centre of Gravity (Solid) | 7.743 m.a.BL |
| Free Surface Correction of V.C.G. | 0.740 m |
| Vertic. Centre of Gravity (Corrected) | 8.483 m.a.BL |
| Draft at A.P (moulded) | 4.881 m |
| Draft at LBP/2 (moulded) | 4.381 m |
| Draft at F.P (moulded) | 3.881 m |
| Trim (pos. fwd) | -1.000 m |
| Heel (pos. stbd) | 1.500 Deg. |
| Volume (incl. Shell Plating) | 6449.123 m$^3$ |
| Longit. Centre of Buoyancy | 56.330 m.b.AP |
| Transv. Centre of Buoyancy | -0.212 m.f.CL |
| Vertic. Centre of Buoyancy | 2.523 m.a.BL |
| Area of Waterline | 1982.097 m$^2$ |
| Longit. Centre of Waterline | 54.092 m.b.AP |
| Transv. Centre of Waterline | -0.209 m.f.CL |
| Metacentric Height | 2.130 m |

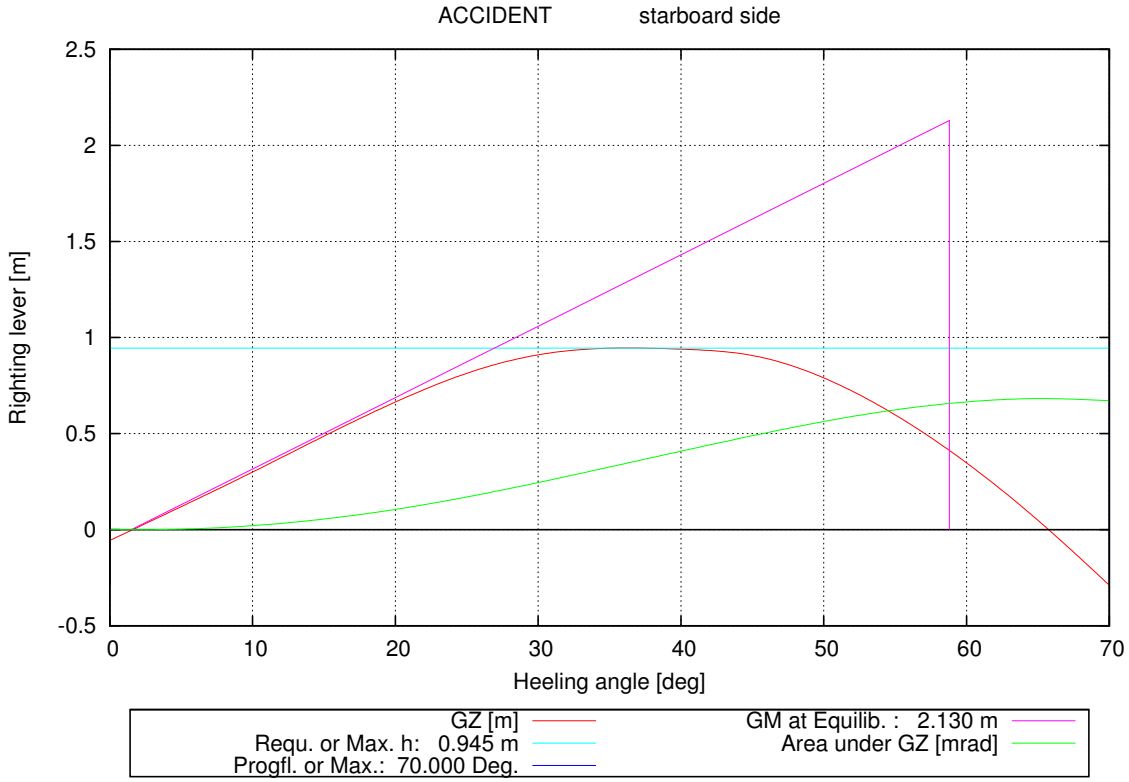


Figure 5.6: Intact lever arm curve of the EUROPEAN GATEWAY

arrangement of the compartments together with the location and size of the damage is shown in Figure 5.7. The flooding paths are illustrated as a graph in Figure 5.8. The most important internal openings are the three watertight doors connecting the Pump Room, the Main Engine Room, the Auxiliary Engine Room and the Stabiliser Room.

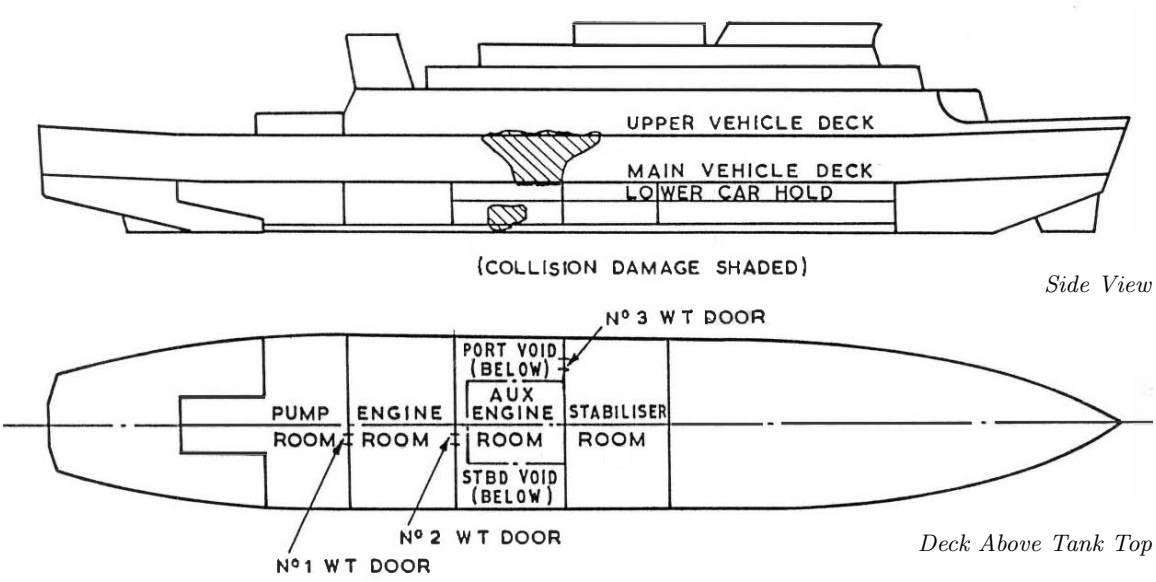


Figure 5.7: Location of the openings and the relevant compartments of the European Gateway (NMI Ltd, 1983)

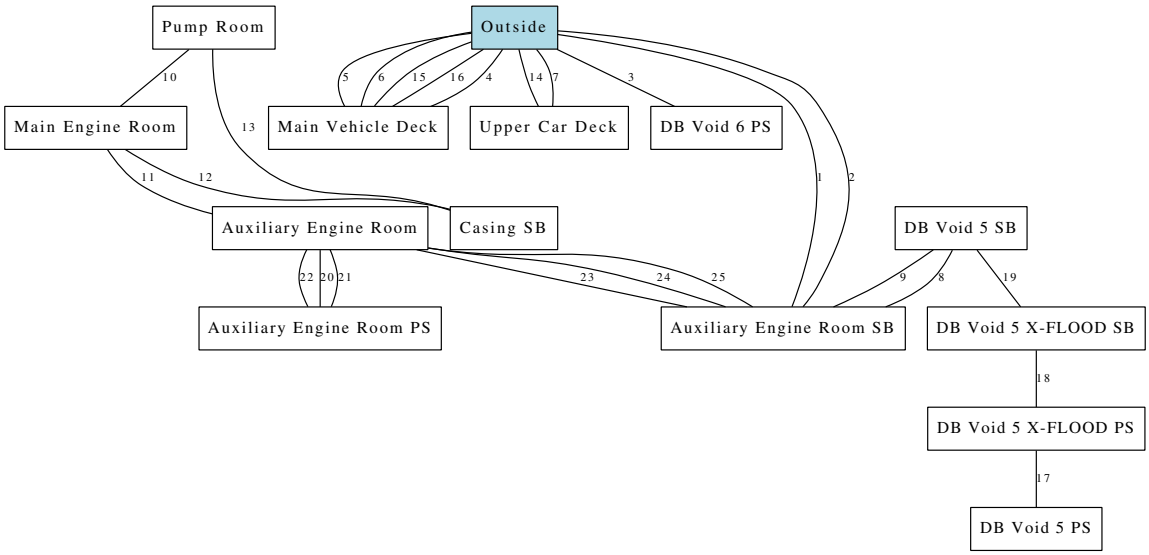


Figure 5.8: Flooding graph of the European Gateway

### 5.1.5 Most Likely Scenario of the Accident

As a first application of the new simulation method, the most likely scenario of the capsizing is investigated and the results are compared to the previous reports. The assumptions are as follows:

1. An initial heel of 1.5 degrees to the starboard side is assumed to be representative for any additional heeling moments caused for example by wind, collision forces and further dynamic effects as described in more detail in Spouge (1985).
2. The asymmetric transient flooding of the Auxiliary Engine Room is modelled by subdividing the compartment into two side and one centre part, which are connected by openings in the same matter as described in Santos et al. (2002). A discharge coefficient of $C_d = 0.2$ is assumed for these openings.
3. The three watertight doors are assumed to be left open during the whole flooding process.

The developments of the heel angle over time obtained by the different authors compared to the results from the new method are shown in Figure 5.9 together with three observations of the crew marked as black dots. In addition, the metacentric height $\overline{\mathrm{GM}}$ is shown on the right vertical axis to control the stability of the vessel during the flooding process.

The time of grounding is estimated by computing the minimum freeboard of the lowest point of the hull. The water depth at the accident location was around 9.7 m (Spouge, 1985, page 61), which is reached by the lowest point after around three minutes.

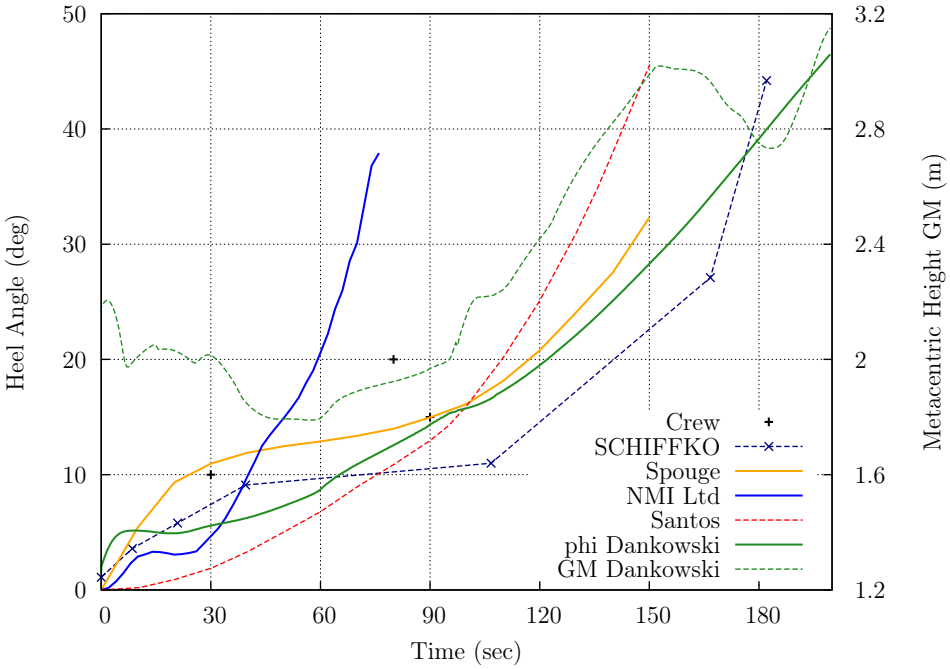


Figure 5.9: Comparison of the heel angle development during the accident of the EUROPEAN GATEWAY issued by different authors

In general, the new method reproduces the heeling over time well. The results are located in between the values of the previous investigations. The sudden heel right at the beginning in the first 30 seconds is not as large as predicted by SCHIFFKO or Spouge, but this can be explained by the fact that they introduced a manual shift of the centre of gravity to account for the asymmetric flooding. Compared to Santos, who used the same asymmetric modelling, the first part of the computed heel angle obtained with the new method matches the observation better. After the sudden heeling, a phase of 90 seconds with a slower increase of heel follows. At around two minutes, the damage to the main deck becomes submerged, which accelerates the heel increase further until the ship runs aground only three minutes after the collision at a heel angle of around 40 degrees.

The metacentric height shows a reasonable stability of the vessel above 1.6 m during the whole flooding process. In the first minute it decreases when large transient free surfaces are developed in the lower compartments. After this point, the value increases again due to the decrease of the overall vertical centre of gravity. The metacentric height slightly decreases again after 150 seconds when the upper decks are submerged.

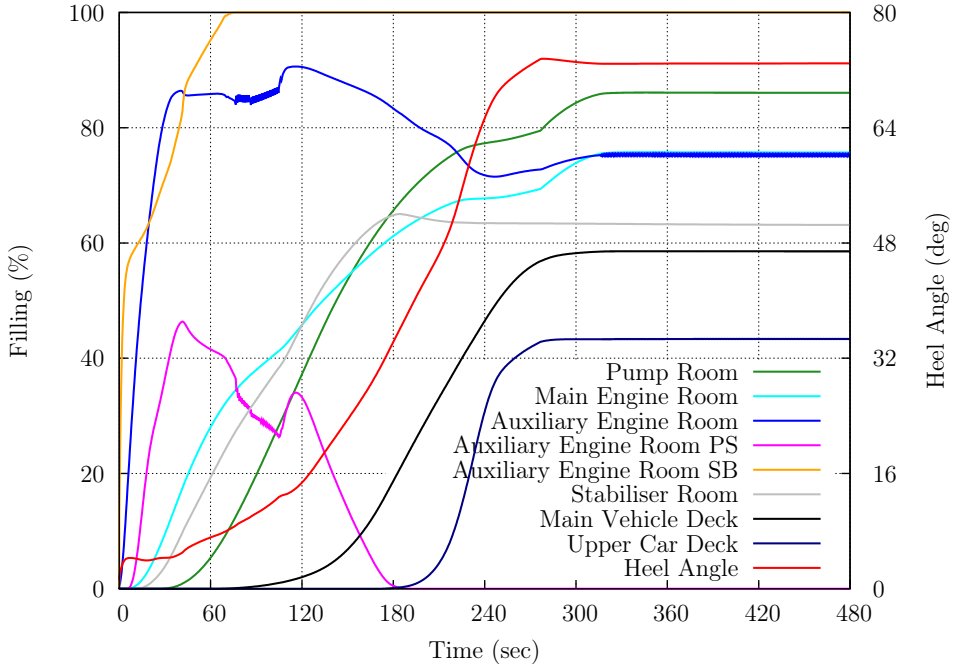


Figure 5.10: Simulated filling levels and heeling over time during the accident of the EUROPEAN GATEWAY

If the simulation is not stopped after the grounding, the ferry comes to rest on its side at a heel angle of around 75 degrees. In Figure 5.10 the filling levels of the different compartments together with the heeling angle are shown over a time period of six minutes assuming that no grounding occurred. It is remarkable that only the starboard Auxiliary Engine Room is completely filled. Due to the large and fast list, water flows back from the port side part of this compartment after around 40 seconds. After three minutes, this compartment becomes empty again, while at the same time the upper deck is flooded. A slower increase of the heeling angle by a more symmetric flooding would probably have resulted in a deeper submerging of the ship caused by a larger amount of water ingress. This would have delayed the whole flooding sequence, even though the overall flood water ingress at the final stage would have been larger.

### 5.1.6 Transient Asymmetric Flooding

The sudden and large heel angle was explained in the previous investigations with the phenomenon of transient asymmetric flooding of the symmetric Auxiliary Engine Room. This fact is enforced by the observation of the crew who saw a “wall of water” spreading across that room (NMI Ltd, 1983).

The transient effect of flood water accumulation on the damaged side of the Auxiliary Engine Room can be modelled by an additional inclination of the water surface in this room, a manual shift of the flood water centre or by an artificial subdivision of the compartment. The latter

was suggested by Santos et al. (2002) and is also used in the current model, because it is best motivated by the real physical behaviour of the flood water: The first transient phase of flooding through a large opening can be compared to a dam-break problem. The propagation velocity of the breaking front is mainly influenced by the water height difference. This is similar to obstruct the water spreading at certain discrete points with artificial walls. The velocity through these walls is also mostly driven by the water height differences on both sides.

The section 70 of the Auxiliary Engine Room is shown in Figure 5.11, which is a part of the general arrangement drawing. The subdivision modelling with regard to the two generators in this room as defined in the computational data model is shown in Figure 5.12. Both figures are section views at the aft end of this compartment looking forward.

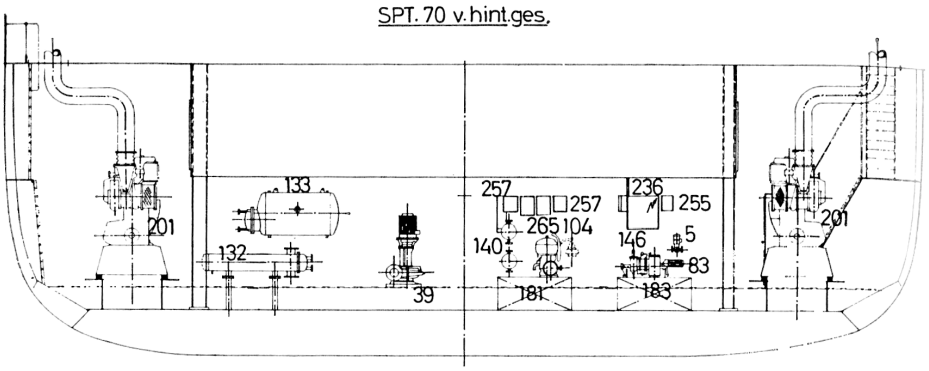


Figure 5.11: View of section 70 of the Auxiliary Engine Room of the European Gateway (Doskocil and Thomsen, 1976)

In the illustration of the computational data model in Figure 5.12, the hull is shown in grey and the openings as filled rectangles in transparent grey. The hydrostatic sections of the compartments are illustrated by lines, the starboard part is shown in green, the centre part of the Auxiliary Engine Room in blue. The generators are modelled as negative sub-spaces coloured in red. The other halve of the port side generator belongs to the port side compartment, which data model is not shown here.

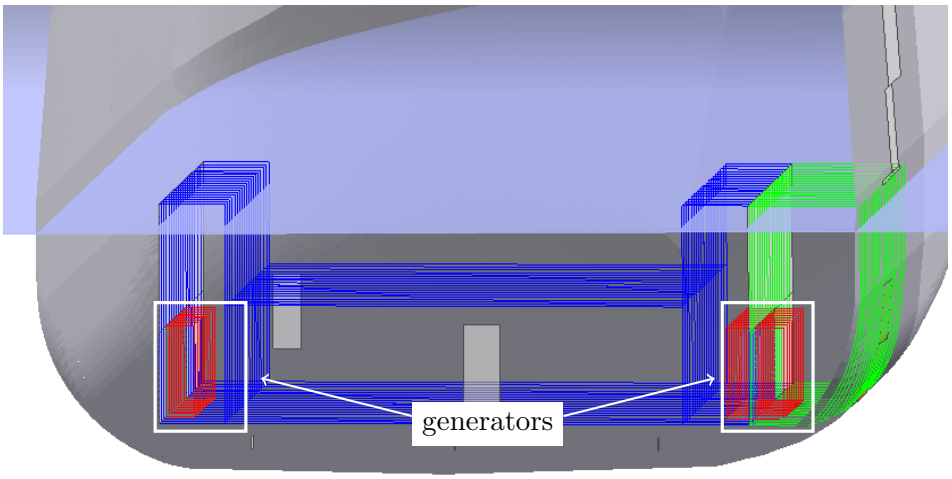


Figure 5.12: Cross-section view of the Auxiliary Engine Room of the European Gateway in the computational data model

Furthermore, another small asymmetry is present in the flooding system. The double bottom compartment below the generators also has small holes below the starboard generator. These holes were caused by the movement of the starboard generator that led to a rupture of the tank top below the engine foundation. The double bottom compartment consists of two side compartments that are connected by a cross-flooding duct. Even though previous investigations mentioned that the influence is small (Spouge, 1985), it is included in the current model by sub-dividing the double bottom compartment and connecting the sub-compartments with openings.

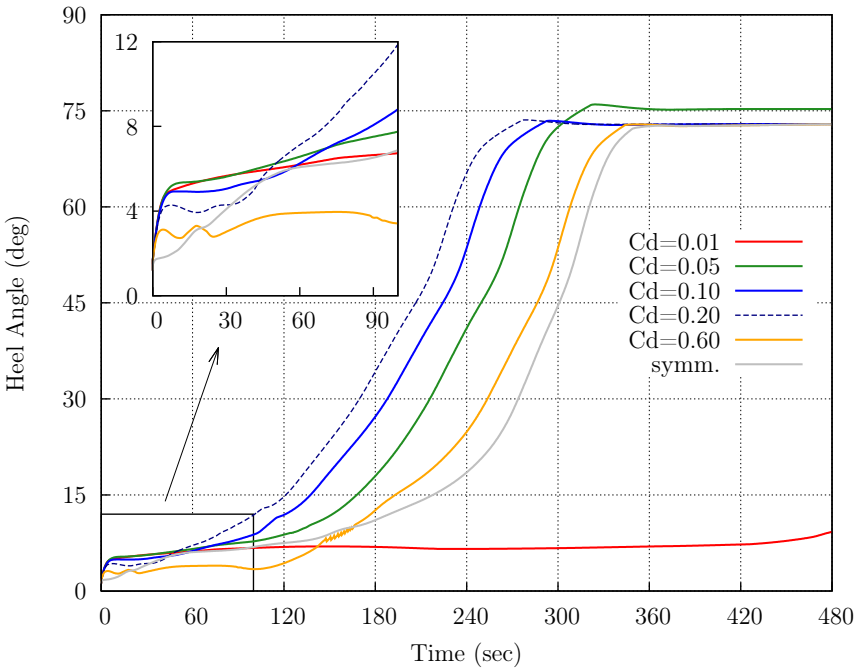


Figure 5.13: Heeling over time of the European Gateway for different discharge coefficients of the artificial walls

To further investigate the transient flooding effect, the discharge coefficient for the artificial walls around the generators is varied. The results of this variation study are shown in Figure 5.13. In addition, the subdivision of the compartment is removed to simulate the symmetric case, which is marked in the plot with "symm.".

The most interesting result of this study is that the symmetric case also leads to a rapid capsize, even though the sudden increase of heel is not that strong and the whole flooding sequence is delayed. However, a small asymmetry still exist in this damage case, which is caused by the already mentioned damage to the double bottom compartment with its cross-flooding duct and the assumed initial heel angle of 1.5 degrees to account for any external heeling moments. The newly developed numerical method is feasible to resolve this small asymmetry. Even without a further subdivision of the Auxiliary Engine Room, the resulting rapid capsize of the vessel is correctly predicted.

However, it is also true that the fast heel increase in the first seconds can only be resolved if the Auxiliary Engine Room is subdivided in one centre and two side compartments. For the smallest discharge coefficient of the artificial walls of $C_d = 0.01$, the heel angle does not exceed more than eight degrees. Values above 0.01 lead to the observed fast capsizing, while a larger discharge coefficient results in a faster heel angle development. This behaviour changes for a

discharge coefficient of $C_d = 0.6$, which is more similar to the symmetric flooding case. Both cases lead again to a delay of the heel angle increase compared to smaller values of $C_d$.

There are two contradicting factors leading to this behaviour: A small discharge coefficient increases the asymmetry of the flooding by preventing the water from immediately spreading through the whole compartment, while a large discharge coefficient accelerates the overall flood water ingress. The water can leave the starboard part of the Auxiliary Engine Room subjected to the damage faster, what, at the same time, prevents the water level inside the ship from becoming equal to the outside water level. This means that discharge coefficients for these artificial openings have to be selected carefully to appropriately model the transient asymmetric flooding effect.

### 5.1.7 Closure of Watertight Doors

During the investigation of the accident, the question arose whether a faster closure of the watertight doors would have prevented the capsizing. This issue has also been investigated in NMI Ltd (1983) in more detail. The results obtained with the present method are illustrated for three different setups in Figure 5.14:

1. Watertight door number 3 closed
2. Watertight door number 2 closed
3. All three doors closed within 20 to 50 seconds

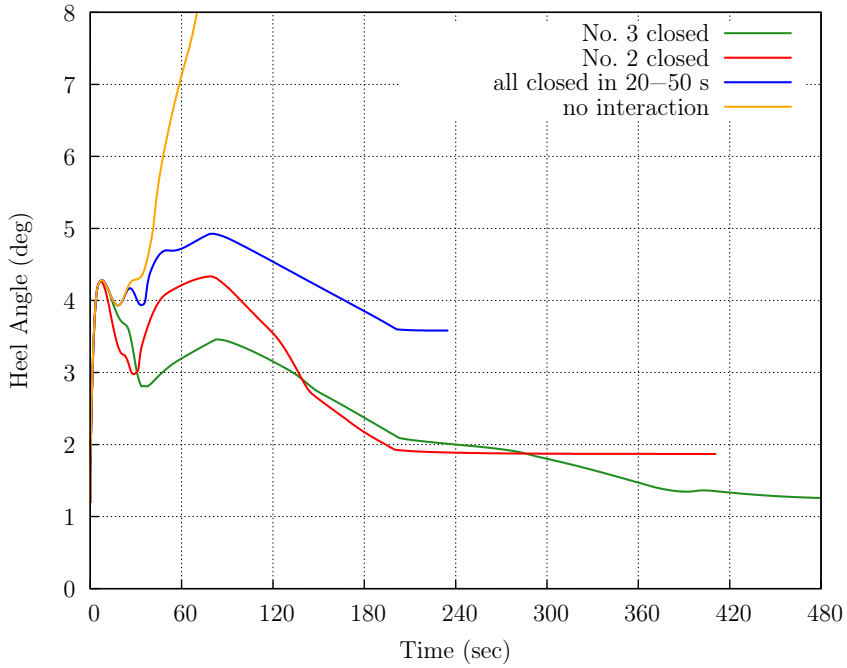


Figure 5.14: Heel angle development for three different watertight door closing scenarios

If door number 3 is closed from the beginning, the ship reaches a stable state after around eight minutes. This stable state is reached after only four minutes, if door number 2 were closed. The final heel angle is slightly larger for the third investigated scenario, when all doors are closed automatically within 30 seconds after an initial response time of 20 seconds. In this scenario a stable equilibrium is reached after around three minutes.

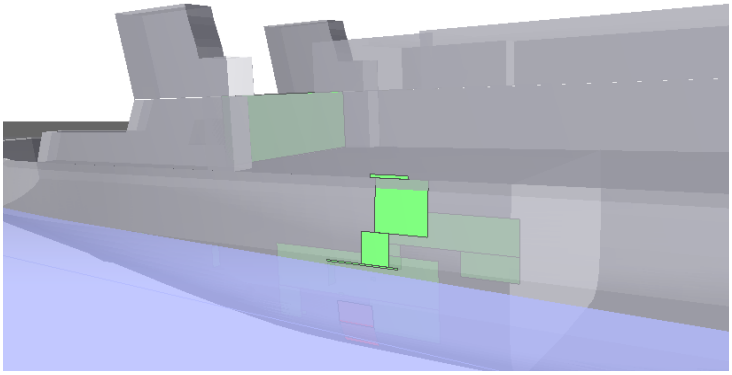

Figure 5.15: Final floating position with watertight door number 3 closed

However, this stable state bears the risk that the upper damage to the main deck has only a very small freeboard to the mean surrounding water surface (see Figure 5.15). Any wave or small dynamic motion would lead to a flooding of the main deck and an immediate capsize of the ship. The closure of the doors would probably only have delayed the capsize, but this might have been sufficient to avoid some of the casualties. The same conclusion has also been drawn by the Report of Court based on the technical investigation of NMI Ltd (1983). It should be noted, that current regulations require that watertight doors must be capable of being closed in not more than 60 seconds (IMO, 2009, Chapter II-1, Part B-2, Regulation 13, paragraph 5.1).

The key issue that led to the sudden and severe capsize, was the flooding of the main deck. However, the flood water ingress through the large side damage to the main deck was only possible, because of the combination of the initial heel angle, which was caused by the transient asymmetric flooding, and the reduced freeboard. This submerging was caused by the flooding of buoyancy volume in the lower parts of the ship, which are only accessible through left open watertight doors.

### 5.1.8 Summary of the Investigation

The accident with all major effects has been successfully computed with the proposed numerical simulation method. The very fast capsize of the European Gateway is accurately computed by the new method. The effect of transient asymmetric flooding can be modelled by an artificial subdivision of the relevant compartments. However, also very small asymmetries in the flooding system are appropriately taken into account by the flooding simulation.

The main cause of the accident was found to be the combination of a lower side damage followed by a transient asymmetric flooding together with the submerging of the main vehicle caused by the upper damage. It should be noted, that a similar pattern of heel angle development, though at an increased flooding time, has been presented in Papanikolaou et al. (2003) for the investigation of the Express Samina accident.

Potential improvements to avoid this kind of accidents in the future are a larger freeboard of the main deck and an improved closure policy of watertight doors. In addition, the buoyancy reserve of the upper car deck can for example be improved by a small double side shell located on parts of the main deck. This would at the same time improve the capability to withstand collisions, which lead to a water ingress. Furthermore, any possible asymmetries of the inner subdivision of ships should be avoided, even though these asymmetries might be small and not very obvious at first sight.

## 5.2 The S.S. Heraklion Accident

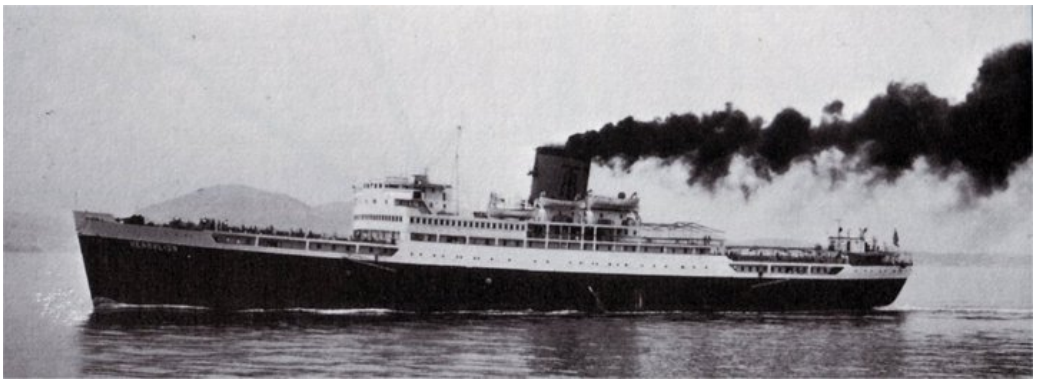

Figure 5.16: Photo of the S.S. Heraklion (via E-Mail from Sklavenitis, 2011)

The S.S. Heraklion capsized and sank in heavy weather conditions on 8th December, 1966 in the Aegean Sea on its voyage from Crete to Piraeus causing the loss of over 200 people's life. A photo of the vessel on voyage is shown in Figure 5.16. The last route of the vessel is shown in Figure 5.17. The accident happened close to the island of Milos and Ananes.

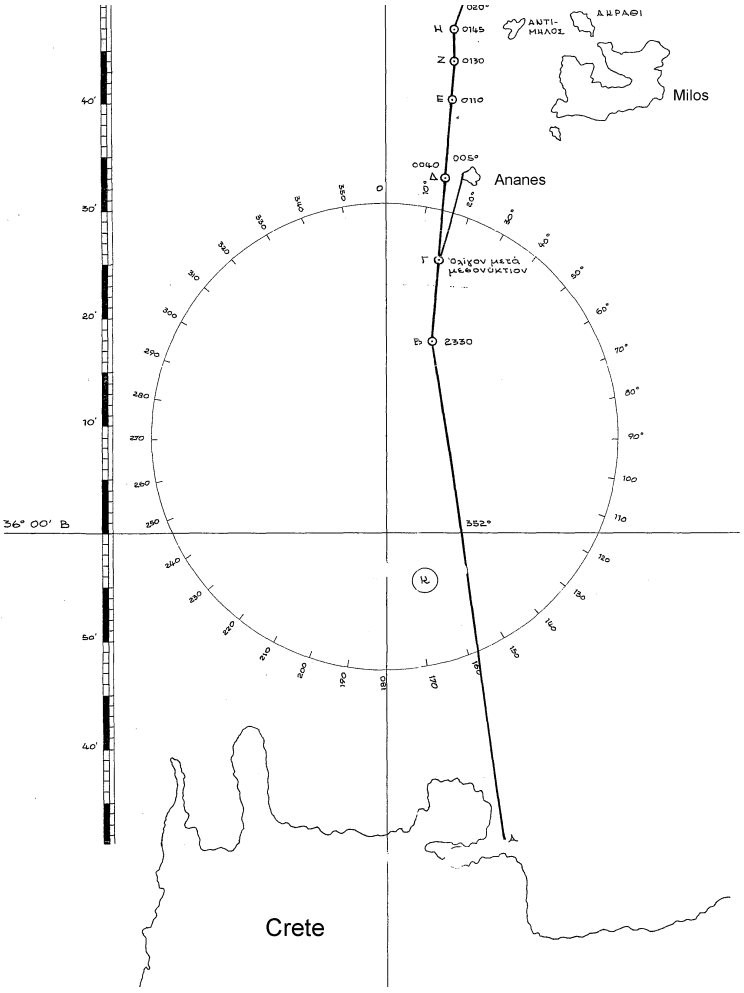


Figure 5.17: Route of the last voyage of the Heraklion

According to former investigations, the main cause of the accident was a a transversely stowed, 34 tons large reefer truck on the vehicle deck, which started to move in rough sea conditions leading to the damaging and loss of a large side door. The resulting water ingress and the large scale flooding of the car deck led to the capsize and finally to the sinking of the vessel. This accident is likely to be one of the first ferry accidents caused by the water-on-deck phenomenon.

The focus of this investigation is to describe the general flooding events after the loss of the side door. Even though the accident occurred in heavy weather leading to large ship motions, the general rough flooding events can be described by the quasi-hydrostatic flooding simulation in the time domain, as presented in the following.

### 5.2.1 General Description of the Vessel

The ship was originally built as the S.S. LEICESTERSHIRE by the Fairfield Shipbuilding and Engineering Company in Glasgow, Scotland, in 1949 as hull number 2562 to operate the UK to Burma route as a combined passenger and cargo ship. It was later converted to a passenger ferry, which was sailing on routes in the Aegean Sea. Her main particulars are given in Table 5.3.

Table 5.3: Main particulars of the HERAKLION

| | | |
|---|---|---|
| Length over all | $L_{\mathrm{OA}}$ | 146.46 m |
| Length between perpendiculars | $L_{\mathrm{PP}}$ | 143.26 m |
| Breadth Moulded | $B$ | 18.29 m |
| Depth to Upper Deck | $H_1$ | 10.83 m |
| Depth to Main Vehicle Deck | $H$ | 5.35 m |
| Draught Design | $T$ | 4.53 m |
| Service Speed | $V_S$ | 17.00 kn |

### 5.2.2 Previous Accident Investigations

The available documents from previous investigations are listed in the following:

- Official Accident Report (Fragoulis, 1967)
- Official Report of the Accident Investigation Board (Hellenic Maritime Accident Investigation Board, 1968)
- Additional Accident Report (Georgiadis and Antoniou, 1968)
- Accident Report (Wendel, 1970)
- Technical Drawings by the Naval Architect A. Theodoridis, Piraeus, May 1965

Based on these documents, the ship data model and the accident situation is reconstructed. The general arrangement drawing composed from the available technical drawings is shown in Figure 5.18. In addition to the previous investigations, as an outcome from a cooperation with the Ship Design Laboratory of the National Technical University of Athens (NTUA-SDL), further aspects of the accident have recently been investigated in Papanikolaou et al. (2012) and Krüger et al. (2012).

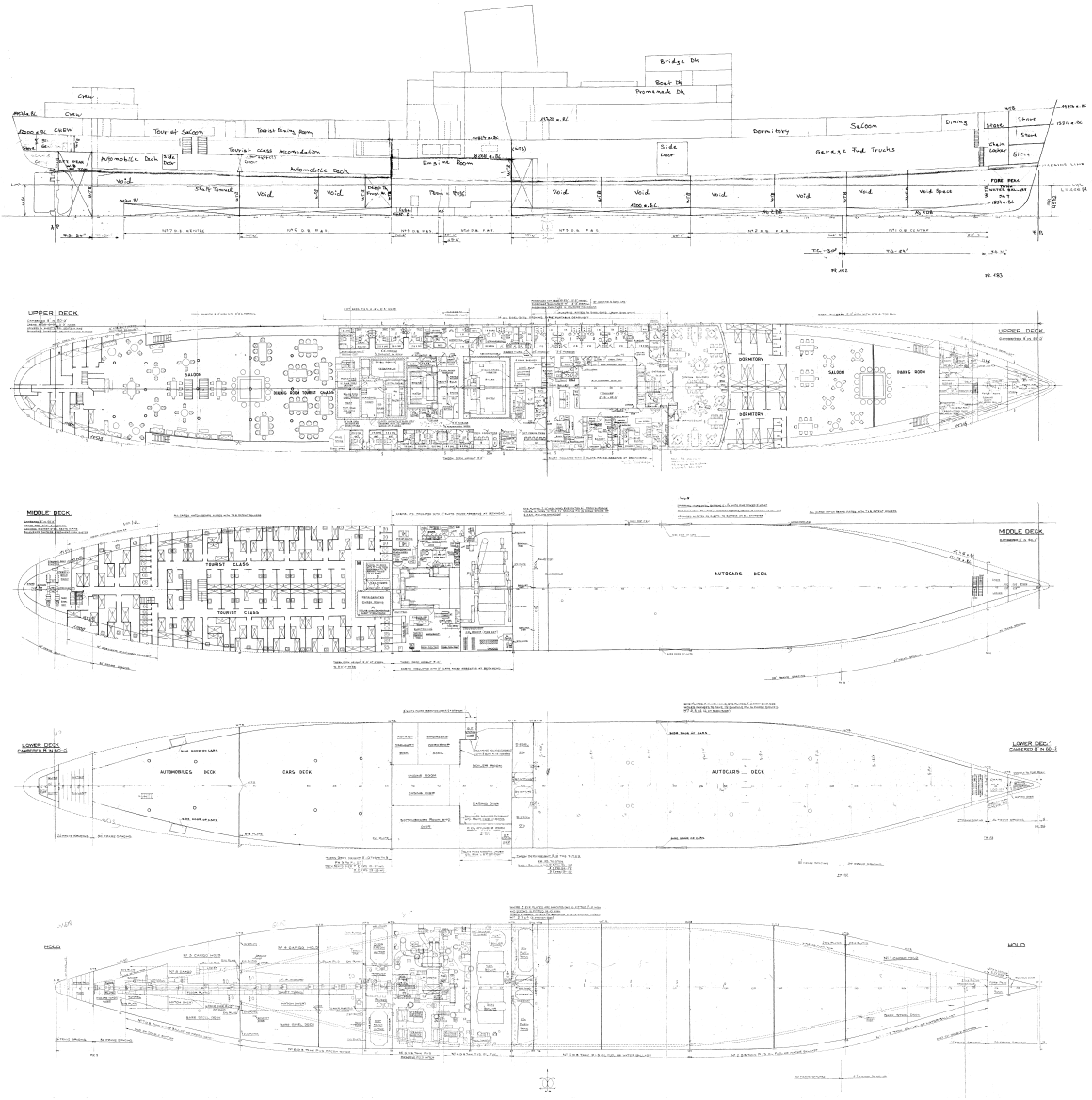


Figure 5.18: Side and deck views of the HERAKLION

### 5.2.3 Final Voyage Condition

The loading condition during the final voyage is thoroughly reconstructed in cooperation with the NTUA-SDL, based on the information provided in the accident reports and the capacity plan. In addition, the heeling moment due to wind pressure and the cargo shift as described in Wendel (1970) led to a heeling angle of approximately 11.5 degrees. These additional heeling moments are modelled as a transverse shift of the centre of gravity, which is equivalent to a cosine shape heeling lever. The condition of the vessel prior to flooding is summarised in Table 5.4 together with the intact lever arm curve shown in Figure 5.19.

For the flooding simulation, the whole buoyancy body of the ship including all superstructures has to be modelled, even though these parts are not water- nor weather tight according to the regulations. However, in the scope of flooding simulations, these parts have to be included, because they may contribute to the buoyancy volume, at least for a limited period of time.

Table 5.4: Loading condition of the HERAKLION prior to sinking

| | |
|---|---|
| Shell Plating Factor | 1.006 - |
| Density of Sea Water | 1.025 t/m$^3$ |
| Ships Weight | 7546.962 t |
| Longit. Centre of Gravity | 67.369 m.b.AP |
| Transv. Centre of Gravity | -0.197 m.f.CL |
| Vertic. Centre of Gravity (Solid) | 7.714 m.a.BL |
| Free Surface Correction of V.C.G. | 0.079 m |
| Vertic. Centre of Gravity (Corrected) | 7.793 m.a.BL |
| Draught at A.P (moulded) | 6.021 m |
| Draught at LBP/2 (moulded) | 4.434 m |
| Draught at F.P (moulded) | 2.847 m |
| Trim (pos. fwd) | -3.173 m |
| Heel (pos. stbd) | 11.500 Deg. |
| Volume (incl. Shell Plating) | 7362.890 m$^3$ |
| Longit. Centre of Buoyancy | 67.254 m.b.AP |
| Transv. Centre of Buoyancy | -1.232 m.f.CL |
| Vertic. Centre of Buoyancy | 2.704 m.a.BL |
| Area of Waterline | 1982.864 m$^2$ |
| Longit. Centre of Waterline | 69.183 m.b.AP |
| Transv. Centre of Waterline | -1.231 m.f.CL |
| Metacentric Height | 1.128 m |

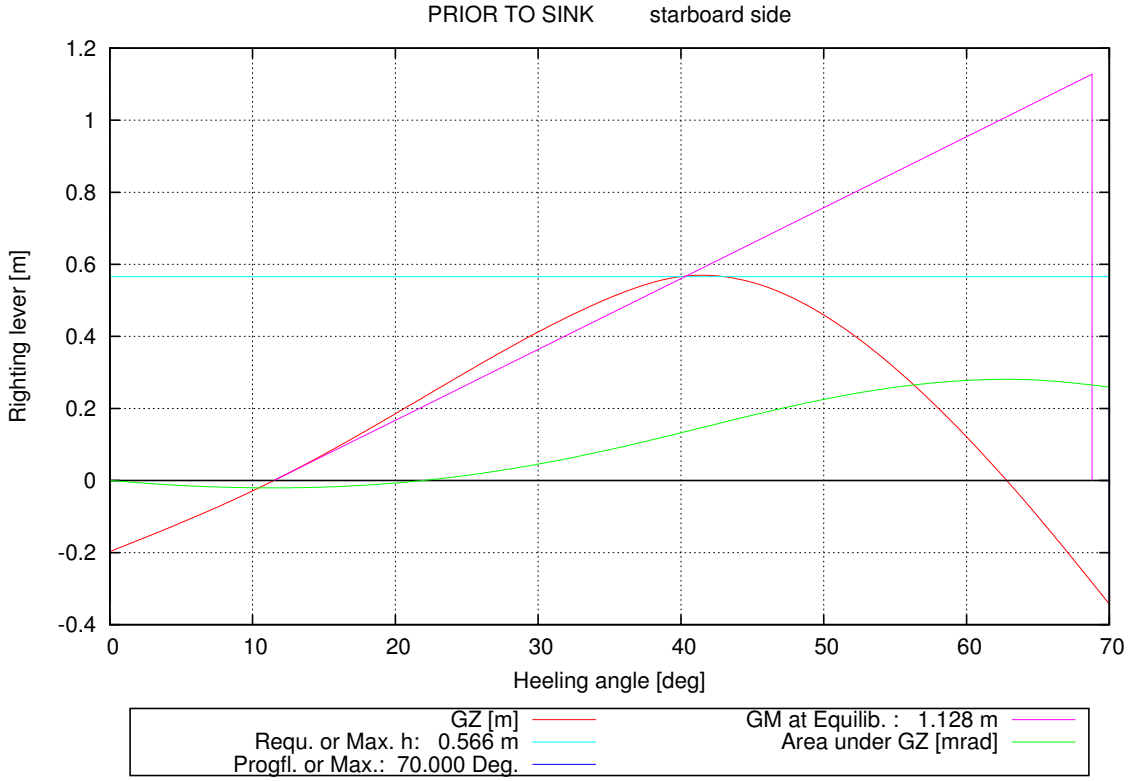


Figure 5.19: Intact lever arm curve of the HERAKLION prior to sinking (including shift of transverse centre of gravity)

In addition, all relevant internal and external openings, like windows and doors on the upper deck, are considered. Pressure head conditions for the collapse of some of the openings are added, while others are assumed to withstand no water pressure at all. A total number of 96 openings are defined, connecting 78 compartments, including the ones on the upper decks.

An illustration of the computational model including all openings is shown in Figure 5.20. Important openings are the large side door of the vehicle deck leading to the first initial water ingress and the side openings on the upper decks relevant for the later phase of flooding. The small windows on the upper decks are represented by several large and narrow openings with a relatively low discharge coefficient. In addition, parts of the upper deck are further subdivided in transverse direction to prevent unrealistic large free surfaces to occur.

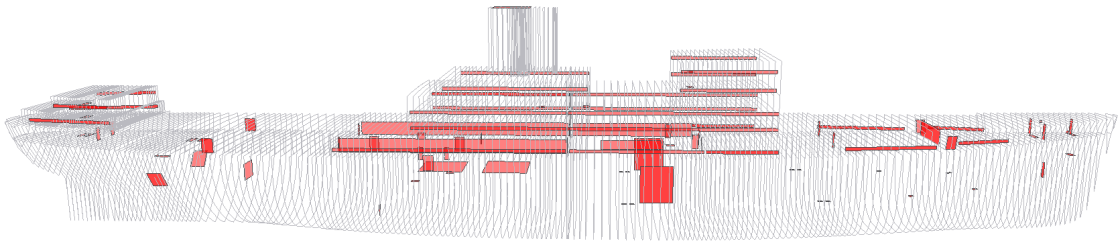

Figure 5.20: Hydrostatic model of the HERAKLION with all considered openings

### 5.2.4 Most Likely Scenario of the Accident

With the prescribed loading condition of the ship, the flooding simulation stops after only a few moments, because the water levels of the vehicle deck and the outside sea become equal. This equilibrium state is certainly not a very stable one, since the quasi-static simulation neglects the dynamic motions of the vessel. To overcome this pseudo stable point, the metacentric height is lowered by an increase of the vertical centre of gravity by an offset of 10 cm. This critical point will be discussed in more detail in Subsection 5.2.5 by a sensitivity analysis driven by the vertical centre of gravity.

The results of the flooding simulation, i.e. the development of the heel angle, the trim angle, the displacement and the metacentric height over time are shown in Figure 5.21. The distribution of the flood water can be depicted from the relative volume fillings shown in Figure 5.22 for selected compartments. A selection of frames of interesting time steps is given in Figure 5.23.

After around two minutes the heeling increases dramatically for around one minute, until the upper decks become immersed to provide additional buoyancy. On the upper deck, the Dining Room, which is located close to the main section, is flooded first through broken side windows (see also Figure 5.22). Due to the forward trim, the flooding of the Tourist Saloon which is located in the aft part of the ship, is a little delayed in time. A slower flooding phase follows, until after ten minutes the last deck before the bridge, the Boat Deck, becomes submerged at a heeling angle of around 75 degrees. A fast increase of the heeling follows, before the funnel becomes submerged only around 14 minutes after the loss of the side door.

The immersion of the funnel leads to a tremendous down-flooding into the Engine Room, which is also shown in Figure 5.22. The large vertical extension of the funnel requires a very accurate calculation: The flooding of the upper part of the funnel would lead to a large heeling moment,

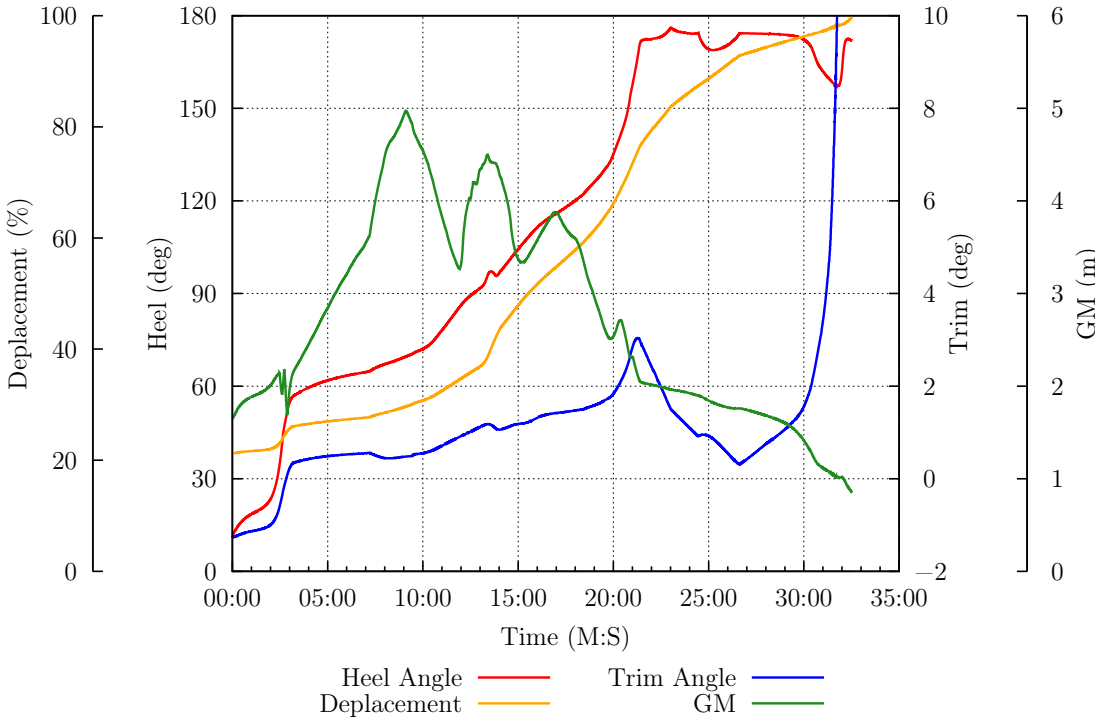


Figure 5.21: Time dependent development of heel, trim, displacement and metacentric height for the most likely scenario of the HERAKLION accident

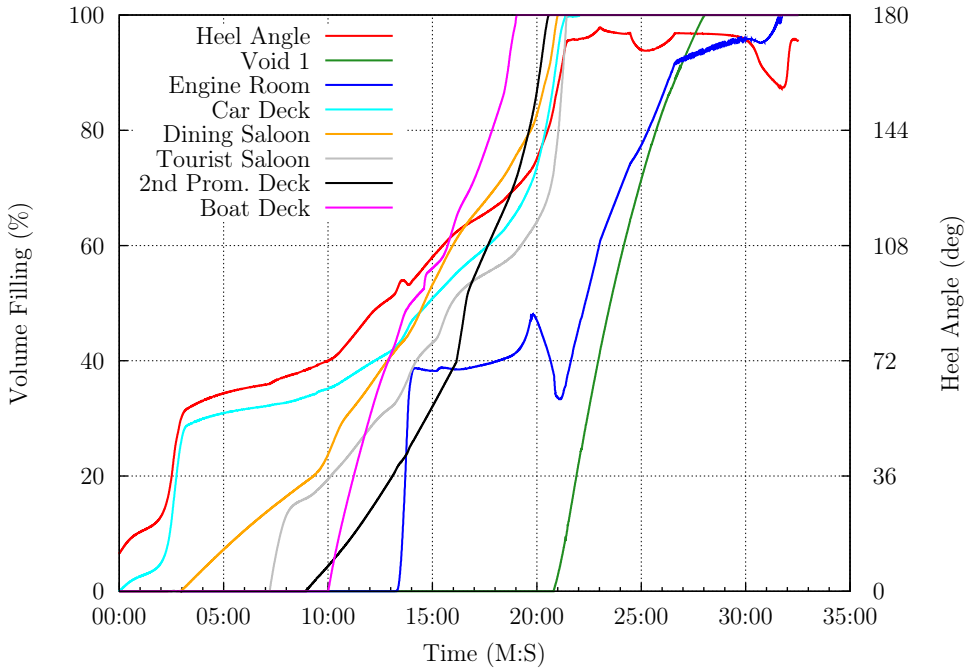


Figure 5.22: Development of volume fillings for selected compartments for the most likely scenario of the HERAKLION accident

while the down-flooding to the lower part of the funnel and the Engine Room located here, stabilises the ship shortly at this point.

After around 18 minutes, the ship moves from approximately 120 degrees up to 170 degrees of heel angle in just three minutes caused by the immersion of the superstructures from the other side. Void spaces below the vehicle deck, represented by Void 1 in Figure 5.22, are flooded from inspection manholes located on the port side. After around 30 minutes, the trim rapidly increases before the ship disappears completely from the sea surface and all reserved buoyancy is lost.

The uncertainty regarding the development of the progressive flooding process increases beyond 50-60 degrees heel angle due to the fact that the detailed internal subdivision and the characteristics of the involved openings is only reasonably estimated.

However, the reconstructed flooding scenario is roughly in line with the statements of the witnesses.

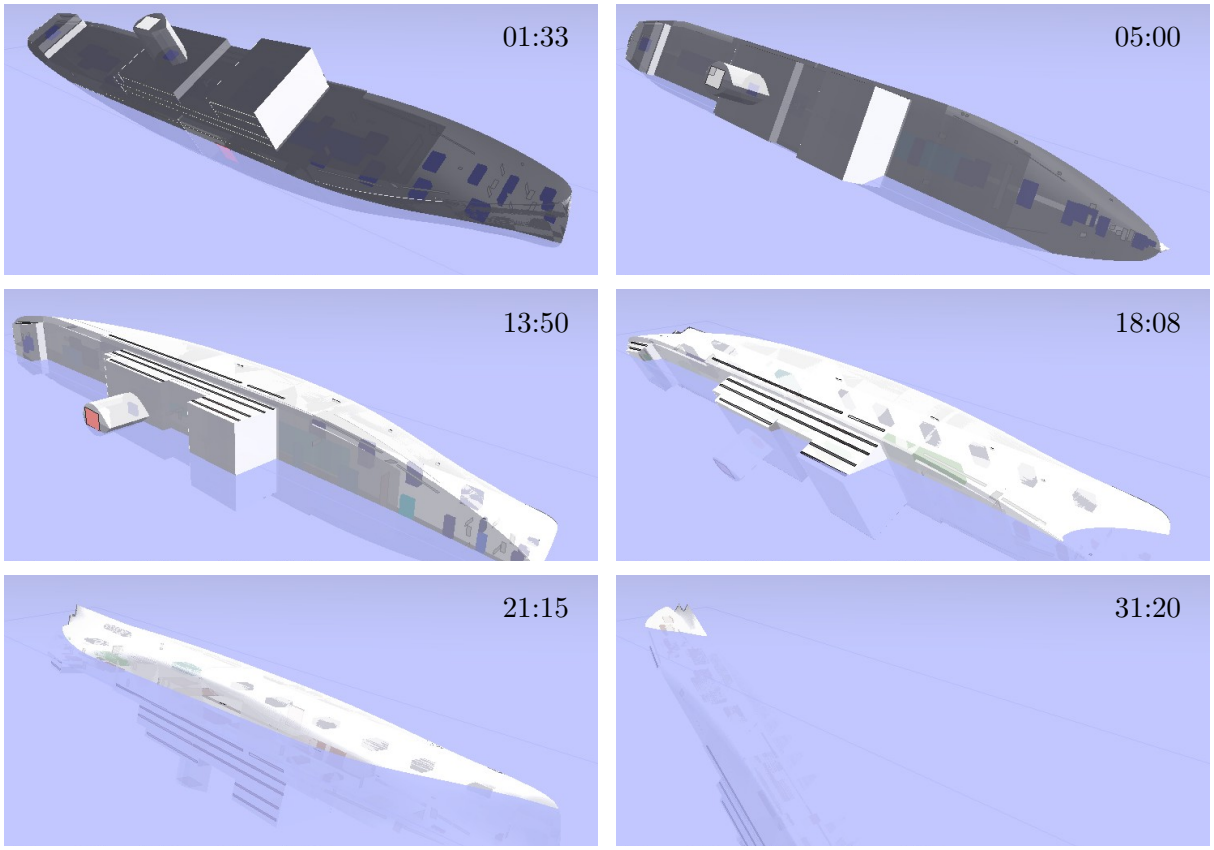


Figure 5.23: Selected frames of the flooding simulation of the HERAKLION

### 5.2.5 Sensitivity Analysis of Vehicle Deck Immersion

As already mentioned in the last section, the first phase of the vehicle deck flooding through the damaged side door may result in a pseudo-stable situation when both water levels become equal. In Figure 5.24 the heeling angles over time for different vertical centres of gravity ($\overline{\mathrm{KG}}$) are plotted. For lower values of $\overline{\mathrm{KG}}$, the flooding stops after one to two minutes.

After a critical threshold value of 10 cm increase in the $\overline{\mathrm{KG}}$ is exceeded, the heeling ascends

very fast after three minutes. Only the small change of 1 cm in the $\overline{\text{KG}}$ value distinguishes, if the vessel heels further or if a pseudo-stable equilibrium is reached at around 18 degrees of heel angle. A larger value for the centre of gravity is not chosen, because this would differ too much from the reconstructed loading condition.

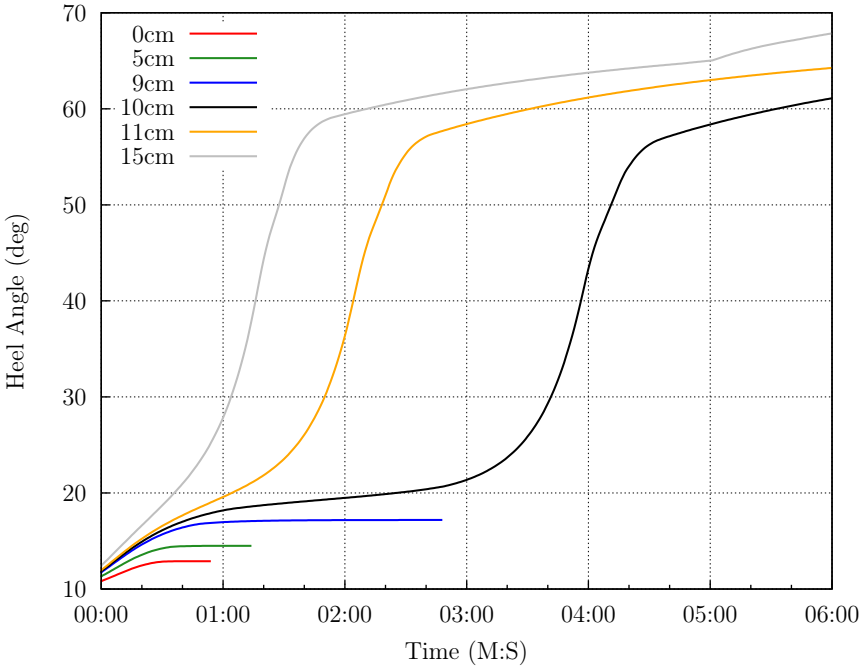


Figure 5.24: Heel angles for different $\overline{\text{KG}}$ variations of the HERAKLION

The instability of this situation becomes even more obvious when lever arm curves for the damaged case of the main vehicle deck are compared with the initial $\overline{\text{KG}}$ value. In Figure 5.25 three different lever arm curves are shown.

The red and blue curves are the lever arm curves calculated for the case that the vehicle deck is assumed to be a damaged compartment applying the lost buoyancy method. For the increased $\overline{\text{KG}}$ value, here the red curve, no righting lever is left and the ship would capsize immediately. However, also the maximum of the blue lever curve with the lower $\overline{\text{KG}}$ value amounts to only less than one millimetre. Any additional heeling moment would lead immediately to the capsize of the ship. For the black curve, the upper superstructure is also included in the buoyancy body, but its influence is only important for angles greater than 40 degrees.

In addition, the floodwater mass of 104.4 tons obtained by the lost buoyancy method is added to the loading condition and a new lever arm curve with fluid shifting moments is calculated for this case shown as the green curve. This is equivalent to the added mass method for damage calculations.

At this point the question arises what a lever arm curve represents: It illustrates the capability of a ship to withstand additional heeling moments. This means that if flooding simulations in the time domain are performed, the computation of the lever arm for each heeling angle becomes time dependent as well. If an additional heeling moment is taken into account in the situation of a flooded compartment, which is connected to the outside and no difference in the water levels is present, any additional heel angle will lead to a further flood water ingress. This dynamic coupling makes it complicated to compute a lever arm curve in this situation.

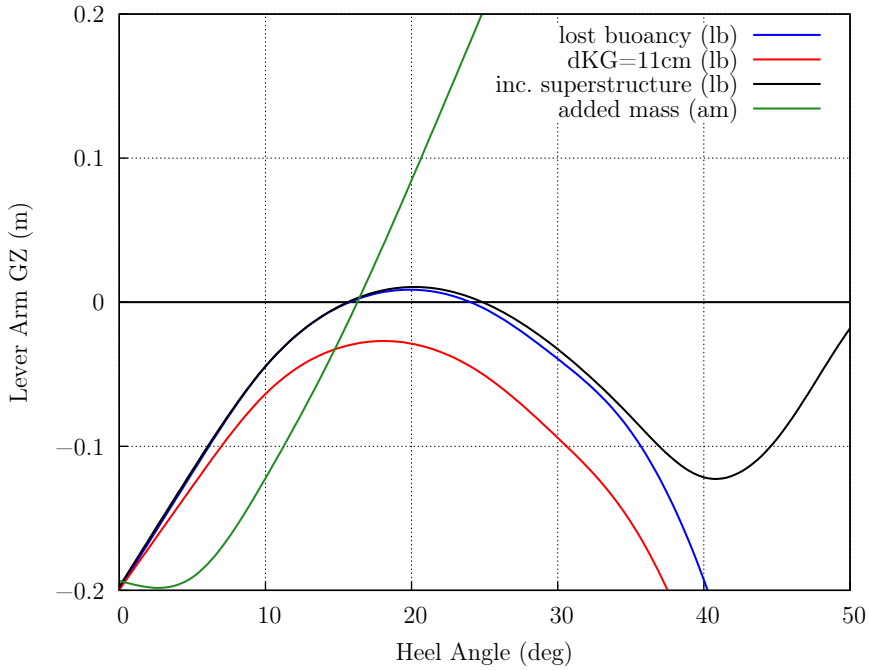


Figure 5.25: Comparison of lever arm curves for different conditions and vertical centres of gravity of the HERAKLION

A proposal is to successively increase a heeling lever and to perform a flooding simulation for a specified duration until a new heeling angle is reached. This gives a series of heeling angles together with the corresponding righting lever. The important parameter in this case would be the time duration of one heeling lever step.

The classical damage case lever arm calculation with the lost buoyancy method is equivalent to the case, when for each heeling angle the flooding simulation is performed until convergence, but only if the initial flooding case is already converged as well. An equalisation time of zero assumes that no water exchange occurs and the floodwater mass is kept constant, which is equivalent to the added mass method.

The sketched reasons above make it difficult to use a lever arm curve to characterise the stability of the vessel during its time dependent progressive flooding. The computation of lever arm curves is only useful in a converged flooding condition but not during intermediate stages of flooding. A better indication if a certain flooding process is stable, is only provided by further flooding simulations with an assumed additional heeling moment right from the beginning.

### 5.2.6 Watertight Integrity of the Car Deck

The forward car deck has been added during the conversion of the vessel to a passenger ferry. As mentioned in Papanikolaou et al. (2012), the watertight integrity of this deck at the time of the accident is questionable. To answer the influence of a flood water ingress through this deck with regard to the sinking sequence, a short study is performed. It is assumed that on both sides of the car deck six manholes were located, each with the dimension of 400 x 600 mm. Even though the original drawings showed only manholes on the port side, the others are modelled to represent the insufficient watertight integrity of the deck in this region.

The capability of the deck to withstand water ingress is modelled by a variation of the discharge

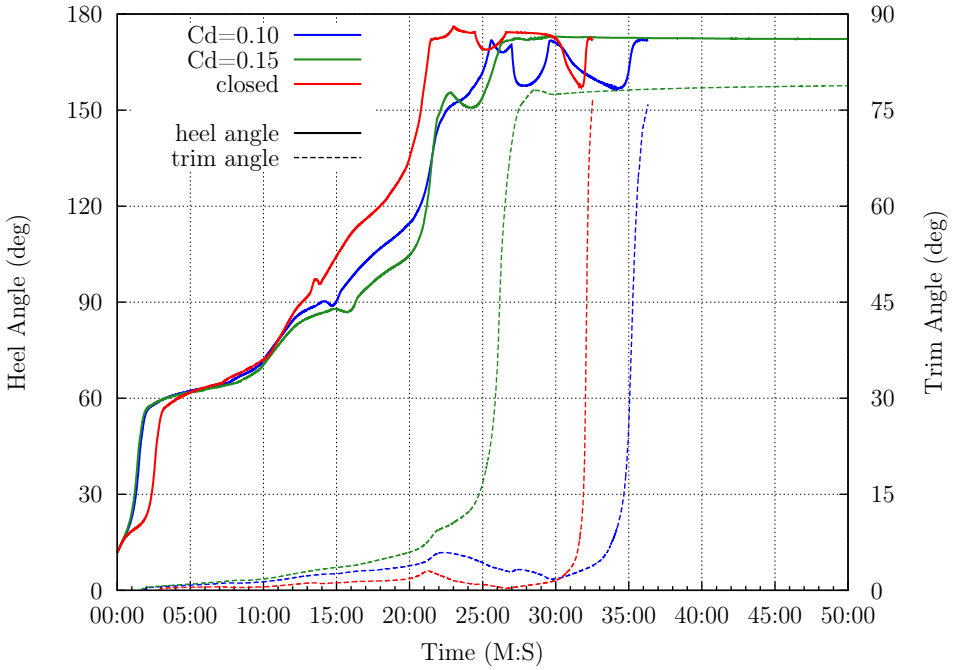


Figure 5.26: Influence of the car deck down-flooding on the heel and trim angle during the HERAKLION accident

coefficient of these manhole openings. The development of the heel and trim angle depending on the assumed discharge coefficient is shown in Figure 5.26. For all three cases, the increased $\overline{\mathrm{KG}}$ of 10 cm is used.

It is very interesting to observe, that a possible down-flooding strongly influences the sinking behaviour. The down-flooding to the void spaces extends the overall flooding sequence by a few minutes. In the initial phase, the heeling angle increases slightly faster. After around ten minutes the flooding is delayed by two to three minutes compared to the initial scenario. At around 22 minutes, the down-flooding leads to an increase of the trim angle due to the fact that more water can enter the forward part of the ship at an earlier phase. For the larger opening to the void spaces with an assumed $C_d = 0.15$, this fact actually leads to a completely different final floating position. The ship becomes unstable in longitudinal direction and capsizes over the bow. The trim rapidly increases to around 80 degrees, which leads to a final floating position in which the vessel floats like a buoy. To further illustrate the situation after 50 minutes in this scenario, the current floating position of the ship is shown in Figure 5.27.

Only a very small amount of water can now enter the ship, since compartments with reserve buoyancy in the aft part can no longer be flooded. Even some water egress occurs here, because openings are now above the waterline and a sinking of the vessel is no longer possible for this configuration. This means that the scenario with an assumed $C_d = 0.15$ can be excluded, while the smaller value represents a realistic alternative scenario.

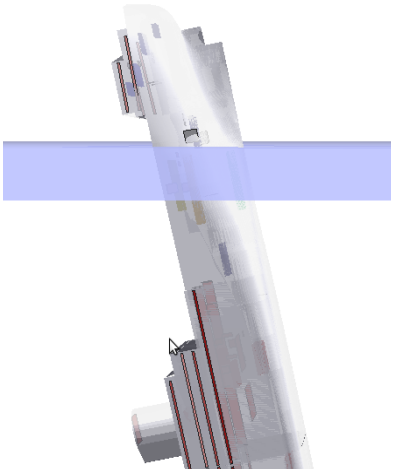

Figure 5.27: Floating position of the HERAKLION after 50 minutes with down-flooding through deck openings with $C_d = 0.15$

### 5.2.7 Summary of the Investigation

In general, the simulated sinking behaviour after the water ingress matches quite well with the statements of the witnesses mentioned in the previous investigations. The whole flooding behaviour of the ship seems to be reasonable. Advanced sea-keeping simulations may provide more accurate results, but the average flooding process is well reproduced by the presented method. Another interesting aspect is the shown sensibility to small changes in the $\overline{\mathrm{KG}}$, which represents additional heeling moments. The dynamic coupling of the ship's motion and the water ingress makes the flooding very sensitive to small changes in the initial conditions.

Furthermore, the influence of a possible down-flooding of the void spaces below the forward car deck has successfully been investigated. The down-flooding leads to a decrease of the $\overline{\mathrm{KG}}$. However, the effect of the developed large transient free surface is much stronger, which in total decreases the $\overline{\mathrm{GM}}$ in this phase.

The developed method is suitable to study several scenarios within a short period to figure out the most likely scenario. It is very interesting to observe that a small change in the initial assumptions strongly influences the overall sinking sequence. For example, the last scenario with a discharge coefficient of $C_d = 0.15$ is very unlikely, because such a large trim angle was not observed by the witnesses. This way certain scenarios can definitely be excluded.

For a numerical flooding simulation method, it is of crucial importance that the method is able to identify sensitivities of the flooding process to certain input parameters. The newly developed method can reveal these sensitivities and it provides reasonable results for the studied scenarios in combination with a fast runtime.

## 5.3 The M.V. Estonia Accident

The ESTONIA accident took place in the night between the 27th and 28th September, 1994 causing the death of 842 people. During heavy weather on her route from Tallinn in Estland to Stockholm in Sweden the vessel capsized and sunk after a severe water ingress through the damaged bow visor opening. A photo of the ESTONIA is shown in Figure 5.28.


Figure 5.28: Photo of the ESTONIA with open bow visor (Jaeger, 2008)

The aim of the following study is not to re-investigate the whole sequence of events leading to the accident and the loss of the ship. In general, the conditions are assumed to be similar to the ones reconstructed by the German group of experts in their previous investigations, namely Kehren (2009) and Valanto (2009). This study will mainly focus on the very complex progressive flooding sequence of the internal subdivision caused by the large water ingress through the open bow door. The purpose of this investigation is to validate the newly developed method with another carefully investigated real ship accident to show the advantages but also the limitations of the method.

Even though the accident occurred in rough sea conditions with large dynamic motions of the vessel and the ingressed flood water, the general sinking sequence of the vessel can be predicted by the developed quasi-static simulation method, if the most important dynamic effects are sufficiently taken into account and appropriately simplified.

The accident was triggered by several complex effects:

- The large vessel motions in rough sea conditions, especially the pitch and roll motions
- A relative high speed of the vessel leading to the development of a bow wave by the vessels own wave system
- The dynamic wave impacts affecting especially the opening of the bow visor but also external openings like windows and doors
- The last turning manoeuvre of the vessel to prevent further water ingress, but which also led to an additional heeling moment

In the next section an overview of previous investigations and a general description of the vessel are given. This is followed by remarks on the special requirements of the ship data model for the progressive flooding simulation. After this, the most likely sinking scenario is presented and a sensitivity analysis of several factors influencing the flooding sequence is conducted.

### 5.3.1 Previous Accident Investigations

Extensive research has been carried out to better understand and investigate the phenomena leading to this tragic accident (as already mentioned in Subsection 1.2.2). The first official investigation was published by the Joint Accident Investigation Commission (JAIC) only a few years after the accident in 1997. Since this report did not sufficiently answer all questions, the Swedish Governmental Agency for Innovation Systems (VINNOVA) initiated a new research project in 2004 to further investigate the events leading to this severe accident.

Within this research project, two consortia have been formed, one lead by the Swedish SSPA, the other by the German HSVA (Hamburg Ship Model Basin). Our institute as a subcontractor of the HSVA was responsible for the reconstruction of the later phase of the sinking sequence. The results of the two consortia were published in the final reports of this research project (Krüger and Kehren, 2008; SSPA Consortium, 2008). In addition, original drawings from the yard are available.

### 5.3.2 General Description of the Vessel

The ship was originally built in 1979 as the M.V. VIKING SALLY with yard number S590 by Jos L. Meyer Werft GmbH in Papenburg, Germany, for the first owner AB Sally of Mariehamn, Finland. Two years after a major conversion in 1991, the vessel was sold to Nordström & Thulin of Stockholm, Sweden. The vessel received her final name M.V. ESTONIA and started to serve routes between Sweden and Estland. The main particulars are given in Table 5.5. A general arrangement drawing of all decks together with a side view is given in Figure 5.29 and 5.30.

Table 5.5: Main particulars of the ESTONIA

| | | |
|---|---|---|
| Length over all | $L_{\mathrm{OA}}$ | 157.02 m |
| Length between perpendiculars | $L_{\mathrm{PP}}$ | 137.40 m |
| Breadth Moulded | $B$ | 24.20 m |
| Depth to Upper Deck | $H_1$ | 13.40 m |
| Depth to Main Vehicle Deck | $H$ | 7.65 m |
| Draught Design | $T$ | 5.57 m |
| Service Speed | $V_S$ | 21.20 kn |

The hull form including all upper decks and the compartmentation are based on the data model that was used for the study of Krüger and Kehren (2008). However, it was necessary to model the inner subdivision more precisely and to add various openings to this data model to take the special requirements for flooding simulations into account.

### 5.3.3 Final Voyage Condition

The final loading condition of the ESTONIA on her last voyage is published in Kehren (2009) and summarised in Table 5.6. The corresponding intact lever arm curve is shown in Figure 5.31.

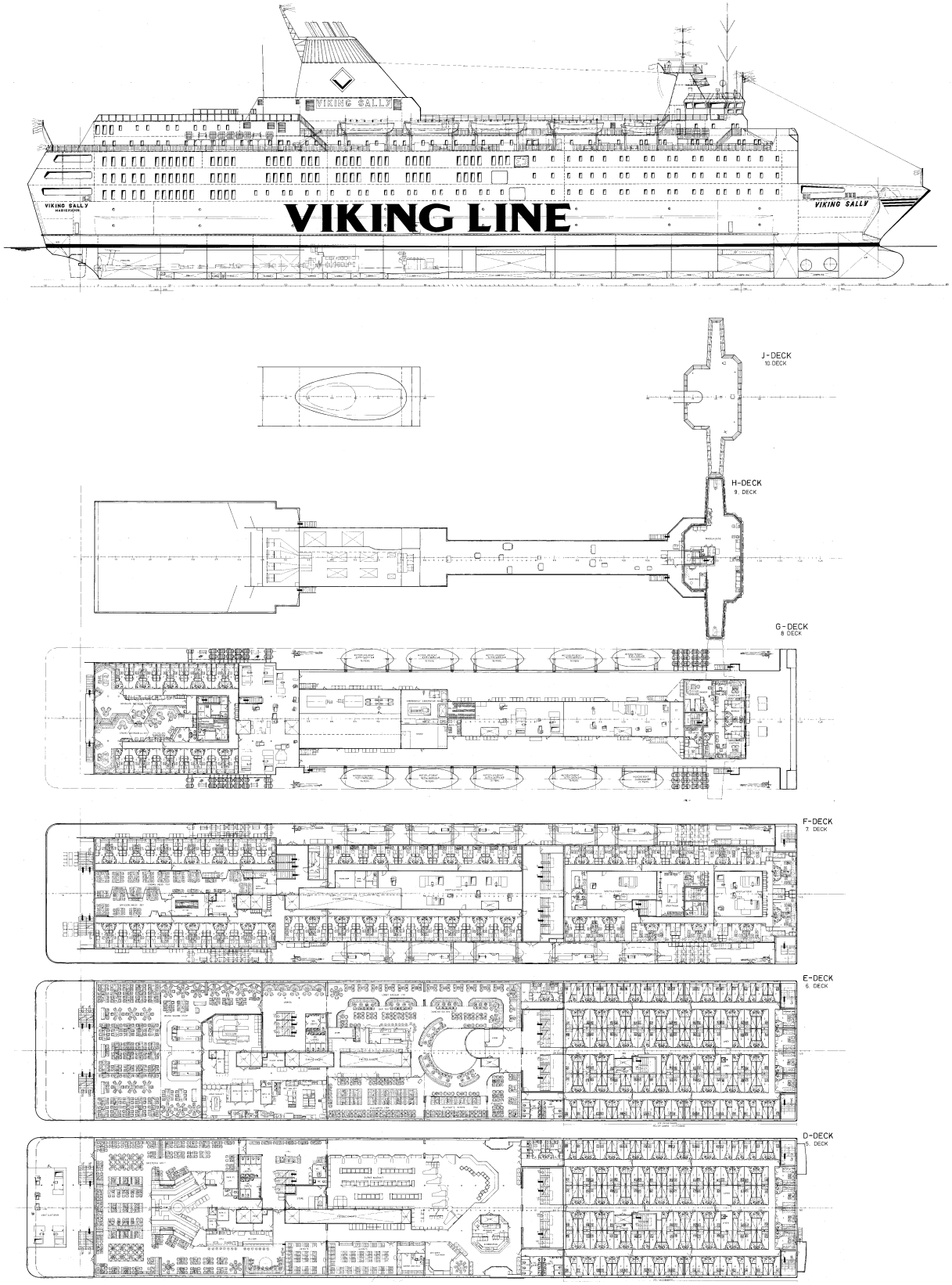


Figure 5.29: Side view and upper decks of the Estonia (MEYER WERFT GmbH, 1980, unpublished)

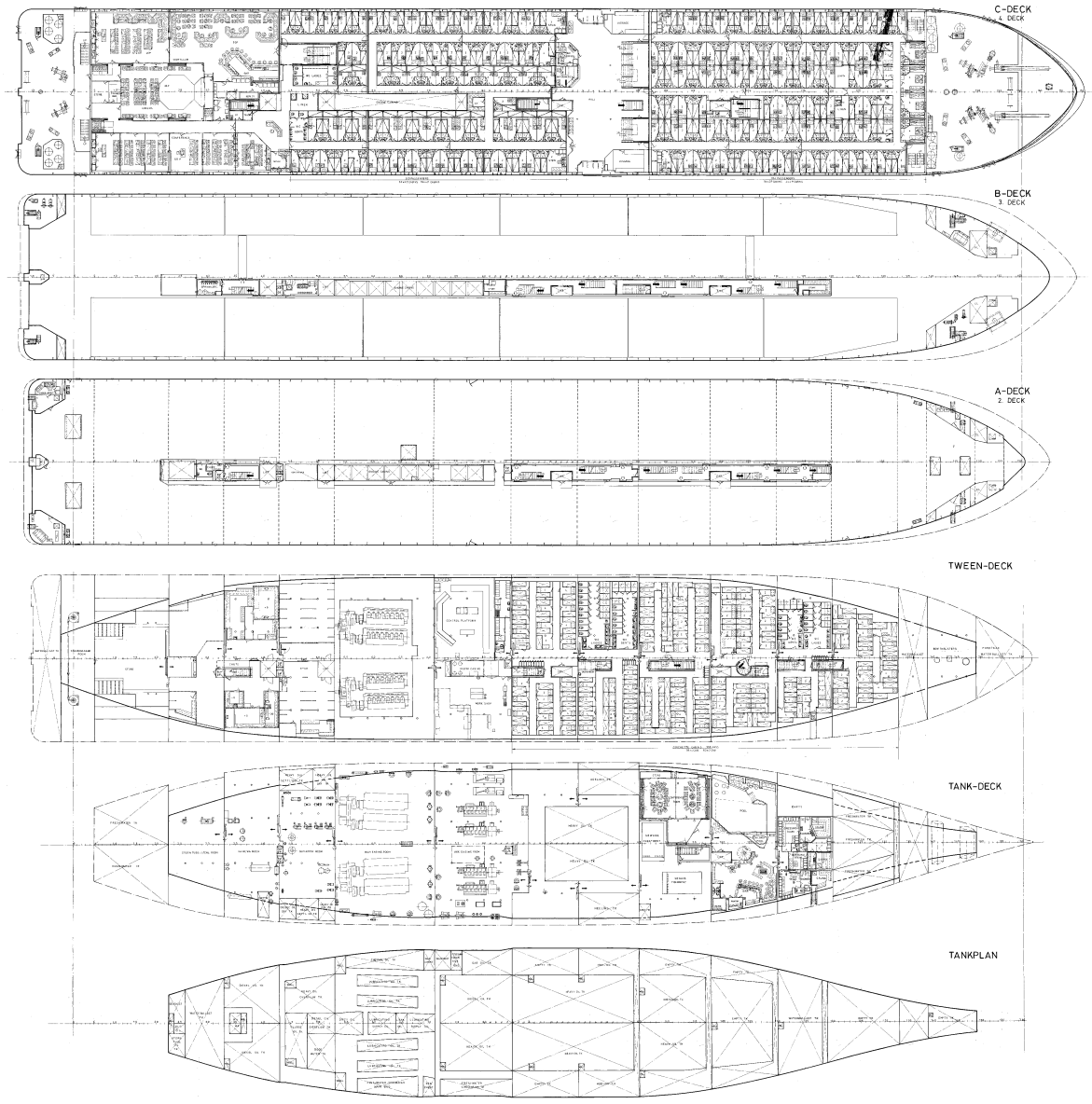


Figure 5.30: Lower decks of the ESTONIA (MEYER WERFT GmbH, 1980, unpublished)

Table 5.6: Final loading condition of the ESTONIA during the last voyage

| | |
|---|---|
| Shell Plating Factor | 1.007 - |
| Density of Sea Water | 1.004 t/m$^3$ |
| Ships Weight | 11945.914 t |
| Longit. Centre of Gravity | 63.090 m.b.AP |
| Transv. Centre of Gravity | -0.033 m.f.CL |
| Vertic. Centre of Gravity (Solid) | 10.602 m.a.BL |
| Free Surface Correction of V.C.G. | 0.100 m |
| Vertic. Centre of Gravity (Corrected) | 10.702 m.a.BL |
| Draught at A.P (moulded) | 5.733 m |
| Draught at LBP/2 (moulded) | 5.300 m |
| Draught at F.P (moulded) | 4.867 m |
| Trim (pos. fwd) | -0.866 m |
| Heel (pos. stbd) | 1.439 Deg. |
| Volume (incl. Shell Plating) | 11898.320 m$^3$ |
| Longit. Centre of Buoyancy | 63.041 m.b.AP |
| Transv. Centre of Buoyancy | -0.229 m.f.CL |
| Vertic. Centre of Buoyancy | 2.887 m.a.BL |
| Area of Waterline | 2824.712 m$^2$ |
| Longit. Centre of Waterline | 58.415 m.b.AP |
| Transv. Centre of Waterline | -0.359 m.f.CL |
| Metacentric Height | 1.303 m |

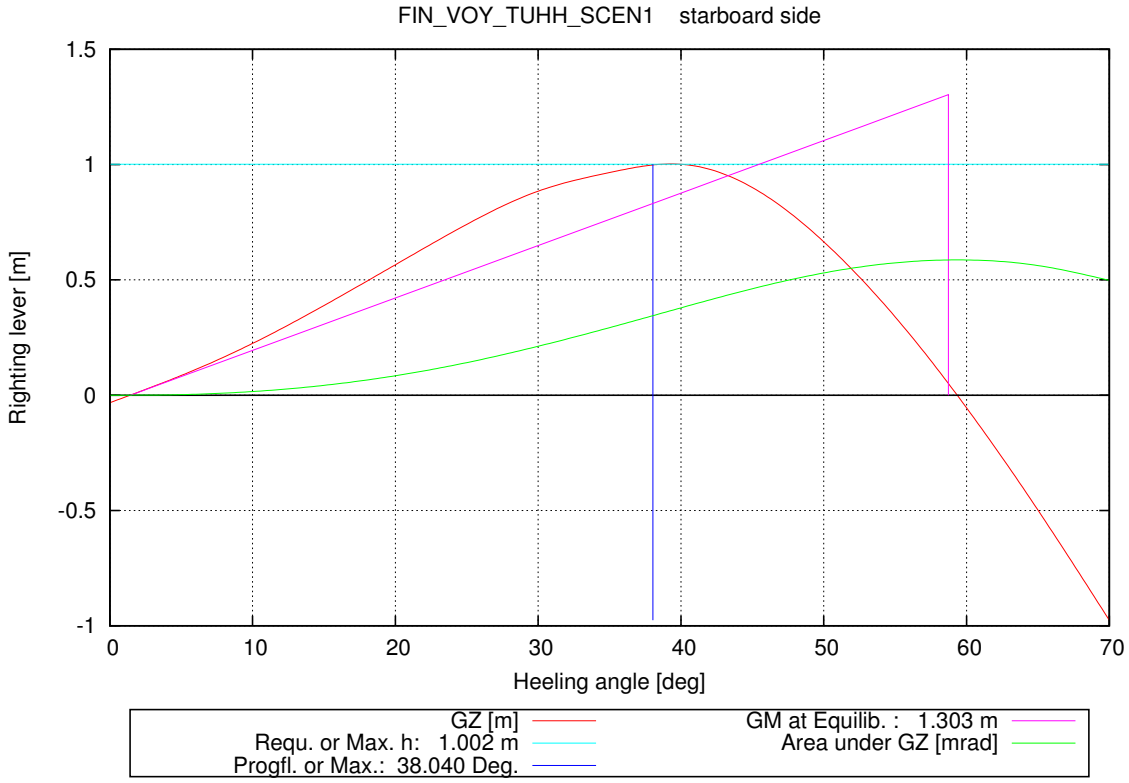


Figure 5.31: Intact lever arm curve of the ESTONIA before the accident

### 5.3.4 Considered Openings

It is assumed that the water entered the ship through the open bow door resulting in a flooding of the main car deck. From the main car deck, the water ingressed through the ventilation system and doors to other parts of the ship. At larger heel angles, the external side ventilation of compartments located in the lower part of the ship became submerged. The side windows collapsed after their maximum allowable pressure height was exceeded, which allowed water to enter the upper decks. The openings will be described more detailed in the following.

#### The Bow Visor Opening and the Ramp

Like in the previous investigations of the ESTONIA accident, it is assumed that the loss of the bow visor due to structural failure caused the initial water ingress and the flooding of the main car deck. A technical side view drawing and a photo of the visor after salvage is shown in Figure 5.32.

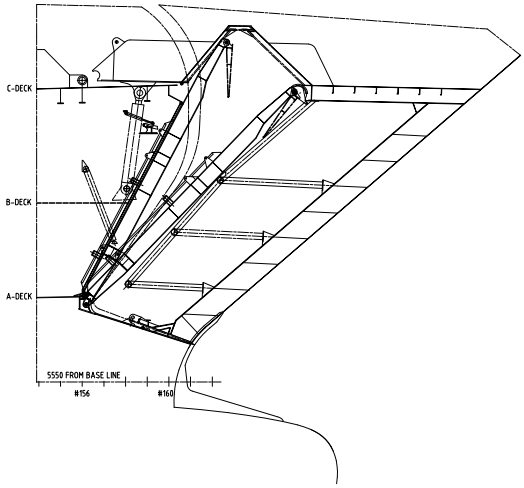


(a) Side view of the open visor (Carlsson, 2008)

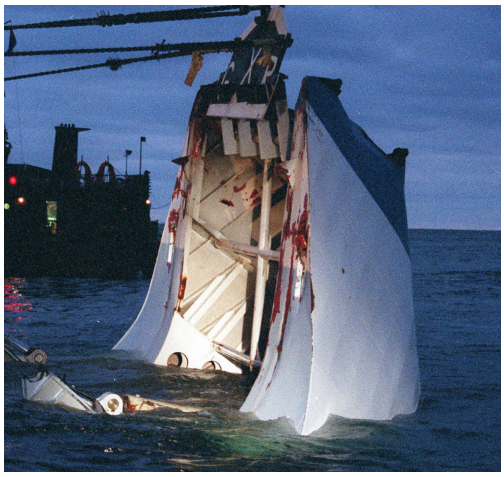

(b) Photo of the bow visor after salvage (Avikainen, 2004)

Figure 5.32: The bow visor of the ESTONIA

The following flooding simulations will start at the point in time when the bow visor was completely lost, which is assumed to be at 1:00 o'clock local ship time. The open bow door will be idealised by a rectangular opening with an assumed discharge coefficient of $C_d = 0.2$ to account for obstruction of the flow by the bow ramp.

The structural failure of the bow visor led to the open bow door and an exposure of the main vehicle deck to the open sea. However, the water ingress has only been possible in the presence of waves and the large motions in the rough sea conditions during the time of the accident. At calm water conditions without the movement of the ship, even with the bow visor and ramp completely removed, no water ingress would have been possible, because the freeboard of the main car deck to the water surface was approximately two meters.

One regular model wave as described in Subsection 3.4.4 is assumed to model the water ingress to the main car deck caused by the waves and the ship motions. In addition, due to the relatively high forward speed of the ESTONIA, a speed dependent bow wave and the dynamic sinkage of

the ship has to be considered as well. These effects are modelled in the simulation by artificially lowering the corresponding bow visor opening by a speed dependent function $h(u)$. This function depends on an assumed initial submerging $h_0 = 1.5\,\text{m}$ (Kehren, 2009, page 108), the squared ratio of the current speed $u$ and the initial speed $u_0 = 15\,\text{knots}$ of the vessel:

$$h(u) = \left(\frac{u}{u_0}\right)^2 \cdot h_0. \tag{5.1}$$

This additional submerging of the opening is reduced, when the ship slows down until a value of zero is reached when the vessel stops. The function $h(u)$ is also used to take into account the influence on the water ingress of the relative motion of the ship to the waves due to the vessel's heave and pitch motion.

It is further assumed that the front ramp, which was still attached to the vessel on the seabed, closed due to gravity after a heel angle of 90 degrees was exceeded according to Carlsson (2008). In the simulation, the discharge coefficient of this conditional opening is set to zero, if 90 degrees of heel angle is exceeded.

#### Vertical Openings

The following openings are responsible for the vertical down- or up-flooding through the decks:

1. Ventilation Ducts
2. Emergency Exits
3. Lifts
4. Stairs

The ventilation system ducts allow water to enter the compartments below the main deck after the outside air intakes are submerged. The emergency exits and lifts are further flooding paths, which partly lead to the lower decks. The staircases are quite large vertical openings connecting the different decks. On the lower decks, the stairs are located in the centre casing.

#### Windows and Doors

The locations and dimensions of all windows are known from the available drawings. The assumed breaking loads of the windows are taken from Kehren (2009, page 116): The pressure head criterion before collapsing is 4.16 m for small windows and 3.55 m for large windows. Since these values are estimated for the calm water case, the values are enlarged by two meters in the presence of a regular model wave. For a limited time the windows might withstand an increased water column height, when the wave crest is passing the ship. The location and the dimensions of internal fire doors and watertight sliding doors are known from the original drawings provided by the building yard.

#### Further Openings

The watertight integrity and dimensions of most of the doors and windows are known from detailed drawings. However, for some doors, no further information except their location shown in the general arrangement drawings are known. Appropriate assumptions are required for these

openings. A summary of the assumed properties depending on the type of the opening is given in Table 5.7. These values are only assumed, if no other information about the opening in question is available.

Table 5.7: Assumed properties for openings of the ESTONIA for which only incomplete information is available

| Type | Coefficient (-) | Pressure Height (m) | Extension (m) | Coaming (m) |
|---|---|---|---|---|
| Lift | 0.2 | -1 | 2.0 x 1.60 | 0.10 |
| Internal Door | 0.3 | 1 | 2.0 x 0.80 | 0.10 |
| Internal A-60 Fire Door | 0.3 | 2 | 2.0 x 0.80 | 0.10 |
| Emergency Exit | 0.4 | -1 | 1.7 x 0.65 | 0.25 |
| Stair Cases | 0.4 | -1 | - | - |

### 5.3.5 Internal Subdivision

For the flooding simulation, also the non-watertight parts of the vessel like the upper decks and the superstructures have to be taken into account. In addition, a more detailed model with additional subdivisions of the compartmentations are required compared to classical damage stability calculations. The water ingress would otherwise lead to unrealistic large free surfaces resulting in extensive heel and trim moments. For example, the cabins are subdivided by the alleys preventing the flood water to immediately spread over the whole deck in transverse direction. An example for the typical modelling of the internal subdivision is shown in Figure 5.33, which is a part of the 4th deck, the C-Deck. The green lines mark the considered walls.

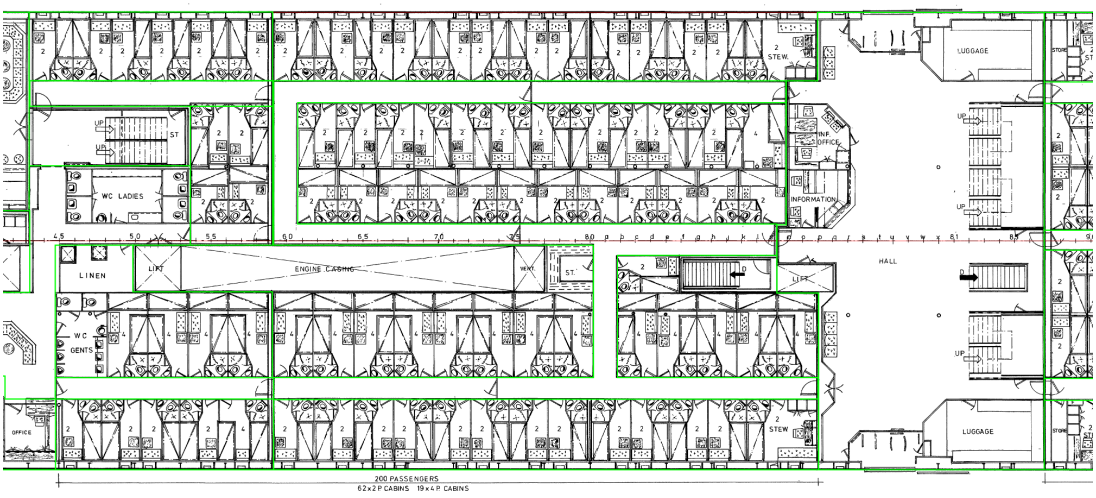


Figure 5.33: Example for a refined subdivision on the 4th deck of the ESTONIA

The walls that are not watertight are modelled as additional openings, which prevent the water from flooding immediately through the whole deck in the first phase of the flooding. The openings that represent the walls are idealised to have the same extension and effective door opening area as the real cabin walls. This simplification reduces the modelling effort, because

otherwise each cabin door needs to be defined. In addition, the detailed condition during the time of the accident for each cabin door in question, e.g. whether it is open or closed, is unknown anyway.

The idealised wall opening is defined by correcting the discharge coefficient $C_d$ accordingly. The standard cabin door has an assumed area of $A_0 = 1.6\,\mathrm{m}^2$ with a width of 0.8 m and a height of 2.0 m together with an assumed coaming of 0.1 m. It is further assumed that such a door has a discharge coefficient of $C_{d0} = 0.6$ and a 50 % probability ($p = 0.5$) to be open at the time of flooding. The corrected discharge coefficient $C_d$ can be computed from the actual opening area $A$ and the number $n$ of standard cabin doors, if the effective area of the doors $A_{e1}$ is set equal to the effective area $A_{e2}$ of the simplified opening:

$$A_{e1} = n \cdot p \cdot C_{d0} \cdot A_0, \tag{5.2}$$

$$A_{e2} = C_d \cdot A, \tag{5.3}$$

$$C_d = p \cdot C_{d0} \cdot A_0 \cdot \frac{n}{A} = 0.48 \cdot \frac{n}{A}. \tag{5.4}$$

### 5.3.6 Track of the Vessel

The same track of the ESTONIA as described in Valanto (2009, page 56) will be used. For consistency the original sketch of the track is shown in Figure 5.34.

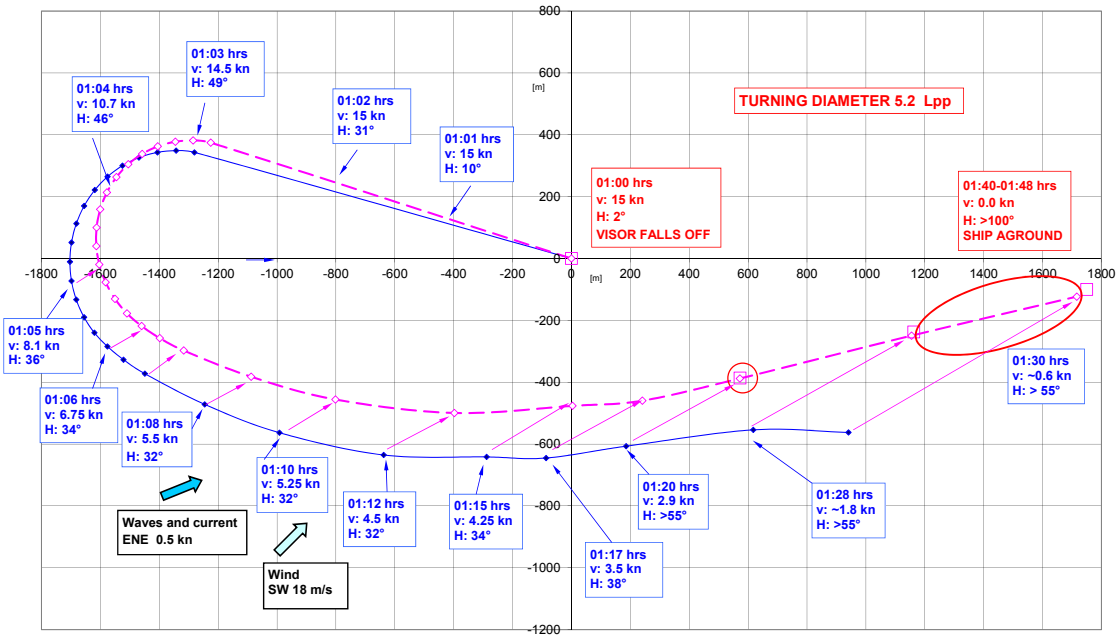


Figure 5.34: Track of the ESTONIA according to Valanto (2009)

#### Relative Position in the Wave Pattern

The change in the heading together with the varying forward speed influences the relative position of the vessel in the wave pattern. This means that the ESTONIA is exposed to a changing wave encounter frequency, which influences the fluctuation of the inflow through the open bow visor. The relative position is added as an additional offset $x_1$ in Equation 3.8 for the determination of the current position and height of the regular model wave.

### Influence of the Forward Speed on the Inflow

The decreasing velocity reduces the current bow wave height $h(u)$ according to Equation 5.1. In addition, the forward speed of the vessel may further increase the inflow through the open bow door by the relative velocity $u_r$ of the opening to the waves. The average inflow velocity $u$ can be determined from the initial volume flux $Q_0$, which depends on the pressure height difference, together with the submerged area of the opening $A_s$ and its discharge coefficient $C_d$. The relative velocity $u_r$ is added to this value and the volume flux is recalculated. Summarising this yields the following formula for the corrected inflow flux:

$$Q = (u + u_r) \cdot C_d \cdot A_s \qquad \text{with} \quad u = \frac{Q_0}{C_d \cdot A_s}, \tag{5.5}$$

$$Q = Q_0 + u_r \cdot C_d \cdot A_s. \tag{5.6}$$

Local effects like a change in the orbital wave velocities are neglected.

### Turning Circle Moment

The turning of the vessel induces a turning circle moment, which is described by

$$M_T = r(t) \cdot \Delta \cdot \cos(\varphi) \cdot \left(\overline{\mathrm{KG}} - \frac{T}{2}\right) \cdot \frac{u^2}{R}. \tag{5.7}$$

The turning circle radius $R$ is assumed to be constant and the velocity $u$ is the current forward speed of the vessel. The displacement $\Delta$, the vertical centre of gravity $\overline{\mathrm{KG}}$ and the mean draught $T$ are taken from the current state of the vessel during the simulation, where the mass of the ingressed flood water is included in the displacement.

For the development of the turning moment, a shape function $r(t)$ depending on the current time is used to describe the inertia of the ship. The development of this function is the same as used by the HSVA in Valanto (2009) and shown in Figure 5.35.

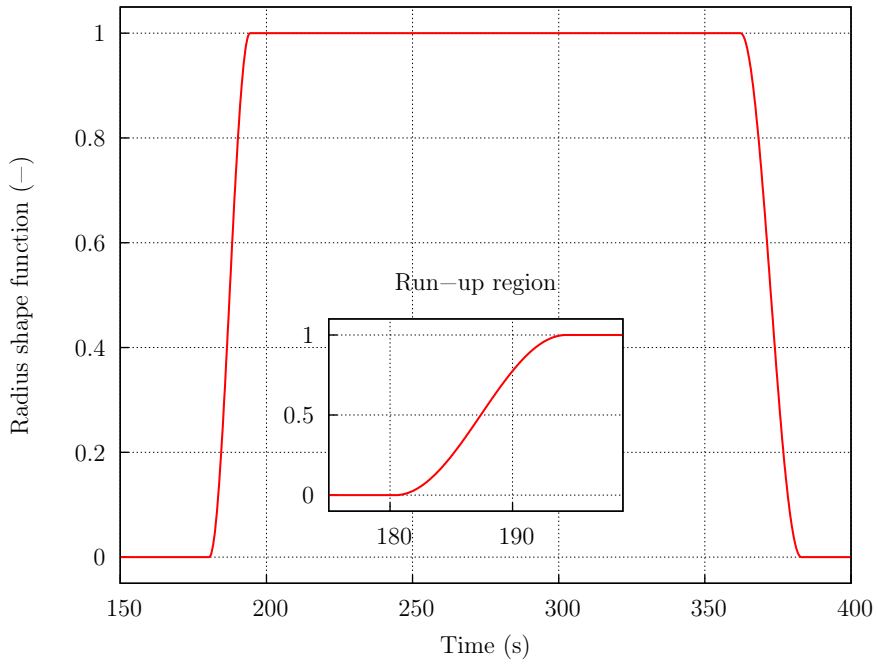


Figure 5.35: Shape function of the turning moment of the ESTONIA

The function in the region of the run-up between $t_1$ and $t_2$ is defined as:

$$r(t) = \cos\left(\frac{1}{2} + \frac{\pi}{2} \cdot \left[1 - \frac{t - t_1}{t_2 - t_1}\right]\right). \tag{5.8}$$

Using this kind of shape function allows a smooth development of the turning moment over time.

### 5.3.7 Most Likely Sinking Scenario

With the assumptions mentioned above, the final and most likely sinking scenario can be summarised as follows:

- A regular model wave of a height of 5 m and a length of 100 m (period approximate 8 seconds) is used to model the water ingress through the open bow door.
- The bow wave and the dynamic sinkage is modelled by an additional submerging of the bow door opening by initially 1.5 m. It is dynamically lowered by the square of the ship's speed.
- The vessel moves on a track as shown in Figure 5.34. The position of the vessel relative to the waves is corrected according to its current position, what influences the wave encounter frequency.
- The additional heeling moments are the turning moment, which depends on the track and the state of the vessel, and the moment caused by the cargo shift.
- The cargo shift is modelled according to Kehren (2009, page 127) as an conditional shift: The vehicle cargo of 1,100 tons is shifted by 1 m to starboard after a heel angle of 30 degrees is reached. The shift further increases by 0.5 m after 60 degrees of steady list is passed.
- The breaking loads of the windows are increased by 2 m to account for temporarily wave loads.
- The conditions of all other internal and external openings are considered as mentioned above in Subsection 5.3.4 and 5.3.5.
- All compartments are assumed to be fully ventilated, i.e. no air compression is taken into account.
- The configuration of the watertight doors are taken from scenario S6 of Jasionowski and Vassalos (2008), where some of the doors are assumed to be left open after the flooding started.
- According to Valanto (2009), the water depth at the accident location is approximately 74 m. The simulation stops when the lowest point of the vessel hits the seabed.

The estimated list developments issued by the different author's are compared to the results of the new method in Figure 5.36. The list development of the new method for the most likely sinking scenario is located in between the results of the other authors and matches the statements of the witnesses quite well.

Compared to the results of the other authors and the witnesses, the heel is first slightly underestimated by the new quasi-static method. This can be explained by the fact that no dynamic motions are simulated, even though heavy roll and pitch motions have been observed, which both have a large influence on the water ingress through the open bow door.

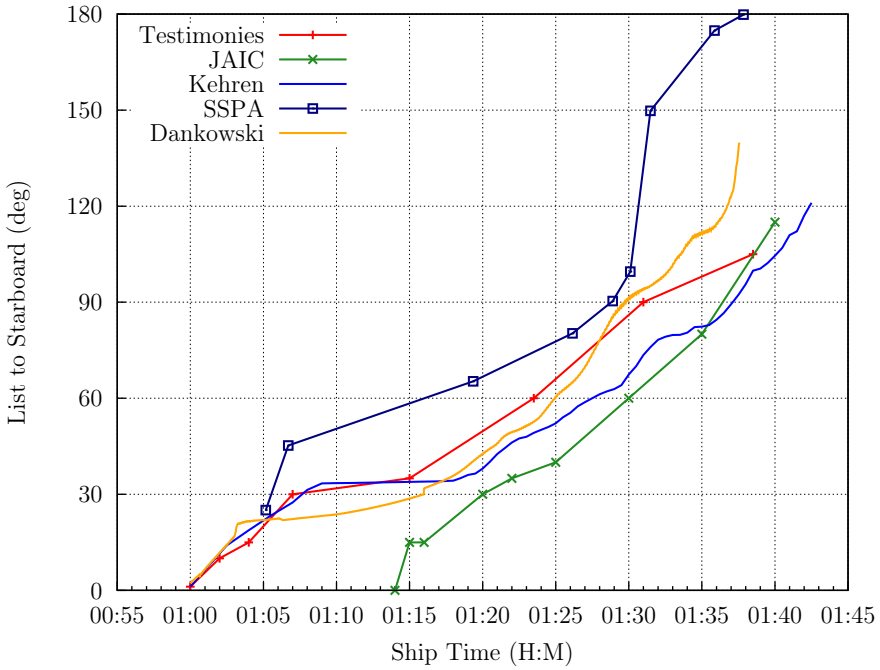


Figure 5.36: List Development of the ESTONIA issued by different authors

In addition, the large dynamic roll motion made it probably difficult for the witnesses to estimate the mean steady list of the ship in the early phase of the flooding. The duration of the plateau of approximately 15-20 minutes is well reproduced. Furthermore, the later list development and the overall time matches very well with the statements of the witnesses.

### 5.3.8 Sensitivity Analysis

To better understand the influence of different factors on the sinking sequence, a sensitivity analysis with regard to the following parameters is performed:

1. An additional increased breaking load of the windows by one meter
2. An increased discharge coefficient of $C_d = 0.3$ for the bow door opening
3. The complete closure of all watertight doors
4. Influence of the closure of the bow ramp beyond 90 degrees heel

The heel angle development for the first three scenarios is shown in Figure 5.37 together with the most likely, default scenario described before.

To start with the last one, the late closure of the bow ramp due to gravity did not have any influence, the motion of the vessel was exactly the same compared to the default scenario. This can be explained by the fact that after an angle of 90 degrees is passed, the vessel is already flooded by a large amount of water and the influence of the inflow of water on the vehicle deck is no longer relevant for the later sinking sequence.

As expected, the increase of the breaking load of the windows by one meter leads to a delay in the flooding process after around 22 minutes, while the shape of the heel angle development stays almost the same. In addition, the overall flooding time until the seabed is reached, is almost the same as for the default scenario.

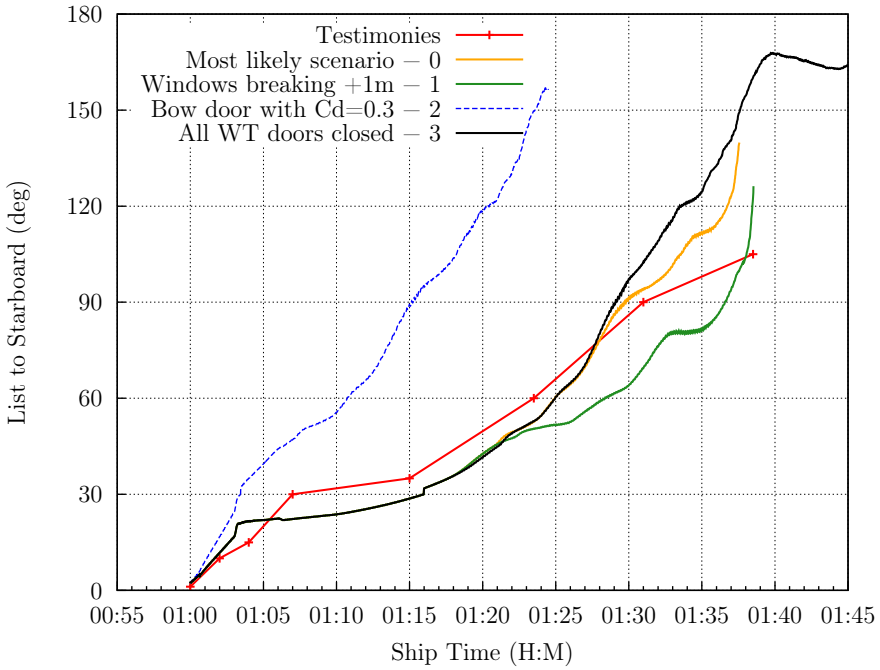


Figure 5.37: Heel angle development for different scenarios of the ESTONIA sinking sequence

A relative large influence can be observed from the increase of the discharge coefficient of the bow door opening by 50 % to a value of $C_d = 0.3$. It results in a more unrealistic scenario, because the heel angle increase is very fast leading to an overall predicted flooding time of less than 25 minutes, which contradicts the statements of the witnesses.

At last, it is interesting to observe that the influence of the closure of all watertight sliding doors below the main deck on the overall flooding process is very small. This is explained by the sequence of flooding: The initial water entrance is located above the main deck, which leads very fast to a large heel angle and allows less water to enter the lower parts of the vessel, while the non-watertight upper decks are flooded faster mainly through the broken side windows. The complete closure of all doors has, in this special case, actually a negative influence on the later phase of the sinking. At around 1:27 the heel angle starts to increase faster compared to the default scenario, because lesser weight is located in lower parts of the vessel. At the end after 1:40, some of the still completely closed compartments below the main deck provide enough buoyancy reserve to let the capsized ship float longer upside down. However, in contrast to this, a fast sinking of the capsized vessel has been observed by the witnesses.

### 5.3.9 Summary of the Investigation

Even though the effort to create a sufficiently detailed data model that can be used for flooding simulations is very large, it is worth for the investigation of such large-scale flooding accidents. These investigations help to better understand the behaviour of ships in the case of flooding.

For the case of the ESTONIA accident, the general flooding sequence is well reproduced by the newly developed method, even though dynamic motions of the flood water and the vessel are neglected. However, it is also of crucial importance to correctly model other relevant influences like for example the additional turning moments and the track of the vessel.

By variation studies, the most likely sinking scenario can be found by excluding parameter

settings, which lead to unobserved or unrealistic results. The discharge coefficient of the bow opening is for example such a parameter. On the one hand, a too low value leads to an early stop of the flooding process. On the other hand, a too large value results in an unrealistic fast increase of the heel angle. Therefore, the bandwidth of the correct value is quite small. The flooding process is very sensitive with regard to a parameter like this.

Limits of such a quasi-static approach are for example the dynamic spreading of flood water on the port side of the centre casing, which may lead to additional down-flooding through lifts and staircases located on this side. This spreading cannot be captured, when a planar water surface on the whole main car deck is assumed.

# CHAPTER 6

# Conclusion and Outlook

## 6.1 Conclusion

A new numerical flooding simulation method has been developed and successfully validated on the basis of the standard ITTC benchmark model tests recommended for this type of problem and the re-investigation of three real, full scale ship accidents. For the selected accidents, sufficient data material was available and they have been carefully investigated by different research groups before. The most likely scenarios of the accidents are well reproduced by the re-investigation with the new method.

In addition, the method is capable of identifying sensitivities of the flooding process to certain parameters, for example the influence of the vertical centre of gravity on the vehicle deck flooding as shown for the HERAKLION accident. However, also more dynamic effects like the transient asymmetric flooding effect, which occurred during the EUROPEAN GATEWAY accident, can be simulated. If appropriate assumptions are made, even more complex situations like the last turning manoeuvre of the ESTONIA can be handled by the new method as well.

The method provides a fast and robust tool for the accurate time domain simulation of the flood water ingress and spreading inside the vessel. Complex three dimensional ship compartment geometries can be treated. Due to the fast runtime of the method, several possible scenarios can efficiently be investigated. The study of different scenarios is very important to gain a more detailed insight of the effects that occurred during an accident and to quickly answer the question about the main causes and the chain of events, which led to the accident. The investigation of real accidents increases the knowledge of the physical effects, which influence the capability of a ship to survive a damage to its watertight integrity.

The proposed method fills the gap between conventional damage stability calculations of the final stage of flooding and more advanced, but also time consuming sea-keeping analyses of the motions of damaged ships. The correct numerical simulation of the flood water ingress and the spreading inside a ship in the time domain is a useful and valuable contribution to assess the vulnerability of new ship designs in the case of damage.

## 6.2 Outlook

Further interesting accident investigations can now be carried out by applying this successfully validated new flooding method. This would allow to better understand the chain of events and main causes, which led to these accidents.

One useful extension of the method would be a grounding and submerging module to use also the knowledge about the final position of the vessel on the seabed to identify the most likely scenario of an accident. This would allow to calculate the movement of the vessel, even after the ship has completely vanished from the water surface or after grounding to the seabed occurred by taking into account the reaction grounding forces.

Another extension would be to combine the flooding module with a Monte Carlo based damage stability calculation method to automatically and correctly identify critical intermediate stages of flooding, which might occur in a damage case. This would solve the problem how to correctly treat intermediate stages of flooding as required for the current SOLAS 2009 damage stability regulations. A combination with Monte Carlo methods would provide even further information like the distribution of the time-to-flood for a certain ship design and characteristic values such as an average survival time after the ship has been damaged.

Furthermore, it seems to be promising to couple the flooding module with an appropriate non-linear sea-keeping code like E4-ROLLS to efficiently simulate a damaged ship in a natural sea state. In addition, this requires the correct dynamic simulation of the entrapped flood water inside the compartments, while the interchange through the openings and the spreading of the flood water is computed by the proposed method.

In certain cases, it might be required to model the influence of air compression and air flow. It has been shown that in this case the correct timing in the determination of entrapped air is the crucial part to obtain appropriate results. However, the inclusion of air flow in the model would allow to further study the influence of air interchange through openings on the flooding sequence. Other useful extensions are the inclusion of structural elements like longitudinal strength calculations to assess for examples accidents like the TITANIC disaster or the unloading operation of semi-submersible heavy lift vessels.

# CHAPTER 7

## Bibliography


Arndt, B. (1983). MF EUROPEAN GATEWAY Damage Investigations. Technical report, SCHIFFKO GmbH.

Avikainen, J. (2004). HELSINGIN SANOMAT. `http://www.hs.fi/english/picture/1135219486183`. AP Images.

Brekas, F. (2011). MARFAMAR F/B Penelope, Drapetsona, 24/10/11. `http://www.adriaticandaegeanferries.com/agoudimoslines/peeeng.html`.

Carette, N., van Daalen, E., and Ypma, E. (2008). Computations on MV Estonia: FREDYN Simulations of Flooding of Superstructure Deck No. 4. Final Report 20374-2-RD, MARIN.

Carlsson, J.-O. (2008). M/V ESTONIA Bow arrangement collapse – Sequence of events. Technical report, MacGREGOR.

Chanson, H. (2005). Analytical Solution of Dam Break Wave with Flow Resistance: Application to Tsunami Surges. In 31st IAHR Biennial Congress, pages 3341–3353.

Cho, S. K., Sung, H. G., Hong, S. Y., Nam, B. W., and Kim, Y. S. (2010). Study on the motions and flooding process of a damaged ship in waves. In Proceedings of 11th International Ship Stability Workshop, Wageningen, The Netherlands. MOERI/KORDI.

Dand, I. (1988). Hydrodynamic aspects of the sinking of the ferry Herald of Free Enterprise. Transactions of RINA, 130:145–167.

Dankowski, H. and Hatecke, H. (2012). Stability Evaluations of Semi-Submersible Heavy-Lift Vessels by a Progressive Flooding Simulation Tool. In Proceedings of the ASME 2012 31st International Conference on Ocean, Offshore and Arctic Engineering, number ISBN 978-0-7918-4492-2, Rio de Janeiro, Brazil. ASME.

Dankowski, H. and Krüger, S. (2012). A Fast, Direct Approach for the Simulation of Damage Scenarios in the Time Domain. In 11th International Marine Design Conference, Glasgow, UK. University of Strathclyde.

de Kat, J., Brouwer, R., McTaggart, K., and Thomas, W. (1994). Intact ship survivability in extreme waves: new criteria from a research and navy perspective. In Weaver (1994).

de Kat, J. O. (1988). Large Amplitude Ship Motions and Capsizing in Severe Sea Conditions. PhD thesis, University of California, Berkeley.

Diestel, R. (2010). Graph Theory. Springer-Verlag, Heidelberg, fourth edition edition.

Dillingham, J. (1981). Motion Studies of a Vessel with Water on Deck. Marine Technology.

Doskocil, W. and Thomsen, P. (1976). European Gateway - Dreier-Serie eines neuen Ro/Ro-Fährschiffs-Typs von der Schichau Unterweser AG. HANSA Maritime Journal, Nr. 6:449–455.

Fragoulis, V. (1967). Expertise on the Sinking of SS HERAKLION. Technical report, AEENA. (in Greek).

Georgiadis, S. and Antoniou, A. (1968). Expertise on the Sinking of SS HERAKLION. Technical report, AEENA.

Grim, O. (1961). Beitrag zu dem Problem der Sicherheit des Schiffes im Seegang. Schiff und Hafen, 6.

Grochowalski, S., editor (2002). 6th International Ship Stability Workshop Proceedings, Glen Cove, New York, USA. Webb Institute.

Hackett, C. and Bedford, J. G. (1996). The Sinking of S.S. Titanic: Investigated By Modern Techniques. Transactions of RINA, Royal Institution of Naval Architects:73.

Harwich Lifeboat Station (2010). European Gateway. `http://rnli.harwich.org.uk/Stories/EuropeanGateway/EuropeanGateway.htm`.

Hellenic Maritime Accident Investigation Board, A. (1968). Official Report of the Accident Investigation Board Heraklion. Technical report, AEENA.

Hooft, J. P. and Pieffers, J. B. M. (1988). Maneuverability of Frigates in Waves. Marine Technology, 25(4):262–271.

Hutchison, B. L. (1995). Water-on-Deck Accumulation Studies by the SNAME Ad Hoc Ro-Ro Safety Panel. In Proceedings of the First International Ship Stability Workshop, Hamburg, Germany. Germanischer Lloyd.

IMO (1973). Recommendation on a standard method for establishing compliance with the requirements for cross-flooding arrangments in passenger ships. Technical report, International Maritime Organization.

IMO (2007). RESOLUTION MSC.245(83) - Recommendation on a standard method for evaluating cross-flooding arrangments. Technical report, International Maritime Organization.

IMO (2009). SOLAS 2009. International Maritime Organization, consolidated edition. Consolidate text of the International Convention for Safety of Life at Sea, 1974, and its Protocol of 1988: articles, annexes and certificates.

IMO SLF 47/INF.6 (2004). LARGE PASSENGER SHIP SAFETY - Survivability investigation of large passenger ships. 47th session.

Jaeger, U. (2008). Verhängnisvolle Wende. Der Spiegel, 2:132–133.

Jakubowski, P. and Bieniek, N. (2010). Experiments with leaking and collapsing structures. In FLOODSTAND Project. Napa Ltd and STX Finland.

Jalonen, R., Ruponen, P., Jasionowski, A., Maurier, P., Kajosaari, M., and Papanikolaou, A. (2012). FLOODSTAND – Overview of Achievements. In Spyrou et al. (2012).

Jasionowski, A. (2002). An integrated Approach to Damage Ship Survivability Assessment. PhD thesis, University of Strathclyde.

Jasionowski, A. and Vassalos, D. (2008). Technical Summary of the Investigation on The Sinking Sequence of MV Estonia. Final VIES01-RE-006-AJ, Safety at Sea.

Jasionowski, A., Vassalos, D., and Guarin, L. (2002). Time-based Survival Criteria for Passenger Ro-Ro Vessels. In Grochowalski (2002).

Kehren, F.-I. (2009). The Sinking Sequence of MV Estonia. PhD thesis, Technische Universität Hamburg-Harburg, Denickestr. 22, 21071 Hamburg.

Khaddaj-Mallat, C. (2010). The Transient and Progressive Flooding Stages of Damaged Ro-Ro Vessels: A Systematic Review of Entailed Factors. Journal of Offshore Mechanics and Arctic Engineering.

Konovessis, D. (2006). Maritime and Coastguard Agency Lectureship - Final Report. Technical report, Ship Stability Research Centre, Department of Naval Architecture and Marine Engineering of the Universities of Glasgow and Strathclyde.

Kröger, H.-P. (1987). Simulation der Rollbewegung von Schiffen im Seegang. Technical report, Universitätsbibliothek der Technischen Universität Hamburg-Harburg, Denickestr. 22, 21071 Hamburg.

Krüger, S., Dankowski, H., and Teuscher, C. (2012). Numerical Investigations of the Capsizing Sequence of SS HERAKLION. In Spyrou et al. (2012).

Krüger, S. and Kehren, F.-I. (2008). Hydrostatic Analyses of the Later Phases of the Capsizing and the Sinking of MV ESTONIA. Technical Report Work Package 7, Swedish Governmental Agency for Innovation Systems VINNOVA.

Krüger, S., Streckwall, H., Soeding, H., Schulze, R., Stoehrmann, H., Tellkamp, J., Voigt, C., Kaether, B. L., and Pohl, M. (1999). Offenes Methodenbanksystem für Propulsorentwurf. Abschlussbericht, BMBF, Flensburger Schiffbau-Gesellschaft GmbH & Co. KG.

Letizia, L. (1996). Damage survivability of passenger ships in a seaway. PhD thesis, Strathclyde University, Glasgow (United Kingdom).

Majumder, J., Vassalos, D., Guarin, L., and Vassalos, G. C. (2005). Automated Generation of Shipboard Environment Model for Simulation and Design. In International Conference on Computational Science.

MEYER WERFT GmbH (1980). General Arrangements S 590. Technical report, Schiffswerft.

Moré, J. J., Garbow, B. S., and Hillstrom, K. E. (1980). User Guide for MINPACK-1. Technical Report ANL-80-74, Argonne National Laboratory, Argonne, IL, USA.

NMI Ltd (1983). Investigation into the Sinking of MV EUROPEAN GATEWAY. Technical report, National Maritime Institute (now: British Maritime Institute).

Palazzi, L. and de Kat, J. (2004). Model Experiments and Simulations of a Damaged Ship With Air Flow Taken Into Account. Marine Technology, 41:38–44.

Papanikolaou, A. (2007). Review of Damage Stability of Ships - Recent Developments and Trends. In 10th International Symposium on Practical Design of Ships and Other Floating Structures, PRADS Proceedings, Houston, Texas, United States of America. American Bureau of Shipping.

Papanikolaou, A. (2009). Risk-Based Ship Design - Methods, Tools and Applications. Springer.

Papanikolaou, A., Boulougouris, E., and Sklavenitis, A. (2012). Investigation into the sinking of the RO-RO passenger ferry S.S Heraklion. In Spyrou et al. (2012).

Papanikolaou, A., Spanos, D., Boulougouris, E., Eliopoulou, E., and Alissafaki, A. (2003). Investigation into the Sinking of the Ro-Ro Passenger Ferry EXPRESS SAMINA. In Proceedings of the 8th International Conference on Stability of Ships and Ocean Vehicles, Madrid, Spain. National Technical University of Athens-Ship Design Laboratory.

Papanikolaou, A., Zaraphonitis, G., Spanos, D., Boulougouris, E., and Eliopoulou, E. (2000). Investigation into the capsizing of damaged Ro-Ro passenger ships in waves. In Renilson (2000).

Pawlowski, M. (2003). Accumulation of water on the vehicle deck. Proceedings of the Institution of Mechanical Engineers, Part M: Journal of Engineering for the Maritime Environment, 217(4):201–211.

Petey, F. (1986). Numerical Calculation of Forces and Moments due to Fluid Motions in Tanks and Damaged Compartments. In STAB1986 (1986).

Petey, F. (1988). Ermittlung der Kentersicherheit lecker Schiffe im Seegang aus Bewegungssimulationen. Institut für Schiffbau, Institut für Schiffbau, Hamburg, 487 edition.

Petey, F. (1990). Determination of Capsizing Safety of Damaged Ships by means of Motions Simulations in Waves. In Fourth International Conference on Stability of Ships and Ocean Vehicles, Naples, Italy. University "Federico II" of Naples.

Pittaluga, C. and Giannini, M. (2006). Pressure Losses Estimation for Structural Double Bottom by CFD Technique. Technical report, CETENA.

Renilson, M., editor (2000). Proceedings of the 7th International Conference on Stability of Ships and Ocean Vehicles, Launceston, Tasmania, Australia. The Australian Maritime Engineering CRC Ltd.

Ruponen, P. (2006). Model Tests for the Progressive Flooding of a Boxshaped Barge. Technical report, Helsinki University of Technology.

Ruponen, P. (2007). Progressive Flooding of a Damaged Passenger Ship. PhD thesis, Helsinki University of Technology.

Ruponen, P. (2009). On the Application of Pressure-Correction Method for Simulation of Progressive Flooding. In 10th International Conference on Stability of Ships and Ocean Vehicles.

Ruponen, P., Kurvinen, P., Saisto, I., and Harras, J. (2010). Experimental and Numerical Study on Progressive Flooding in Full-Scale. In RINA Transactions 2010 Part A - International Journal of Maritime Engineering. RINA.

Ruponen, P. and Routi, A.-L. (2011). Guidelines and criteria on leakage occurrence modelling. In FLOODSTAND Project. Napa Ltd and STX Finland.

Sander, R. (1999). Compilation of Henry's Law Constants for Inorganic and Organic Species of Potential Importance in Environmental Chemistry. Technical report, Air Chemistry Department, Max-Planck Institute of Chemistry.

Santos, T. A. (1999). Time Domain Simulation of Accidental Flooding of Roro Ships. Master's thesis, Department of Naval Architecture and Ocean Engineering, University of Glasgow.

Santos, T. A., Dupla, P., and Guedes Soares, C. (2009). Numerical Simulation of the Progressive Flooding of a Box-Shaped Barge. In Proceedings of the 10th International Conference on Stability of Ships and Ocean Vehicles, Lisbon, Portugal. Technical University of Lisbon.

Santos, T. A., Winkle, I. E., and Guedes Soares, C. (2002). Time domain modelling of the transient asymmetric flooding of Ro-Ro ships. Ocean Engineering, 29(6):667–688.

Schreuder, M. (2002). Simulation of damage stability in waves - demonstration of the time-domain simulation program developed at KTH. In Grochowalski (2002).

Schreuder, M. (2005). Time Simulation of the Behaviour of Damaged Ships in Waves. Master thesis, Chalmers University of Technology, Göteborg.

Schreuder, M. (2008). Research Study of Sinking Sequence of m/v ESTONIA - Numerical simulations of foundering scenarios. Technical Report WP 4.1-4.3, Department of Shipping and Marine Technology.

Schreuder, M. (2011). Parameter Study of Numerical Simulation of Parametric Rolling of Ships. In Belenky, V., editor, Proceedings of 12th International Ship Stability Workshop, Sweden. Chalmers University of Technology.

Schröder, R. and Zanke, U. C. E. (2003). Technische Hydraulik: Kompendium für den Wasserbau. Springer, Berlin, 2. auflage edition.

Skaar, D., Vassalos, D., and Jasionowski, A. (2006). The Use of a Meshless CFD Method in Modelling Progressive Flooding and Damaged Stability of Ships. In Proceedings of the 9th International Conference on Stability of Ships and Ocean Vehicles, Rio de Janeiro, Brazil. Univ. of Glasgow and Strathclyde.

Sklavenitis, A. (2011). Persönlicher Kontakt. E-Mail.

Spanos, D. (2002). Theoretical-numerical modelling of large amplitude ship motions and of capsizing in heavy seas. PhD thesis, Ship Design Laboratory, National Technical University of Athens.

Spanos, D. and Papanikolaou, A. (2001). Numerical Study of the Damage Stability of Ships in Intermediate Stages of Flooding. In Francescutto, A., editor, Proceedings of the 5th International Workshop "Stability and Operational Saefety of Ships", Trieste, Italy. National Technical University of Athens.

Spouge, J. R. (1985). The Technical Investigation of the Sinking of the Ro-Ro Ferry EUROPEAN GATEWAY. Transactions of RINA, Royal Institution of Naval Architects:24.

Spyrou, K. J., Themelis, N., and Papanikolaou, A. D., editors (2012). Proceedings of the 11th International Conference on Stability of Ships and Ocean Vehicles, Athens, Greece.

SSPA Consortium (2008). Final Report - Research Study on the Sinking Sequence of MV Estonia. Technical Report 134, SSPA. http://www.safety-at-sea.co.uk/mvestonia.

STAB1986, editor (1986). Third International Conference on Stability of Ships and Ocean Vehicles, Gdansk, Poland. Instytut Okretowy Politechniki Gdanskiej.

Stening, M. (2010). Pressure losses and flow velocities in flow through manholes and cross-ducts. In FLOODSTAND project, number D2.3 in Floodstand Deliverable. Aalto University (TKK).

Stichlmaier, J. (2006). Druckverlust bei der Durchströmung von Lochplatten, chapter Lag, page 1500. Volume I of VDI-Gesellschaft (2006), 10. edition.

Strasser, C., Jasionowski, A., and Vassalos, D. (2009). Calculation of Time-to-Flood of a Box-Shaped Barge by Using CFD. In 10th International Conference on Stability of Ships and Ocean Vehicles.

Söding, H. (1982). Gutachten über die Belastungen des Schiffes E.L.M.A. Tres durch Seegang am Vormittag des 26.11.1981. Technical Report Schrift Nr. 2327, Institut für Schiffbau, Universität Hamburg.

Söding, H. (2001). User Manual of Programs EUMEDES and ARCHIMEDES II.

Söding, H. (2002a). Flow computations for ship safety problems. Ocean Engineering, 29:721–738.

Söding, H. (2002b). Water Ingress, Down- and Cross-Flooding. DCAMM Ph.D.-Course Stability of Ships, Lyngby, Danmark.

Söding, H. and Tonguc, B. (1986). Computing Capsizing Frequencies of Ships in a Seaway. In STAB1986 (1986).

Thornton, N. (2012). Mv European Gateway - Past and Present. http://www.doverferryphotosforums.co.uk/wordpress/mv-european-gateway-past-and-present/.

Todd, T. (2002). Unwinding the Design Spiral. ShipPax STATISTICS 02, pages 10–16.

Valanto, P. (2009). Research for the Parameters of the Damage Stability Rules including the Calculation of Water on Deck of Ro-Ro Passenger Vessels for the amendment of the Directives 2003/25/EC and 98/18/EC. Final Report 1663, European Maritime Safety Agency (EMSA).

van Walree, F., de Kat, J., and Ractliffe, A. (2007). Forensic research into the loss of ships by means of a time domain simulation tool. International Shipbuilding Progress, 54(4):381–407.

van't Veer, R. and de Kat, J. (2000). Experimental and numerical investigation on progressive flooding and sloshing in complex compartment geometries. In Renilson (2000).

van't Veer, R. and Zuidscherwoude, W. (2012). FPSO Green Water on Deck Assessment. In Proceedings of the 2nd International Conference on Violent Flows.

van't Veer, R., Peters, W., Rimpela, A.-L., and de Kat, J. (2004). Exploring the Influence of Different Arrangements of Semi-Watertight Spaces on Survivability of a Damaged Large Passenger Ship. In Xianglu, H., Guoping, M., and Renchuan, Z., editors, Proceedings of 7th International Ship Stability Workshop, Shanghai, China. Shanghai Jiao Tong University.

Vassalos, D., Ikeda, Y., Jasionowski, A., and Kuroda, T. (2004). Transient Flooding on Large Passenger Ships. In Proceedings of the Seventh International Ship Stability Workshop, page 1–3.

Vassalos, D., Letizia, L., Shaw, M., and MacPherson, C. (1998). An Investigation On The Flooding of Damaged RO-RO Ships. In RINA Transactions and Annual Report 1998. The Royal Institution of Naval Architects.

Vassalos, D. and Turan, O. (1994). Damage Scenario Analysis: A Tool for Assessing the Damage Survivability of Passenger Ships. In Weaver (1994).

VDI-Gesellschaft, editor (2006). VDI-Wärmeatlas. Springer Berlin Heidelberg, Berlin, Heidelberg, 10. edition.

Visonneau, M., Queutey, P., and Guilmineau, E. (2010). Results of the computational study on the pressure losses in openings. In FLOODSTAND Project. CNRS.

Walshaw, A. C. and Jobson, D. A. (1979). Mechanics of Fluids. Longman, London; New York, third edition edition.

Weaver, L. E., editor (1994). Fifth International Conference on Stability of Ships and Ocean Vehicles, Melbourne, Florida, USA. Florida Institute of Technology.

Wendel, K. (1970). Gutachten "Heraklion". Technical report, Institut für Schiffbau.

Zaraphonitis, G., Papanikolaou, A., and Spanos, D. (1997). On a 3-D mathematical model of the damage stability of ships in waves. In Bogdanov, P. A., editor, Proceedings of the 6th International Conference on Stability of Ships and Ocean Vehicles, Varna, Bulgaria. National technical University of Athens.

# CHAPTER 8

# Appendix

## 8.1 Determination of Henry's constant

For the solubility of air, the Henry constant for the gas mixture of the ambient air is required. Constants depending on the temperature for various gases can be found in Sander (1999). The ambient air consists of oxygen and nitrogen with the properties that are summarised in Table 8.1.

Table 8.1: Selected properties of oxygen and nitrogen

| Property | | Oxygen $O_2$ | Nitrogen $N_2$ |
|---|---|---|---|
| Molar weights (g/mol) | $M$ | 31.9988 | 28.0134 |
| Partial fractions (-) | $f$ | 0.21 | 0.79 |
| Henry constants (at 25°, mol/(l·atm)) | $k_H^{\ominus}$ | $1.3 \cdot 10^{-3}$ | $6.5 \cdot 10^{-4}$ |
| Temperature constants | $C$ | 1700 | 1300 |

The dependency of the Henry constant on the temperature $T$ is given by:

$$k_H = k_H^{\ominus} \cdot \exp\left[-C \cdot \left(\frac{1}{T} - \frac{1}{T^{\ominus}}\right)\right] \quad \left(\frac{\mathrm{M}}{\mathrm{atm}}\right), \tag{8.1}$$

where $T^{\ominus}$ is the reference temperature. This constant can also be expressed in units of a density:

$$k = k_H \cdot \frac{M}{1\,\mathrm{atm}} = \frac{k_H^{\ominus} \cdot M}{101,325} \cdot \exp\left[-C \cdot \left(\frac{1}{T} - \frac{1}{298.15}\right)\right] \quad \left(\frac{\mathrm{g}}{\mathrm{l}} = \frac{\mathrm{kg}}{\mathrm{m}^3}\right). \tag{8.2}$$

At a temperature of 15°, the constant for air $k_a$ is determined as follows:

$$k_{O_2} = 0.033684 \cdot 10^{-5}, \qquad k_{N_2} = 0.015447 \cdot 10^{-5}, \tag{8.3}$$

$$k_a = 0.21 \cdot k_{O_2} + 0.79 \cdot k_{N_2} = 1.9277 \cdot 10^{-7} = 1.9532 \cdot 10^{-2} \cdot 1\,\mathrm{atm}. \tag{8.4}$$

This means that at atmospheric pressure, the concentration of solute air in water is around 2 percent.

## 8.2 Derivation of the Free Outflow Flux

The detailed derivation of Equation 2.60 is presented in the following. The integral to be solved to determine the volume flux is:

$$Q = \int_A u \, \mathrm{d}A = \int_0^{s_1} u(s) \cdot y(s) \, \mathrm{d}s. \tag{8.5}$$

The velocity is given according to Equation 2.57 as:

$$u(s) = \sqrt{2\,g} \cdot \sqrt{z_a - (z_0 + s_z \cdot s) + \alpha} = \sqrt{2\,g} \cdot \sqrt{h(s)}, \tag{8.6}$$

$$h(s) = z_a - (z_0 + s_z \cdot s) + \alpha. \tag{8.7}$$

The integral of the product of the width function $y(s)$ and the velocity $u(s)$ can be split into two parts

$$u(s) \cdot y(s) = u(s) \cdot y_0 + u(s) \cdot s \cdot \frac{y_1 - y_0}{s_1}, \tag{8.8}$$

which gives us the function for the indefinite integral

$$q(s) = y_0 \cdot \int_s u(s) \, \mathrm{d}s + \frac{y_1 - y_0}{s_1} \cdot \int_s s \cdot u(s) \, \mathrm{d}s. \tag{8.9}$$

Both parts are then integrated separately, yielding

$$\int_s u(s) \, \mathrm{d}s = U(s) = -\frac{2}{3\,s_z} \cdot \sqrt{2\,g} \cdot h(s)^{\frac{3}{2}} \tag{8.10}$$

$$\int_s s \cdot u(s) \, \mathrm{d}s = \frac{U(s)}{5\,s_z} \cdot (2\,h(s) + 5\,s_z\,s) \tag{8.11}$$

$$q(s) = U(s) \cdot \left[ y_0 + \frac{y_1 - y_0}{s_1} \cdot \frac{1}{5\,s_z} \cdot (2\,h(s) + 5\,s_z\,s) \right]. \tag{8.12}$$

The definite integral gives the total flux for one z-stripe:

$$Q = q(s_1) - q(0) = -\frac{2}{3\,s} \cdot \sqrt{2\,g} \cdot \left[ y_1 \cdot h_1^{\frac{3}{2}} - y_0 \cdot h_0^{\frac{3}{2}} + \frac{2\,(y_1 - y_0)}{5\,(z_1 - z_0)} \cdot (h_1^{\frac{5}{2}} - h_0^{\frac{5}{2}}) \right] \tag{8.13}$$

with

$$h_1 = h(s_1) = z_a - z_1 + \alpha \quad \text{and} \quad h_0 = h(0) = z_a - z_0 + \alpha.$$

## 8.3 Fill Level Averaging for Free Outflow

Especially in the first, transient phase of flooding, the difference between two filling levels can be very large. This may result in the overestimation of the flux for the free outflow part of a large opening. Currently, it is assumed that the flux area extents to the maximum filling level.

Even though the correct shape of the free outflow part is unknown, the effective area is probably smaller than the maximum level. The upper limit $z$ is assumed to be between the two water levels $z_a$ and $z_b$, but will reach the upper edge of the opening $z_2$ if the upper part of the opening becomes submerged by the higher water level $z_a$. The velocity of the flow is still determined by the pressure height difference between both compartments.

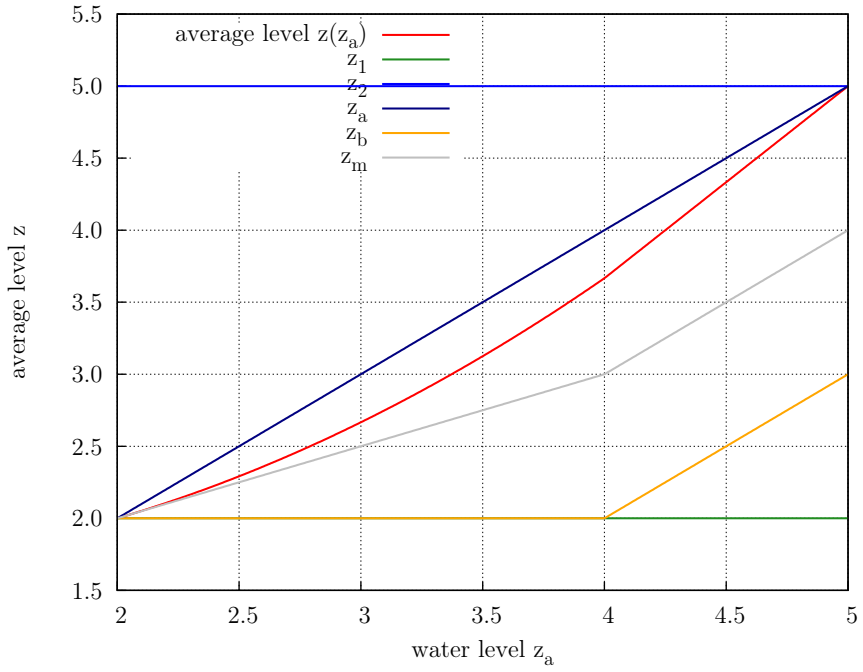


Figure 8.1: Model for the averaged water level in an opening

One reasonable model for the averaged level $z$ is sketched as follows:

$$z_m = z_a \cdot f + z_b \cdot (1 - f) \qquad \text{with} \quad f \in [0, 1], \tag{8.14}$$

$$\bar{z}_a = \frac{z_a - z_1}{z_2 - z_1} \qquad \text{with} \quad \bar{z}_a \in [0, 1], \tag{8.15}$$

$$z = z_m + (z_a - z_m) \cdot \bar{z}_a \tag{8.16}$$

The development of the average water level $z$ depends on the water level $z_a$ and is shown in Figure 8.1 using a constant difference $z_b - z_a$. The $z_1$ value is the lower and the $z_2$ value the upper edge of the opening.

## Curriculum Vitae of the Author

| | |
|---|---|
| **Family Name** | Dankowski |
| **First Name** | Hendrik |
| **Date of Birth** | March 11th, 1980 in Eutin, Germany |
| **12.2007 - today** | Research assistant at the Institute of Ship Design and Ship Safety of Hamburg University of Technology, Germany |
| **10.2005 - 11.2007** | Master of Science program "Computational Sciences in Engineering" at the Technische Universität Carolo-Wilhelmina zu Braunschweig, Germany, Degree: M.Sc. |
| **04.2005 - 08.2005** | Diploma Thesis in collaboration with Flensburger Schiffbau Gesellschaft, Germany |
| **09.2004 - 02.2005** | Internship at Hamburg Ship Model Basin, Germany, Department of Resistance and Propulsion |
| **02.2003** | Internship at the Howaldtswerke - Deutsche Werft AG Kiel, Germany, Department of *Überwasserkonstruktion* |
| **09.2002 - 07.2006** | Studies of Naval Architecture at the University of Applied Science in Kiel, Germany, Degree: Dipl.-Ing. (FH) |
| **02.2002 - 03.2002** | Internship at Howaldtswerke - Deutsche Werft AG Kiel, Germany, Department of *Schiffskörperfertigung* |
| **09.2001 - 08.2002** | Studies of Mechanical Engineering at the University of Applied Science in Konstanz, Germany |
| **08.2001 - 09.2001** | Internship at Siemens AG Turbine Factory in Wesel, Germany |
| **08.2000 - 07.2001** | Alternative Civilian Service at Pflege Diakonie Neumünster, Germany |
| **01.1998 - 06.1998** | Semester Abroad at Quincy High School, Washington State, USA |
| **08.1990 - 07.2000** | Alexander-von-Humboldt-Schule Neumünster, Germany (Secondary School), Degree: Abitur |
| **08.1986 - 07.1990** | Grundschule Bordesholm, Germany (Primary School) |